ENGINEERING EXPERIMENT STATION

COLLEGE OF ENGINEERING

OPEN CYCLE DESICCANT AIR CONDITIONING SYSTEMS

BY

DANIEL R. CRUM

MASTER OF SCIENCE
(MECHANICAL ENGINEERING)

UNIVERSTIY OF WISCONSIN-MADISON

1986

OPEN CYCLE DESICCANT AIR CONDITIONING SYSTEMS

Daniel R. Crum

Under the Supervision of Professor John Mitchell

This thesis presents a study of open cycle desiccant air conditioning systems. Traditional desiccant ventilation and recirculation cycles are reviewed and two advanced desiccant cycles are presented. The advanced cycles employ sensible air coolers in place of direct evaporative coolers.

Variants of indirect evaporative coolers are presented and performance relations and characteristics are formulated. The two most promising coolers are a staged indirect evaporative cooler and a combination cooling tower/heat exchanger.

The various desiccant cycles are simulated for an entire Madison, Wisconsin cooling season when coupled to typical commercial building zones. Histograms of regeneration temperature and thermal COP are presented.

Commercial users of potential desiccant cycles are identified and their total energy expenditure for air conditioning purposes is determined.

An economic life cycle cost comparison is made between the desiccant cycles and a conventional vapor compression air conditioner. Allowable first costs for desiccant systems per ton of installed cooling capacity are calculated. Over the range of zone loading conditions, the desiccant cycles are cost competative with vapor compression equipment.

Estimates of the potential reduction in electrical energy demand and the increase in natural gas sales seen by Wisconsin Power and Light as a result of the possible installation of desiccant systems are made.

ACKNOWLEDGEMENTS

I would like to thank Professors John Mitchell and Bill Beckman for their support throughout this project. They have provided wisdom and valuable technical insights into this study as well as showed encouragement during those most difficult periods. Thanks also go to Professors Jack Duffie and Sandy Klein for their support and friendship.

I also extend my heartfelt thanks to my fellow students in the Solar Lab. Your friendship, kindness and sincere support helped make my graduate studies a positive and memorable experience. Special thanks go to Erik and Ken for sharing with me their knowledge and insights into the world of desiccants.

This project was sponsored by Wisconsin Power and Light Company. The help of George Penn, Carl Dewinkle and Doug Mitchell was greatly appreciated.

Final thanks go to Judy. Thank you for your patience and encouragement throughout my many ups and downs. Your love and prayers have carried me through to this project's end.

TABLE OF CONTENTS

LIST OF FIGURES

FIGURE | PAGE

FIGURE PAGE

FIGURE		PAGE

FIGURE		PAGE

FIGURE | PAGE

LIST OF TABLES

NOMENCLATURE

A	transfer area in wet surface heat exchanger [m^2]
c	flag set to 0 for residential investments, 1 for commercial investments
c_p	specific heat [J/kg°C]
c_{wb}	wet bulb specific heat [J/kg°C]
C	capacitance rate [W/°C]
C^*	ratio of minimum to maximum capacitance flow streams in heat exchanger [dimensionless]
COP	air cooling benefit/energy input [dimensionless]
d	market discount rate
D	ratio of down payment of to initial investment
e	slope of assumed linear saturation line [$°C^{-1}$]
f	fuel inflation rate
F	fraction of inlet air to the air cooler that is delivered to conditioned zone [dimensionless]
$\dot{G}$	instantaneous sensible zone gain [W]
h	enthalpy [J/kg]
h_c	heat transfer coefficient [$W/m^2°C$]
h_D	water vapor transfer coefficient [kg/m^2s]
h_f	enthalpy of liquid water [J/kg]
h_g	enthalpy of water vapor [J/kg]
h_{fg}	latent heat of vaporization [J/kg]
h_{wb}	wet bulb specific heat [J/kg°C]

i	inflation rate
k	constant in Eq. (3.3.11) [dimensionless]
m	mortgage rate
$\dot{m}$	mass flow rate [kg/s]
M	ratio of maintenance to investment
n_L	term of loan
n_d	depreciation lifetime
n_1	minimum of term of loan and years in economic study
n_2	minimum of depreciation lifetime and years in economic study
p	property tax rate
P_1	fuel cost present worth factor
P_2	equipment cost present worth factor
q	heat transfer rate [W]
r	tax credit
S	ratio of salvage to investment
t	effective income tax rate
T	temperature [°C]
U	overall heat transfer coefficient between water film surface and fluid stream in wet surface heat exchanger [$W/m^2 °C$]
W	width of wet surface heat exchanger [m]
$\dot{w}$	work rate [W]
ε_{DEC}	direct evaporative cooler effectiveness [dimensionless]
ε_{HX}	indirect evaporative cooler effectivenss [dimensionless]

ε_h enthalpy effectivenss [dimensionless]

ε_m moisture effectiveness based on ideal dehumidifier [dimensionless]

ε_ω moisture effectiveness based on intersection point method [dimensionless]

Γ_p dehumidifier flow rate parameter [dimensionless]

Δp pressure drop [Pa]

ρ air density [kg/m^3]

ω humidity ratio [kg/kg dry air]

Subscripts

a moist air stream

cc cooling capacity

da dry air

deh dehumidifier

delivered delivered air stream

dew pt dew point conditions

dump dumped air stream

f fluid stream

inlet inlet air stream

max maximum

min minimum

n number of stages

outlet outlet air stream

recirc recirculated zone air

proc process air stream

T	temperature
vent	additional ventilation air
w	at water film surface
wb	wet bulb

Superscripts

'	at saturation conditions

CHAPTER 1: INTRODUCTION

There is a growing concern among power utilities to more fully understand where the energy they produce is going and for what purposes it is being used. It is vital for these utilities to keep abreast of trends and new technologies that are developing within their territory since these developments could alter their plans for future growth. Wisconsin Power and Light is one such concerned utility. WPL serves one-third of Wisconsin's geographical area and annually sells in excess of 5500 GW-Hours of electrical energy to over 326,000 customers. In an attempt to keep pace with new technologies, WPL is funding various projects to determine the feasibility of some of these new technologies. Information gained from these studies aids decision makers in determining how their utility demand may be altered in the future.

Desiccant air conditioning is one such technology that has shown some potential for effecting power utilities energy use and demand. Desiccant air conditioning systems were first proposed by Dunkle in 1965. These cycles use solid rotary desiccant dehumidifiers to dehumidify supply air and heat exchangers and evaporative coolers to cool that dried air. These systems used solar energy as a replacement for the conventional vapor compression machine. Simulation studies at the University of Wisconsin have been aimed at evaluating the potential of these desiccant systems. Nelson [1976] and Jurinak [1982] have simulated these systems in hot, humid weather regions.

Recently, Maclaine-cross and Kang [1985] have proposed and studied a new generation of desiccant cycles in ARI design point computer simulations. These cycles utilize a combination cooling tower/heat exchanger air cooler and initial results indicate that these new coolers boost cycle performance considerably.

The common denominator between all of these desiccant systems, basic or advanced, is their use of thermal energy in place of electrical energy. The conventional vapor compression unit, traditionally mechanically driven, is replaced with open cycle dehumidifying and evaporative cooling. These desiccant systems therefore have the potential of shifting energy demand from the high grade electrical energy to the lower grade thermal energy of natural gas. Because air conditioning operations consume approximately 4% and 7% of the total energy supplied to residences and commercial users in Wisconsin, respectively, there is a significant block of energy in WPL's territory which has the potential for shifting from electricity to natural gas.

The specific objectives of this thesis are the following:

1) Evaluate the potential impact desiccant air conditioning systems may have on WPL's utility demand.
2) Determine the magnitude of the possible reduction in electrical energy usage and the corresponding increase in natural gas sales.
3) Identify and/or develope desiccant air conditioning systems that are suitable to Wisconsin climate and identify the customers in

Wisconsin Power and Light's territory that would be most targetable for such systems.

4) Evaluate the economic feasibility of these systems impacting on the Wisconsin energy market.

To achieve the above objectives, the following information is discussed in the balance of this thesis. In Chapter 2, the fundamentals of both vapor compression and desiccant air conditioning are reviewed. Here, both the dehumidification and the regenerative evaporative cooling processes are discussed. Chapter 3 follows with a discussion of direct and indirect evaporative cooling and a look at new sensible air coolers targeted for desiccant air conditioning systems. In Chapter 4, these new air coolers are incorporated into the traditional desiccant cycles and results from ARI design point computer simulations are examined. The specific component models used in the TRNSYS simulation models are discussed in Chapter 5 and then results for season simulations of an advanced and a classical desiccant cycle are presented in Chapter 6 for Wisconsin weather data. Finally, Chapter 7 presents economic comparisons between conventional vapor compression units and a variety of desiccant cycles. Predictions are then made regarding possible energy reduction and shifts in sold energy. Conclusions are drawn and recommendations are made for further research in Chapter 8.

CHAPTER 2: INTRODUCTION TO DESICCANT AIR CONDITIONING SYSTEMS

Conditioning the air in a building zone involves two fundamental processes. The first is the removal of moisture from the zone air and the second is the sensible cooling of the zone air. To meet an air conditioning load, air must therefore be supplied at a state cooler and drier then that of the conditioned space. Equations (2.0.1) and (2.0.2) are equations used to calculate the air state required of the supply stream.

$$\omega_{supply} = \omega_{zone} - Q_{latent}/(\dot{m}_{supply}*h_{fg}) \qquad (2.0.1)$$

$$h_{supply} = h_{zone} - (Q_{latent} + Q_{sensible})/\dot{m}_{supply} \qquad (2.0.2)$$

Figure 2.0.1 illustrates on a psychrometric chart a typical zone air state and a supply air state required to meet the combination of sensible and latent loads on the zone. The dashed line that runs between these two state points is called the Load Line. Any supply state lying on this line would provide the correct proportion of sensible and latent cooling required to exactly balance the total zone load. As is indicated by Eqs. (2.0.1) and (2.0.2), the larger the supply air flow rate, the smaller the required enthalpy difference required across the supply and return air streams and the shorter the Load Line will be. The latent enthalpy difference, depicted in Fig. 2.0.1 as ΔH_{lat}, is that portion of the total cooling

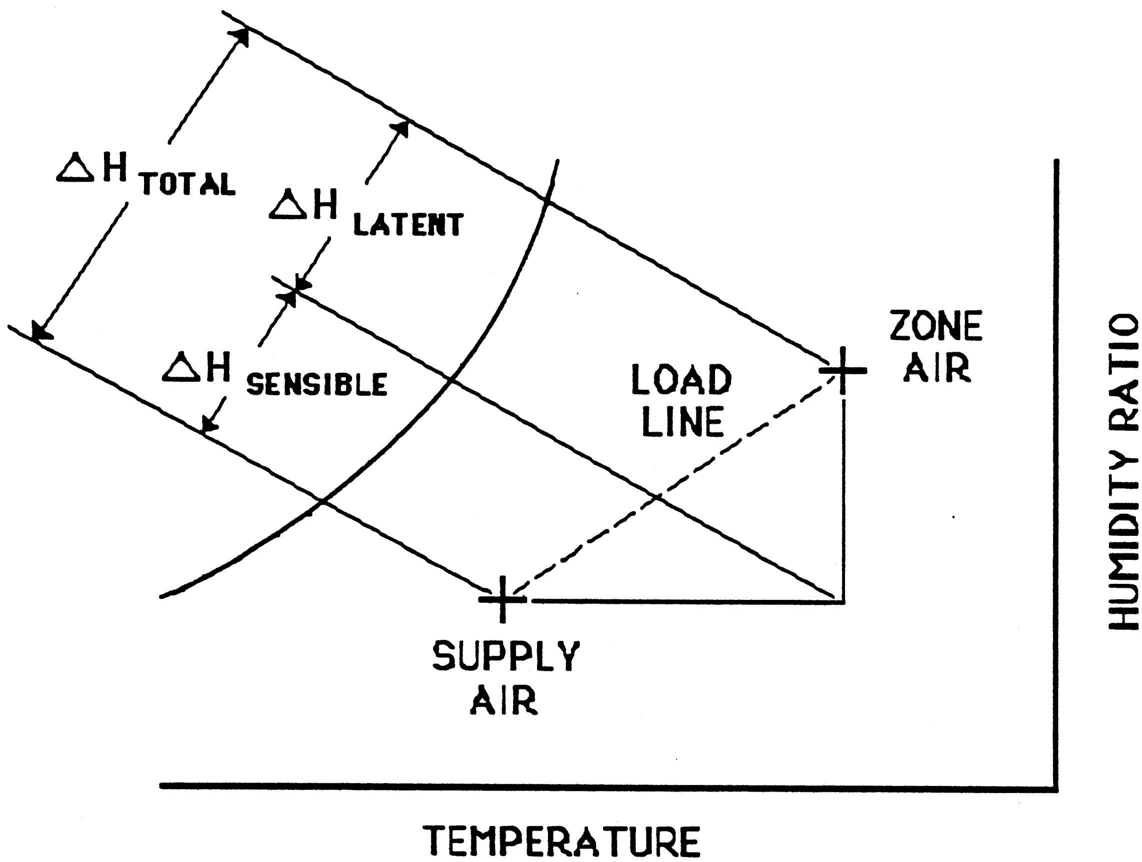

Figure 2.0.1 Sample zone and supply states. Illustrates Load Line and latent and sensible air conditioning components

load required for moisture removal. The enthalpy difference, ΔH_{sen}, is that portion of the total enthalpy difference across the supply and return air streams attributed to sensible cooling. The ratio of the required latent cooling to total cooling load is defined as the Latent Load Ratio (LLR). The values of LLR range from 0 to 1.0 where 1.0 corresponds to a 100% latent air conditioning load.

The conventional means of conditioning a building zone is with a vapor compression machine as illustrated in Fig. 2.0.2. A vapor compression machine is composed of four primary components; an evaporator, a compressor, a condenser and an expansion valve. In operation, the working fluid, usually a freon refrigerant, enters the evaporator as a mixed-phase fluid (F1) and exchanges energy with the warmer zone supply air (A1). Here, the refrigerant changes phase and exits as a saturated vapor (F2) while the zone supply air is cooled and dehumidified (A2). In order to reuse the vaporized refrigerant that exits the evaporator, it must be recondensed. The freon is therefore compressed to a higher pressure (F3) where its boiling temperature is above the temperature of the cooling medium available for condensing purposes. After the refrigerant is condensed in the condenser, (F4), it is throttled through the expansion valve to the evaporator pressure and the cycle is repeated.

A vapor compression machine is inherently just a sensible cooling device. As air blows past the evaporator its temperature is reduced at constant humidity ratio. To dehumidify the supply air, the vapor compression machine must chill the air below its dew point

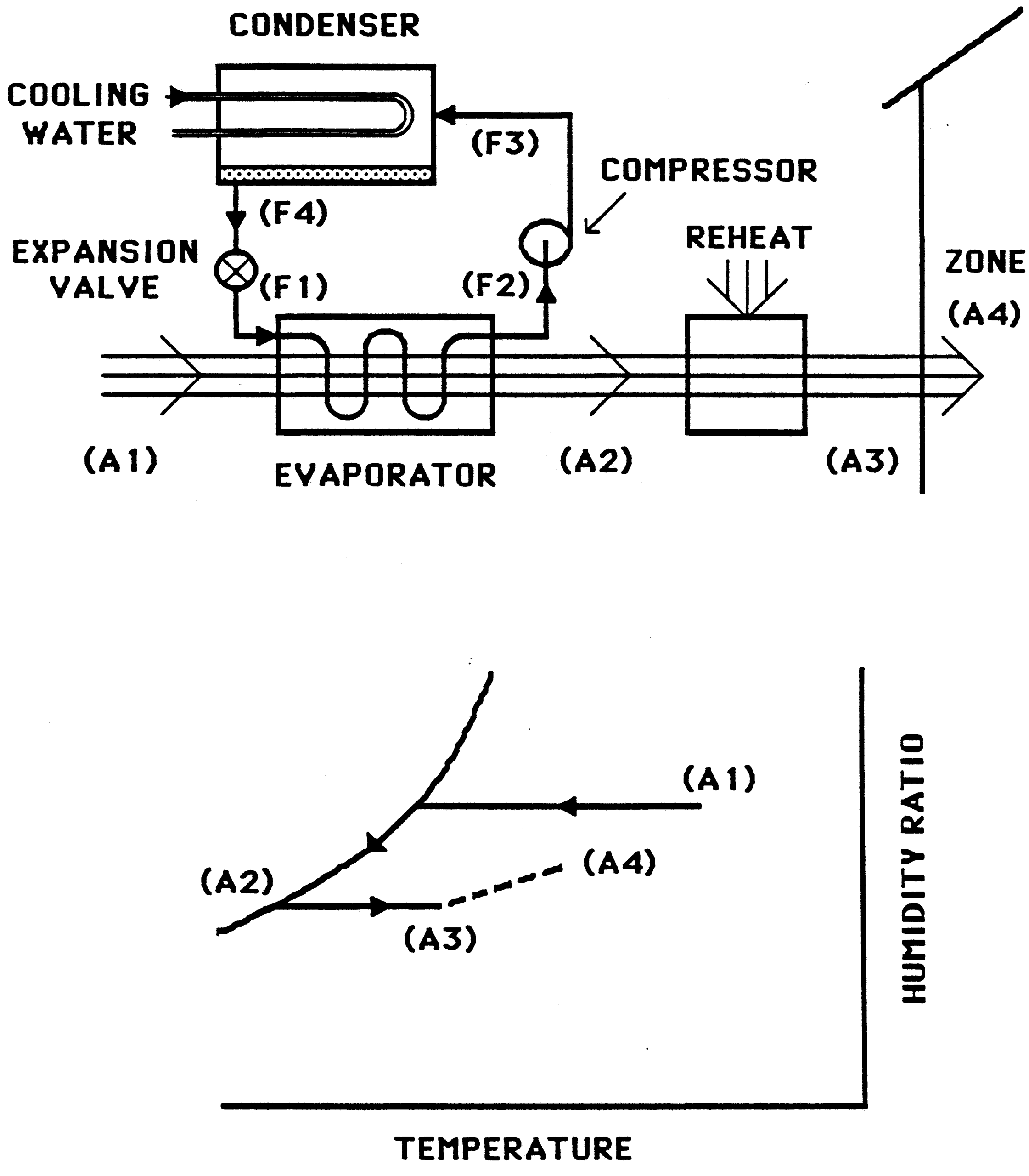

Figure 2.0.2 Conventional vapor compression air conditioner and air states through equipment

temperature and then cool the air at constant 100% relative humidity to the required supply humidity ratio. For supply states that lie away from the saturation line, a final reheat process may be required to reach the final supply temperature.

Section 2.1: The Desiccant Dehumidification Process

Studying Figs. 2.0.1 and 2.0.2 would suggest that an alternative approach to conditioning the supply air would be to first dehumidify the air to the required supply humidity ratio and then somehow cool the air to its supply temperature. A desiccant could perform the dehumidification required of this alternative air conditioning procedure. A desiccant is any drying agent that adsorbs moisture when in contact with moist air. Silica gel and activated carbon are two examples of desiccants often used in dehumidification processes.

The dehumidification process, as shown schematically in Fig. 2.1.1, is an approximately constant enthalpy process [Jurinak; 1982] where the heat of adsorption is released into the air stream resulting in an increase in air temperature. The reduction in the latent air conditioning load is therefore associated with an increase in the sensible cooling load. Because there is a finite amount of moisture that can be adsorbed on the desiccant surface, the desiccant must be periodically regenerated. For this reason, dehumidifiers are often constructed in a rotary configuration as seen in Fig. 2.1.1. With this design, air enters the dehumidifier at state 1 and is dried and heated to state 2 as it flows in the axial direction through the

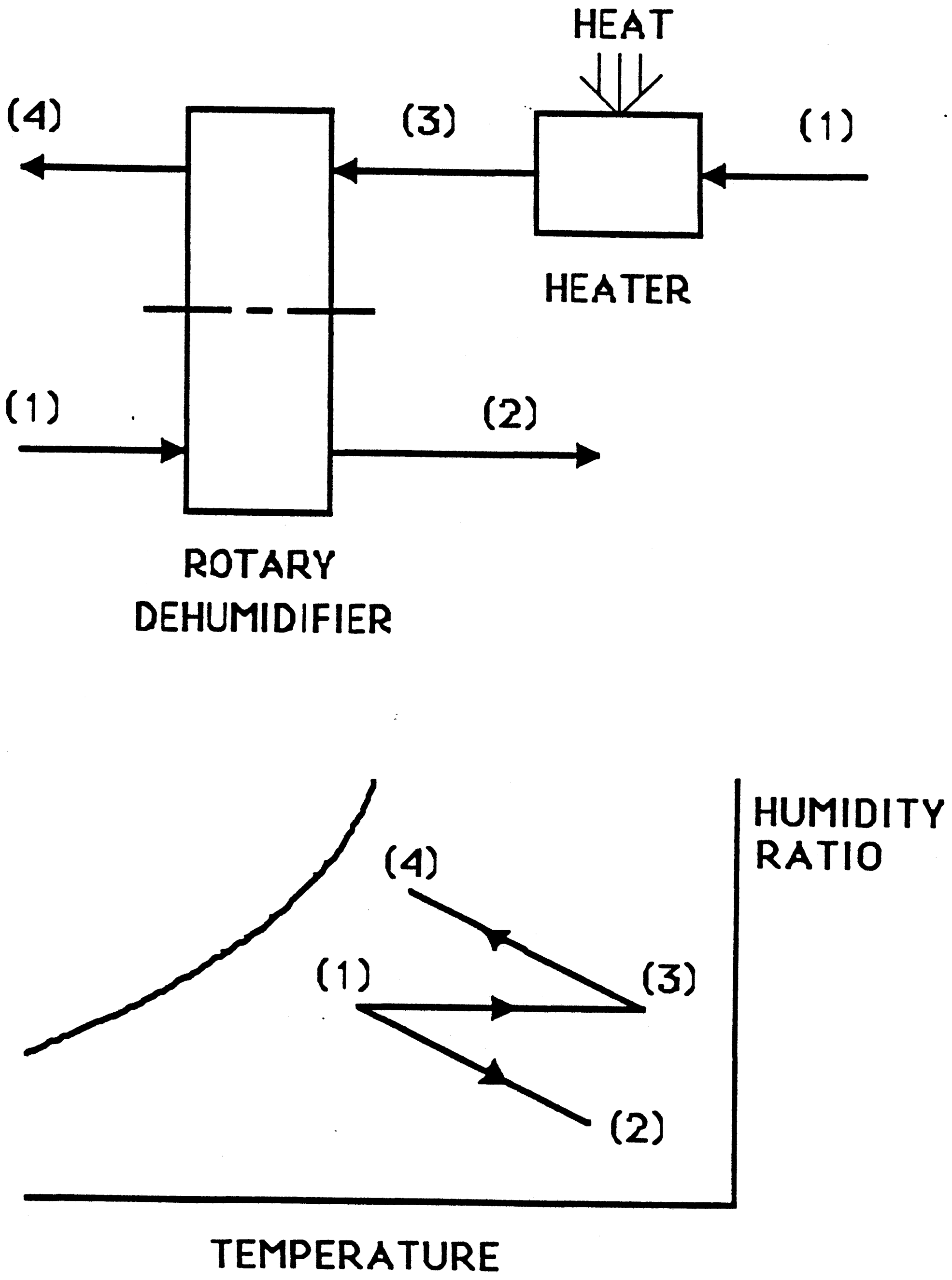

Figure 2.1.1 Schematic diagram and process representation of dehumidification procedure

dehumidifier. The moist desiccant material then rotates through the hot regeneration stream and is purged of the previously adsorbed moisture. The hot regeneration air in Fig. 2.1.1 enters at state 3 and exits at state 4, wet and cool. Because the regeneration stream does not always originate from a source that is hot enough to purge the desiccant, it is usually necessary to add thermal energy to the regeneration air with a heater. This heat addition warms the air from state 1 to 3.

Section 2.2: Regenerative Evaporative Cooling

An alternative air cooling device used in dry and temperate climates is the regenerative evaporative cooler. A schematic diagram of this cooler is illustrated in Fig. 2.2.1. This cooler is an alternative to vapor compression air conditioning in regions where dehumidification is not required. This process uses a sensible air/air heat exchanger and two direct evaporative coolers (See Section 3.1). In this cycle, exhausted zone air at state 4 is cooled and humidified at nearly constant enthalpy to state 5. This cooled air is used as a heat sink for the inlet air at state 1 that is sensibly cooled to state 2. Further cooling is available from the second direct evaporative cooler and air exits from this device at the zone supply state, 3.

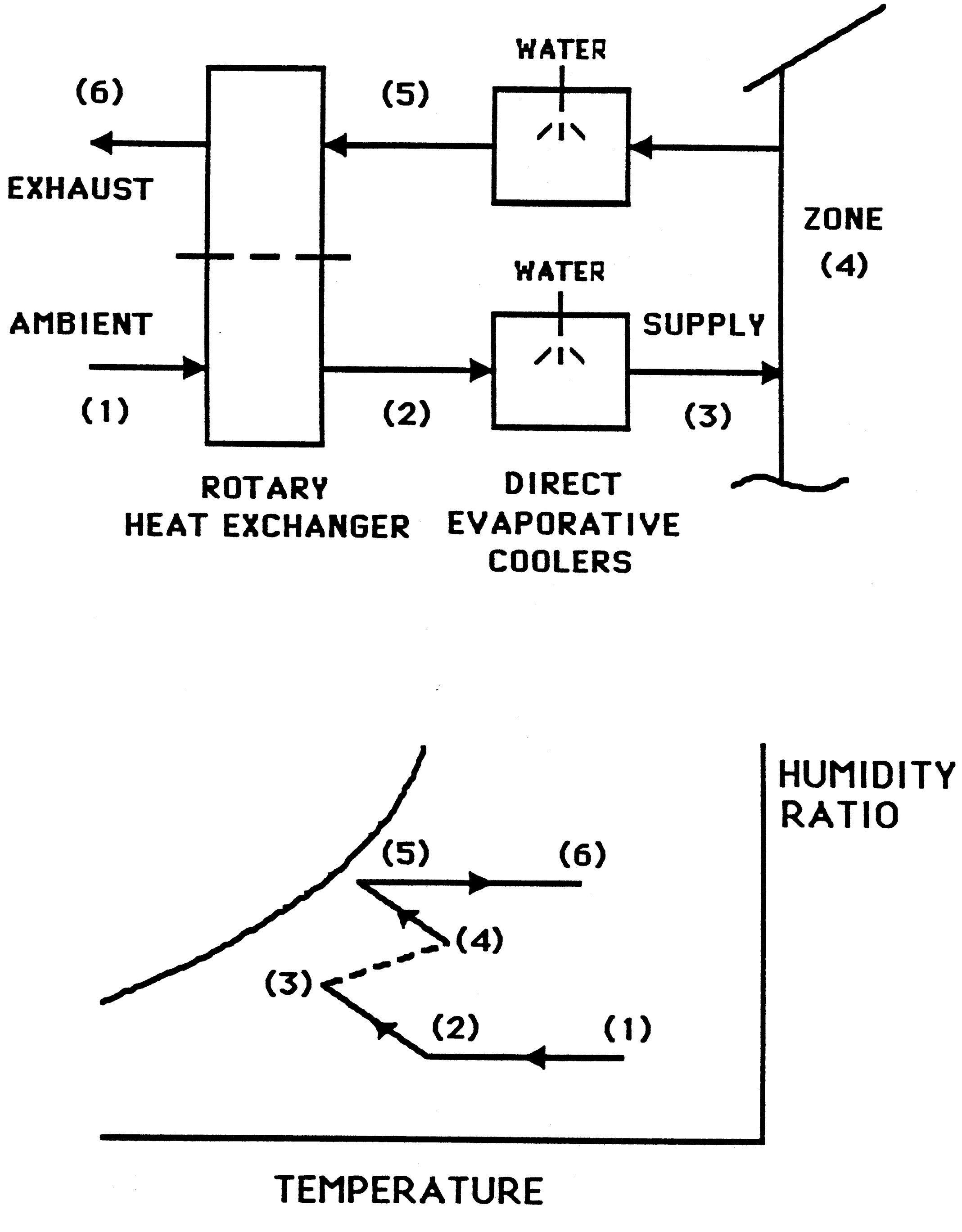

Figure 2.2.1 Schematic diagram and process representation of regenerative evaporative cooler

Section 2.3: Classical Desiccant Air Conditioners

In most climates encountered in the United States, building air conditioning requirements have both latent and sensible components. In these regions, the regenerative evaporative cooler of Section 2.2 may be combined with the desiccant dehumidifier of Section 2.1 to form a machine capable of handling a total (latent and sensible) air conditioning load. Such an air conditioner is a complete substitute for the conventional vapor compression air conditioner discussed earlier.

The classical desiccant air conditioning cycle was first proposed and studied by Dunkle [1961] and later studied by Nelson [1976] and Jurinak [1982]. A schematic diagram and process representation of this air conditioning system is illustrated in Fig. 2.3.1. This particular desiccant cycle operates in a ventilation mode where only fresh air from the ambient is processed through the dehumidifier. In this cycle, ambient air at state 1 is dehumidified and heated to state 2. The state 2 air is then sensibly cooled in the rotary heat exchanger and uses the evaporatively cooled zone exhaust air as its heat sink. The process air is further cooled to the required supply state with the second direct evaporative cooler for use in the zone, state 5. On the exhaust side of the cycle, the evaporatively cooled zone air is sensibly heated to state 7. The exhaust air is further heated in the heater to state 8 where it is then delivered to the dehumidifier at the required regeneration temperature.

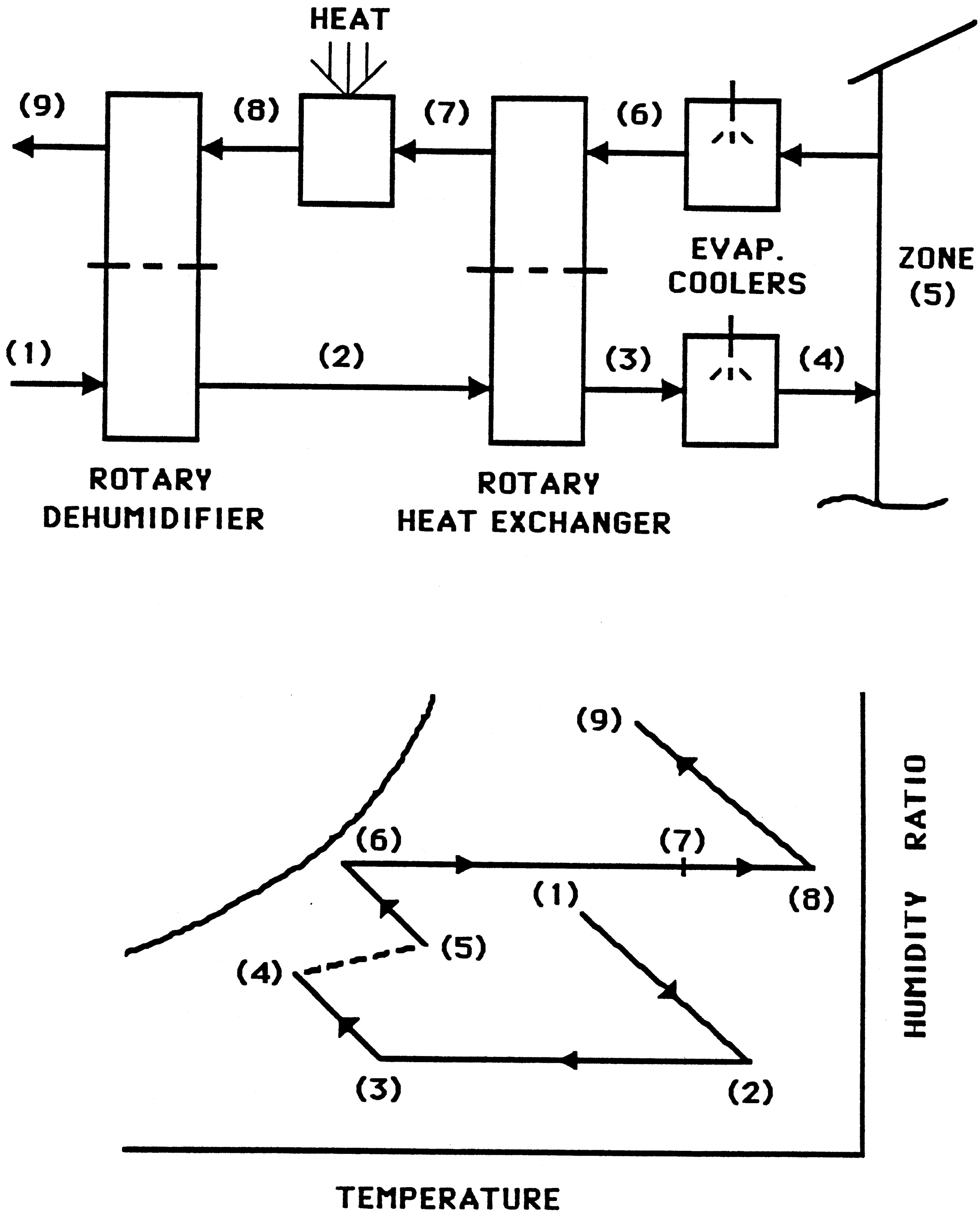

Figure 2.3.1 Schematic diagram and process representation of classical ventilation desiccant air conditioning cycle

The cycle just described may also be configured in a recirculation mode as illustrated in Fig. 2.3.2. The major difference between the ventilation and the recirculation cycle is the origin of the air that is passed through the dehumidifier. The recirculation cycle reprocesses the zone air through the dehumidifier instead of introducing fresh ambient air. The regeneration stream for the recirculation cycle originates from the ambient whereas the ventilation cycle uses zone exhaust air.

When these cycles are simulated at American Refrigeration Institute (ARI) design conditions (Ambient: 35°C, 0.0142 kg/kg; Zone: 26.7°C, 0.0111 kg/kg), the resultant COP's based on thermal energy input for the ventilation and recirculation cycles are 0.77 and 0.54, respectively.

Section 2.4: Differences Between Vapor Compression and Desiccant Air Conditioning

There are several differences between desiccant and vapor compression air conditioning. The first difference is the type of energy required to power these cycles. A vapor compression machine uses high grade electrical energy to power the freon compressor. A desiccant machine uses thermal energy to regenerate the desiccant material. Because desiccant cycles use lower grade thermal energy, these cycles could be powered by waste heat, solar energy or natural gas. In regions where thermal energy sources may be less expensive then electricity, desiccant cycles may be competitive with the higher

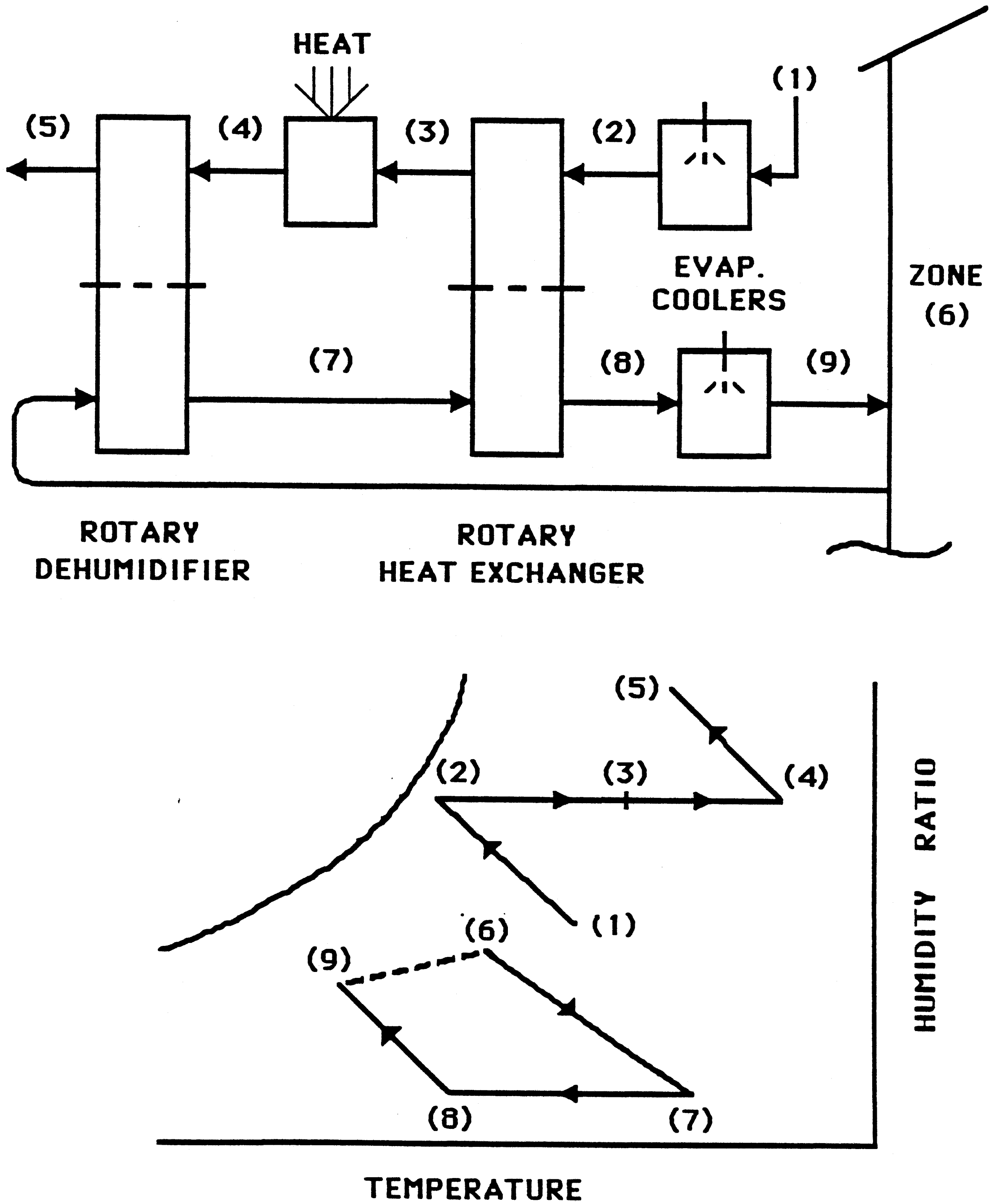

Figure 2.3.2 Schematic diagram and process representation of classical recirculation desiccant air conditioning cycle

performance vapor compression air conditioner. Further, the desiccant cycle may be less expensive to operate during dry periods when the cycle uses the free cooling provided by the regenerative evaporative cooler. Finally, the desiccant air conditioning cycles tend to be more complex than the vapor compression cycles due to the higher number of system components.

CHAPTER 3: SENSIBLE AIR COOLERS FOR USE IN DESICCANT CYCLES

The standard ventilation and recirculation desiccant air conditioning cycles discussed in Chapter 2 use direct evaporative coolers to cool the process air after it exits the dehumidifier. The evaporative cooling process is the exact opposite of the dehumidification process; instead of drying the air, it injects water into the air stream in a nearly constant enthalpy process (See Section 3.1). This injection of water into the dried process stream is therefore counter-productive since the dehumidifier must overdry the process air to allow for future humidifying in the direct evaporative cooler.

It would be beneficial to develope and use air coolers in desiccant air conditioning cycles that do not humidify the process air as it is cooled. The use of such sensible air coolers would enhance the overall system performance by decreasing the amount of drying required by the dehumidifier. This chapter, therefore, reviews direct and indirect evaporative coolers and explores new sensible air coolers targeted for use in desiccant air conditioning systems.

Section 3.1: Direct Evaporative Coolers

A direct evaporative cooler (DEC) is an air conditioning device used to cool and humidify air [ASHRAE Equipment Guide, 1983]. Direct evaporative cooling involves the process of evaporating water into an air stream. Throughout this process, air and water are in direct contact and both heat and mass are exchanged. Figure 3.1.1 shows a

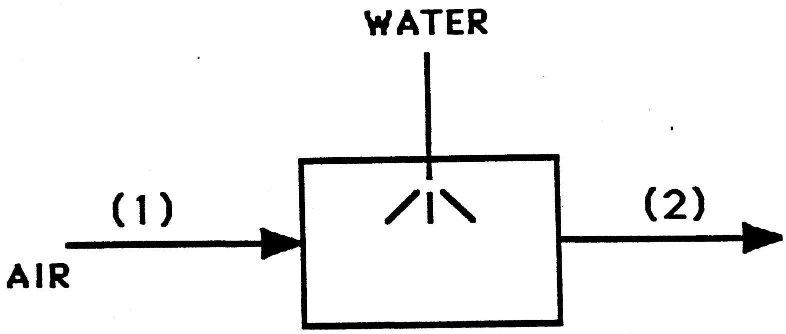

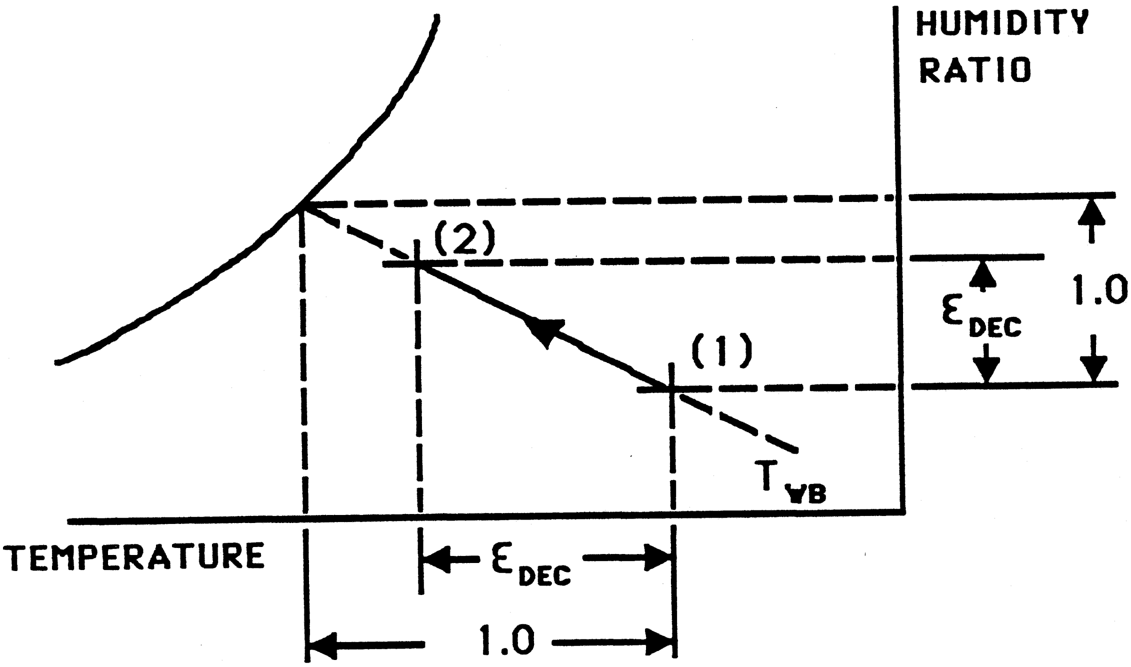

Figure 3.1.1 Schematic diagram and process representation of a simple direct evaporative cooler

schematic representation of a direct evaporative cooler along with the process representation on a psychrometric chart. A direct evaporative cooling process is seen to be a constant wet bulb temperature process. This process is also very nearly a constant enthalpy process. From Fig. 3.1.1, an effectiveness model may be defined to describe the performance of a DEC.

$$\varepsilon_{DEC} = \frac{T_1 - T_2}{T_1 - T_{wb@1}} \qquad (3.1.1)$$

This effectiveness measures the extent to which the air exiting the evaporative cooler approaches the wet bulb temperature of the entering air stream. Since a line of constant wet bulb temperature is linear on the psychrometric diagram, Eq. (3.1.1) may also be written in an equivalent form as:

$$\varepsilon_{DEC} = \frac{\omega_2 - \omega_1}{\omega_{sat} - \omega_1} \qquad (3.1.2)$$

Evaporative cooling of an air stream presents an energy tradeoff since a DEC exchanges a reduction in sensible energy (temperature) with a corresponding increase in latent energy (humidity). A direct evaporative cooler never reduces the total load on an air stream; it merely exchanges one form of the load for another.

The most commonly used type of DEC in air conditioning practice is the wetted media air cooler. This air cooler uses wetted evaporative cooler pads through which the process air is blown. A pumped water distribution system recirculates the sump water so that the evaporative pads are always evenly soaked. In steady-state operating conditions, the water recirculation loop reaches an equilibrium temperature equal to the wet bulb temperature of the inlet air. Figure 3.1.2 shows a plot of air and water temperature in a DEC as a function of the time that the air and water are in contact. This figure further illustrates the effectiveness model described by Eq. (3.1.1). In typical operation, this effectiveness is usually 0.8, however variations in pad face velocities and water flow rates may alter the system's performance.

Simple direct evaporative coolers are being manufactured today. They are used in temperate climates where the ambient wet bulb temperatures are usually lower than that required by the supply air stream. In the United States, these air coolers are typically used in the drier and warmer south-western states.

The only operating cost associated with DEC systems is due to the parasitic power required to operate fans and pumps to recirculate water. Supplying make-up water may also be a factor in operating cost in regions where water is relatively expensive. Typical water consumption rates are approximately 2.5 ml/sec per m^3/sec of air flow per 5°C of air temperature drop.

Section 3.2: Indirect Evaporative Coolers

An indirect evaporative cooler (IEC) is an air conditioning device that sensibly cools process air without increasing the absolute

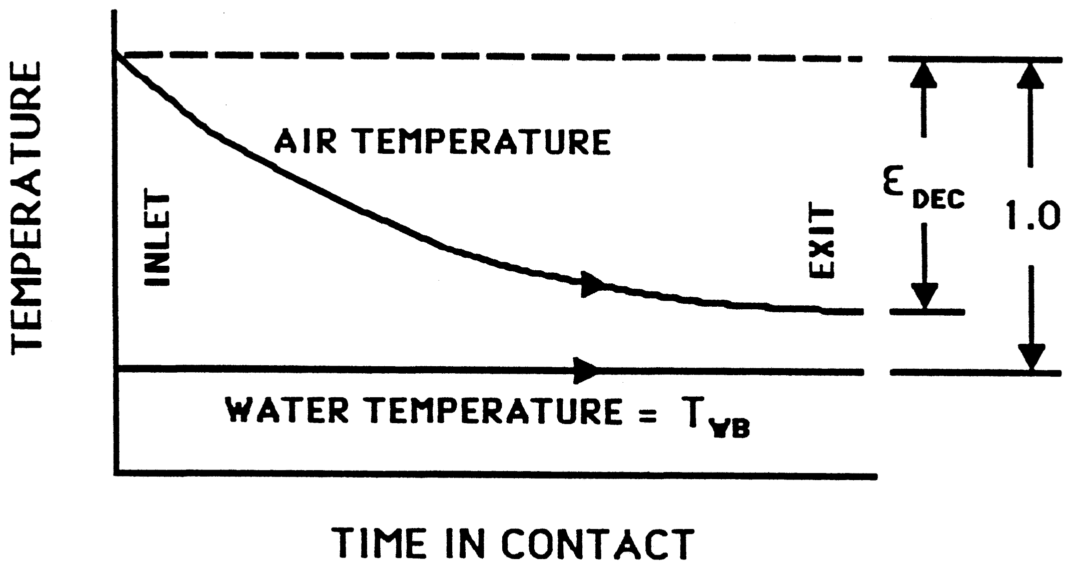

Figure 3.1.2 Air and water temperatures vs time in contact for a simple direct evaporative cooler

humidity ratio of the air [ASHRAE Equipment Guide, 1983]. A schematic diagram and process representation of an IEC is shown in Fig. 3.2.1. This process uses two separate air streams that never mix or come in direct contact. One stream, the "wet stream", goes through an evaporative cooling process and is cooled and humidified to state 3. The second stream, the "process stream", passes through a sensible air/air heat exchanger and uses the cool, wet stream as its heat sink. The process stream is therefore cooled to state 2 and the wet stream is heated to state 4.

The cooling process involved in an IEC is a function of the effectiveness of both the evaporative cooling and the heat exchange process. The effectiveness of the cooling and heat transfer processes are, in turn, functions of the size of the units, and the relative flow rates of the wet and process air streams.

The indirect evaporative cooling process requires no energy input besides that required to overcome fan and water pumping power. Coefficients of performance (air cooling benefit/energy input) for these systems therefore tend to be very high (see Section 3.3).

An IEC, however, is not without its limitations. At best, a single IEC can only cool process air down to the wet bulb temperature of the wet stream. Since the wet stream is typically the ambient, the system performance decreases as the ambient wet bulb temperature increases. As in the case of a direct evaporative cooler, an IEC is best suited for dry and temperate climates. The second major limitation to an IEC system is that the system does not have the capability

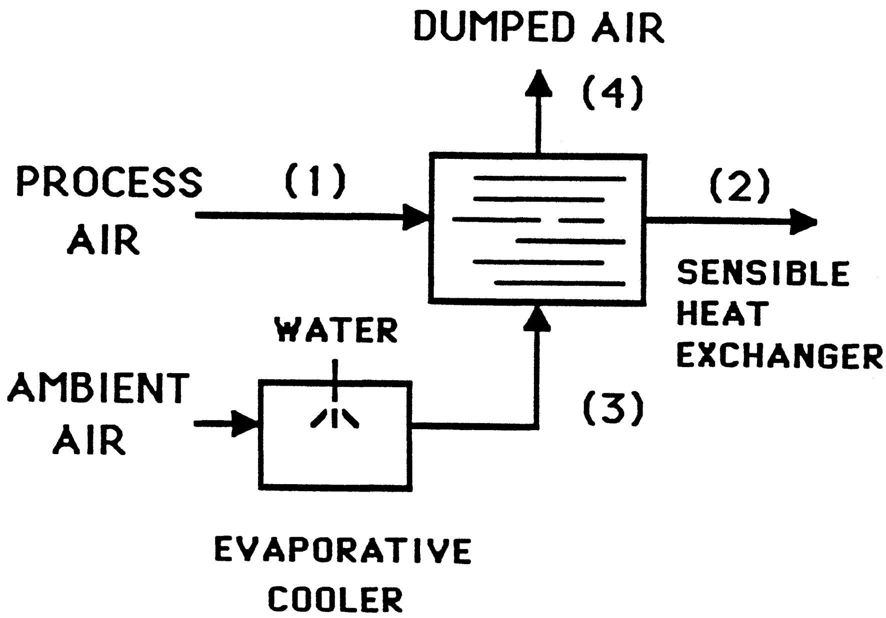

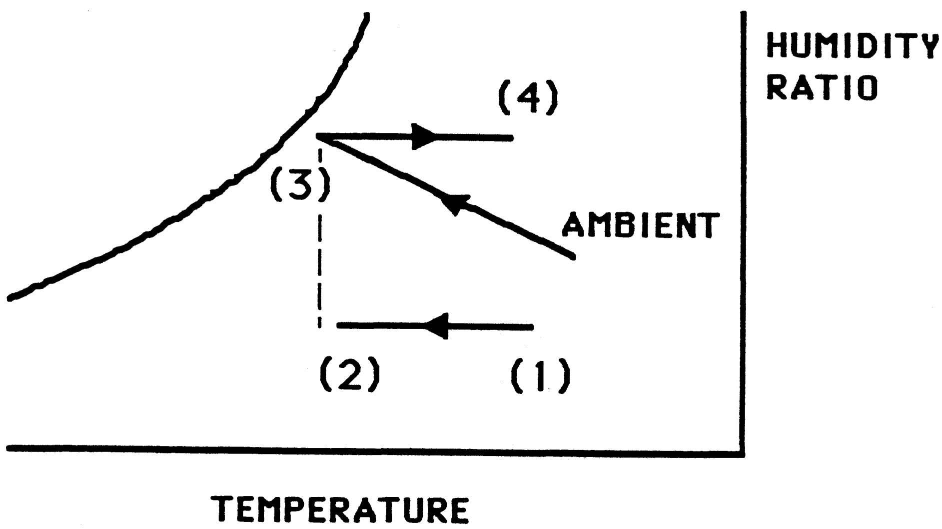

Figure 3.2.1 Schematic diagram and process representation of an indirect evaporative cooler

to dehumidify the inlet process stream. This type of system must therefore be used in conjunction with a dehumidification process in order to meet a total air conditioning (sensible and latent) load on a building zone.

Section 3.3: Single-Stage Indirect Evaporative Coolers

In the indirect evaporative cooler described in Section 3.2 the wet stream air that acts as the heat sink for the warmer process air is usually drawn from the ambient. In this case, the two streams have different sources. In some instances, however, it may be desirable to use a common source for both the wet and process streams. For example, at times the ambient wet bulb temperature may be higher than the inlet temperature of the process stream. In this case, there would be no potential for favorable heat transfer with the process stream. There may also be times when it would be desirable to use more than one indirect evaporative cooler in succession. This concept is referred to as "staging" and is covered in more detail in Section 3.4. In this section, only one IEC with a common source will be considered and will be referred to as a "single-stage IEC". Figure 3.3.1 illustrates such an IEC with a common air source (state 1) and a fraction of the inlet air taken off before the heat exchanger for use as the wet stream.

Equations describing the performance of an IEC start with the definition of the effectiveness of a sensible heat exchanger and a direct evaporative cooler:

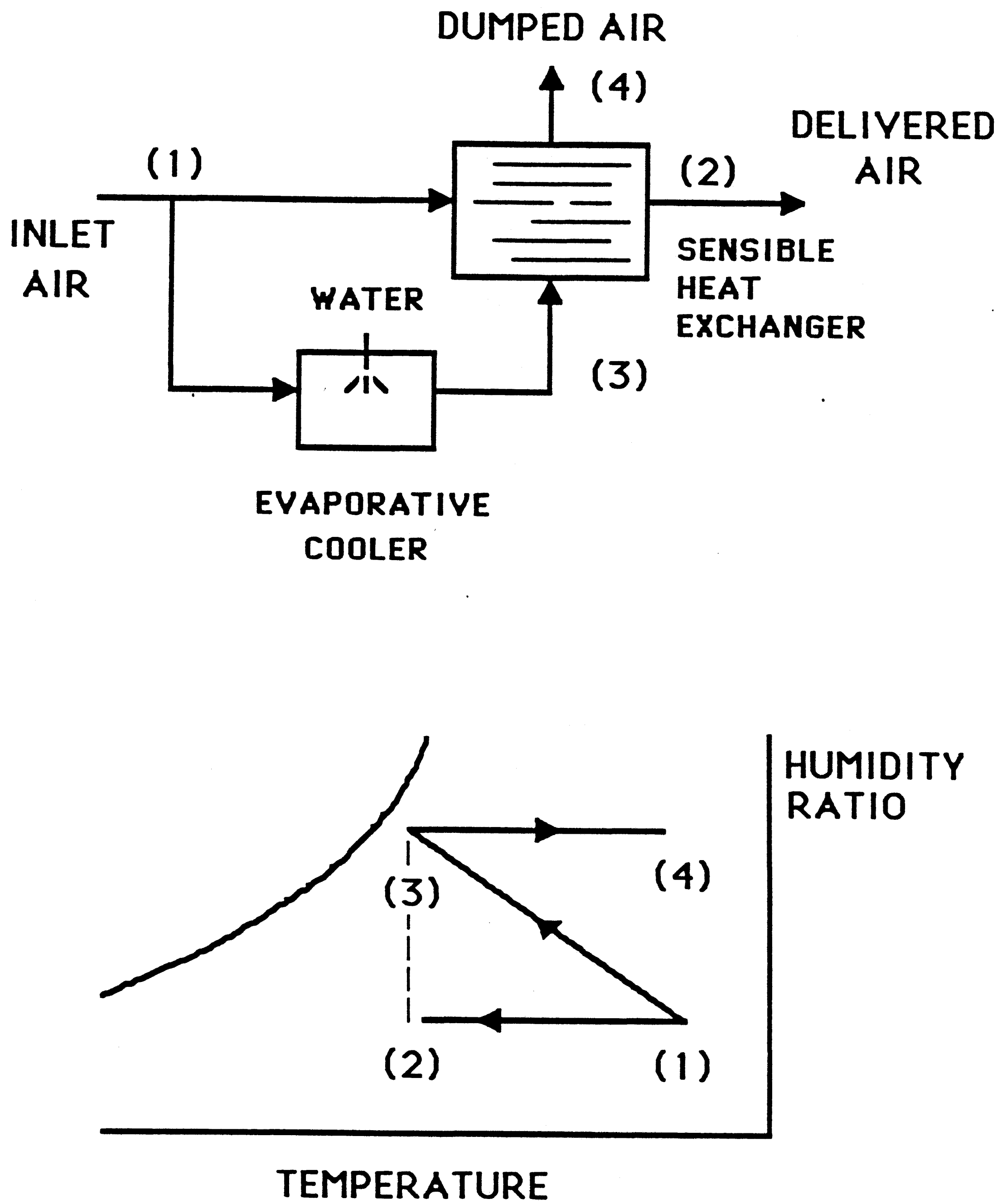

Figure 3.3.1 Schematic diagram and process representation of a single stage indirect evaporative cooler

$$\varepsilon_{HX} = \frac{q}{q_{max}} = \frac{C_{proc}*(T_1 - T_2)}{C_{min}*(T_1 - T_3)} \tag{3.3.1}$$

$$\varepsilon_{DEC} = \frac{T_1 - T_3}{T_1 - T_{wb}} \tag{3.3.2}$$

The effectiveness of a sensible heat exchanger compares the actual heat transfer rate in a heat exchange process to the maximum possible heat transfer rate. The maximum heat transfer rate would be achieved if the minimum heat capacity rate flow stream ($\dot{m}*Cp|min$) experienced the maximum possible temperature change and exited at the inlet temperature of the opposite flow stream.

The effectiveness of a single-stage IEC is defined as the ratio of the actual heat transfer rate from the process flow stream to the maximum possible heat transfer rate from the process stream. The maximum heat transfer rate would be realized if the process stream were cooled all the way to the wet bulb temperature of the wet stream.

$$\varepsilon_{IEC} \triangleq \left.\frac{q}{q_{max}}\right|_{\substack{\text{process}\\ \text{stream}}} = \frac{T_1 - T_2}{T_1 - T_{wb}} \tag{3.3.3}$$

In terms of Eqs. (3.3.1) and (3.3.2), the effectiveness of the IEC may also be written as:

$$\varepsilon_{IEC} = \varepsilon_{HX}*\varepsilon_{DEC}*\frac{C_{min}}{C_{proc}} \tag{3.3.4}$$

Equations (3.3.3) and (3.3.4) are only valid when the inlet air to the heat exchanger and the evaporative cooler are from a common source.

Assuming that there is equal pressure drop across both sides of the IEC, an energy operating cost may be calculated for the single-stage IEC from standard fan laws as:

$$\dot{w} = (\dot{m}_{delivered} + \dot{m}_{dump}) * \frac{\Delta p}{\rho} \tag{3.3.5}$$

Δp is the pressure drop across the heat exchanger and ρ is the density of the air streams. Written in terms of the cost per delivered mass flow rate, Eq. (3.3.5) becomes:

$$\frac{\text{Cost}}{\dot{m}_{del}} = (\frac{\Delta p}{\rho}) * \frac{1.0}{F} \tag{3.3.6}$$

Here a new variable, F, has been introduced to better define what portion of the inlet air to the IEC is being processed and delivered to the building zone. In terms of inlet air, delivered air and dumped air, F is defined as:

$$F \triangleq \frac{\dot{m}_{delivered}}{\dot{m}_{inlet}} = \frac{\dot{m}_{delivered}}{\dot{m}_{delivered} + \dot{m}_{dump}} \tag{3.3.7}$$

The benefit derived from the single stage IEC may also be calculated as:

$$\frac{\text{Benefit}}{\dot{m}_{del}} = \varepsilon_{IEC}*c_p*\Delta T_{max} \tag{3.3.8}$$

Replacing ε_{IEC} with Eq. (3.3.4) yields:

$$\frac{\text{Benefit}}{\dot{m}_{del}} = \varepsilon_{HX} * \frac{\dot{m}_{min}}{\dot{m}_{del}} * c_p*\Delta T_{max}*\varepsilon_{DEC} \tag{3.3.9}$$

where $\Delta Tmax$ is the difference between the dry and wet bulb temperature of the inlet air and $\dot{m}_{min}$ is the minimum mass flow rate through the heat exchanger.

A schematic of both the cost and benefit due to a single stage IEC as a function of the fraction delivered is shown in Fig. 3.3.2. The graph of the benefit is zero at a fraction delivered of 1.0 since the flow rate through the wet side of the heat exchanger is zero. The graph of the cost is infinite at a $F = 0$ since the flow through the wet side of the heat exchanger is now infinite.

The Coefficient of Performance (COP) is defined as the benefit derived from a system divided by the cost of obtaining that benefit. In the case of a single-stage IEC, COP can be obtained by dividing Eq. (3.3.9) by Eq. (3.3.6).

$$\text{COP} = F*\varepsilon_{HX} * \frac{\dot{m}_{min}}{\dot{m}_{del}} *c_p*\varepsilon_{DEC}*\Delta T_{max} * \frac{\rho}{\Delta p} \tag{3.3.10}$$

Equation (3.3.10) may be simplified by grouping together the constants that are not related to the mass flow rates through the IEC. This yields:

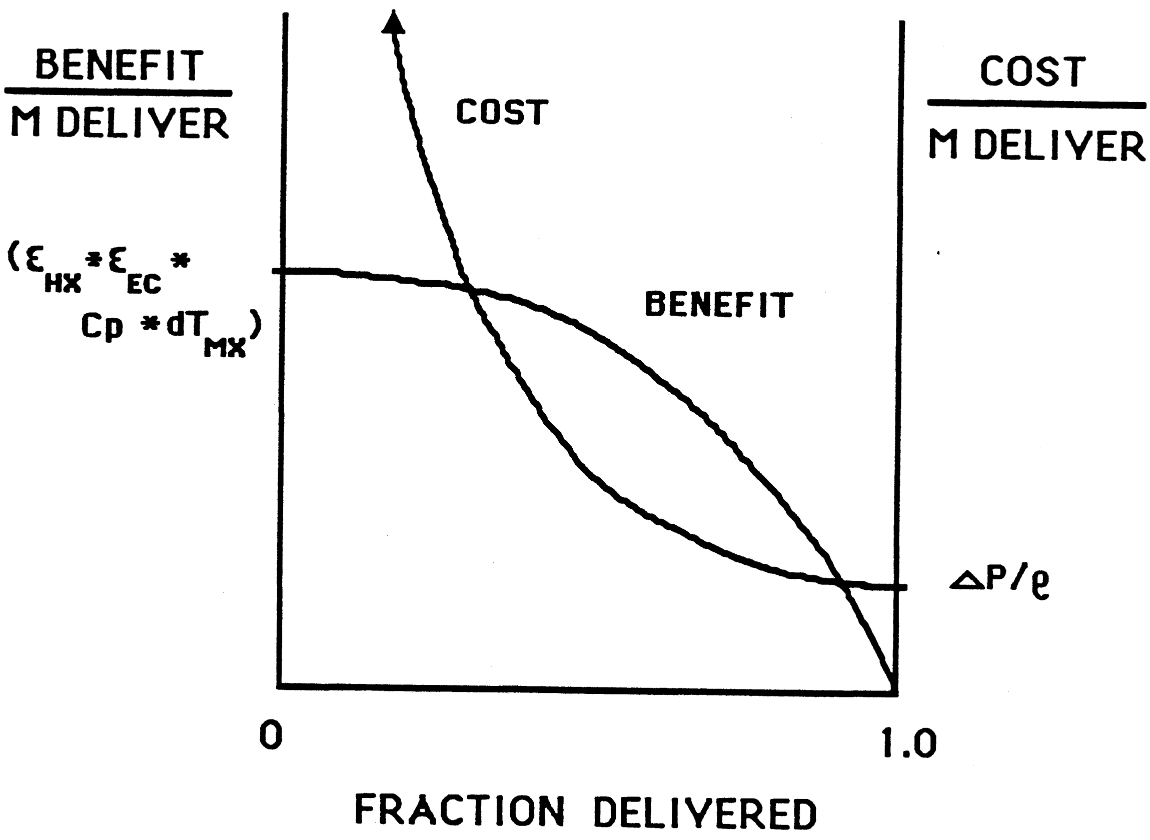

Figure 3.3.2 Illustration of costs and benefits associated with a single-stage indirect evaporative cooler

$$COP = F*\varepsilon_{HX} * \frac{\dot{m}_{min}}{\dot{m}_{del}} * k \qquad (3.3.11)$$

where
$$k = c_p*\varepsilon_{DEC}*\Delta T_{max} * \frac{\rho}{\Delta p} \qquad (3.3.12)$$

The constant, k, of Eq. (3.3.12) is a dimensionless quantity that is a function of the air stream specific heat, the effectiveness of the adiabatic saturation process, the maximum possible temperature difference across the heat exchanger and the pressure drop across the heat exchanger. The maximum temperature difference term, ΔTmax, characterizes where the inlet air lies on the psychrometric chart. Obviously, the hotter and drier the inlet state, the larger both ΔTmax and the COP will be. The COP is also directly proportional to the evaporative cooler effectiveness and is inversely proportional to the pressure drop.

A graph of COP/k vs fraction delivered, F, is shown in Fig. 3.3.3 for varying heat exchanger NTU. The COP is zero at F = 0 and 1 due to infinite costs at F = 0 and zero benefits at F = 1. Further, an optimum COP is seen to exist at a fraction delivered of 0.5 for all values of NTU.

Using the optimum fraction delivered value of 0.5, a heat exchanger NTU of 3.0 and an evaporative cooler effectiveness of 0.8, lines of constant COP can be mapped out on a psychrometric plane. Such a plot is shown in Fig. 3.3.4 for a standard pressure drop of 125 Pa (0.5 in. water). Lines of constant COP have the same shape as

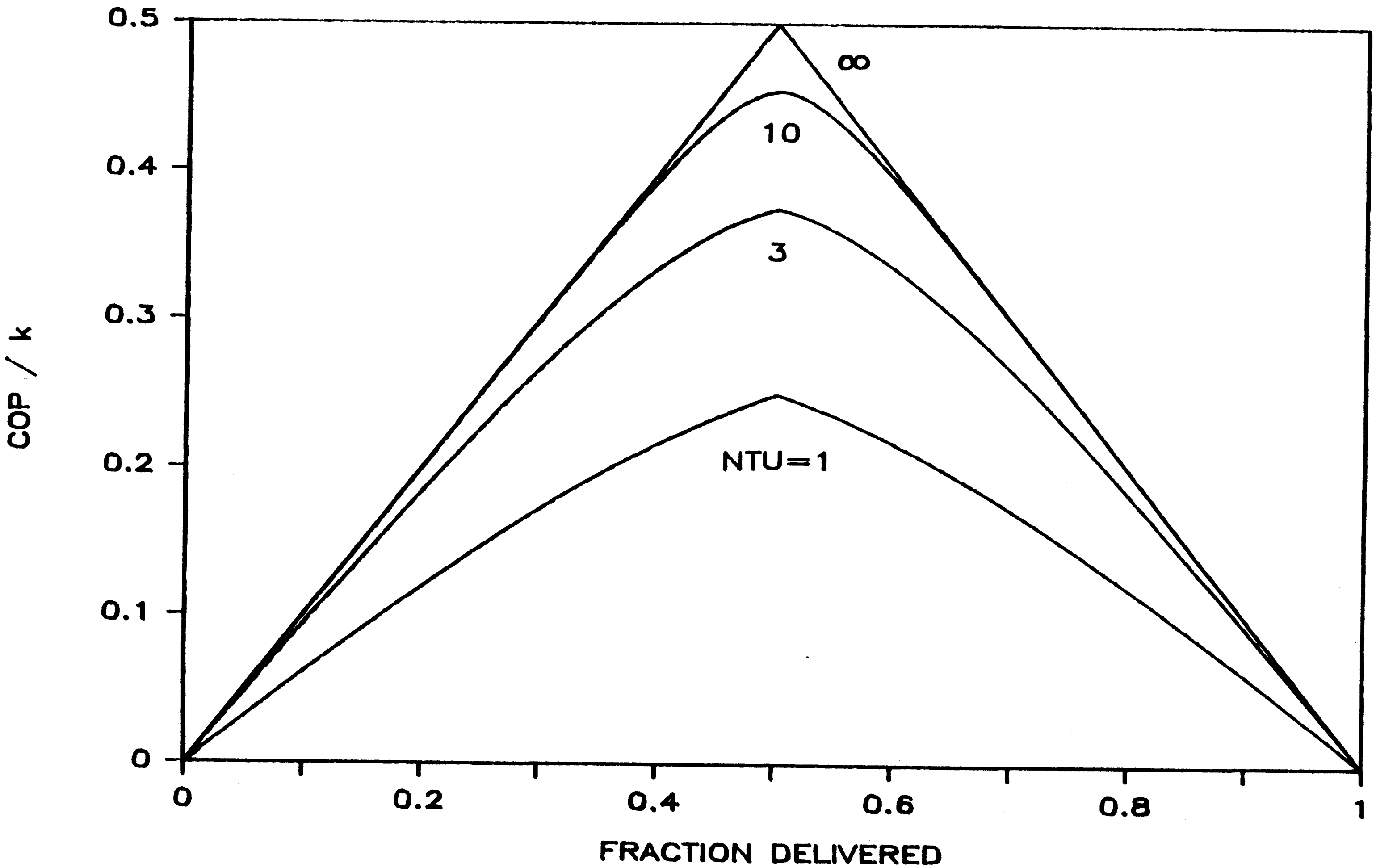

Figure 3.3.3 Single-stage indirect evaporative cooler coefficient of performance vs fraction delivered

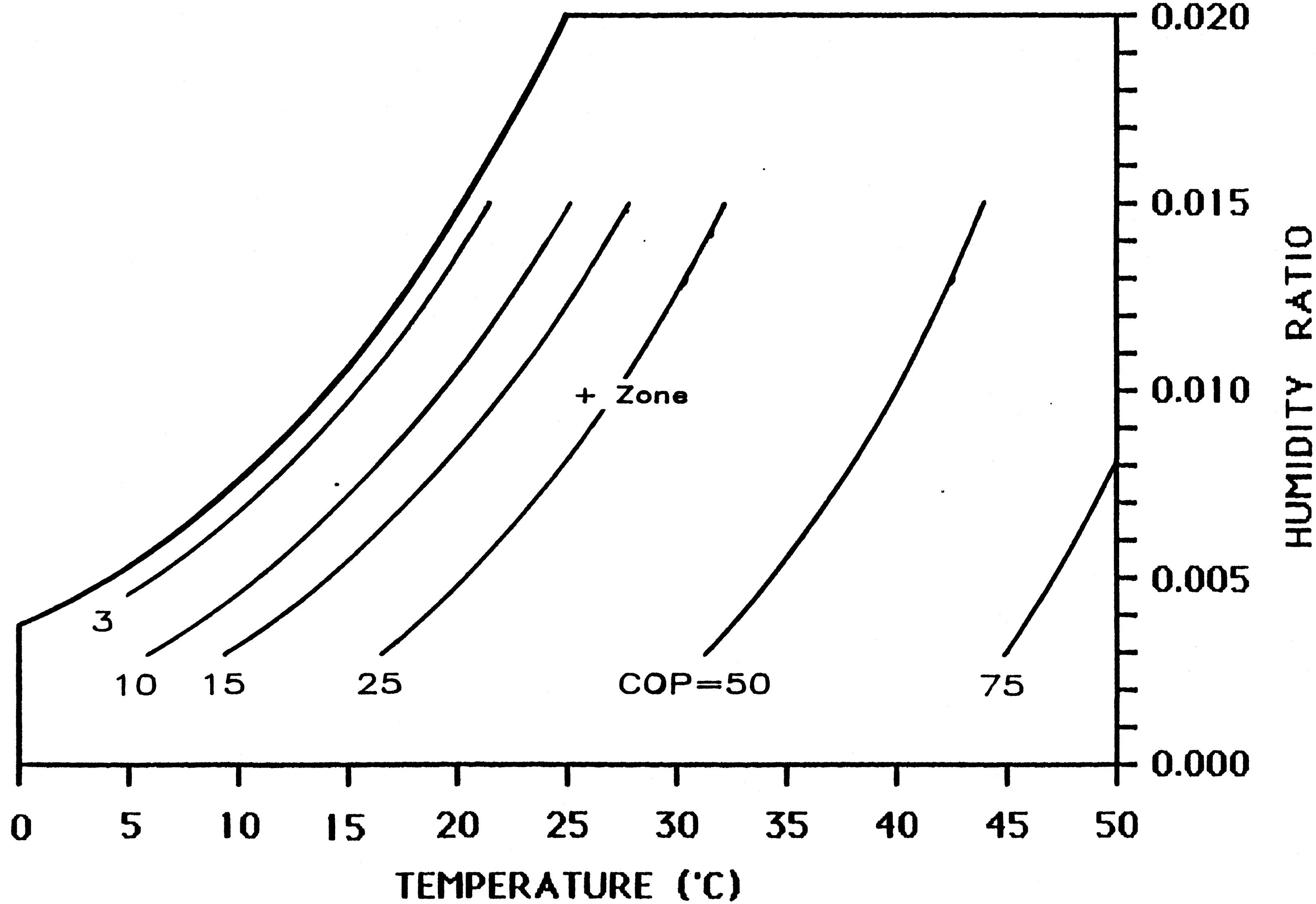

Figure 3.3.4 Lines of constant coefficient of performance for single-stage indirect evaporative cooler. $\varepsilon_{ec}=0.8$ NTU=3.0, fraction delivered=0.5, pressure drop=125 Pa

the saturation curve. In the range of temperature and humidity ratios seen in air-conditioning operations, the COP's range from 15 to 50.

To further investigate the utility of IEC's, two performance parameters are defined as follows:

$$\varepsilon_T = \frac{T_{inlet} - T_{outlet}}{T_{inlet} - T_{dew\ pt.}} \tag{3.3.13}$$

$$\varepsilon_{cc} = \frac{\dot{m}_{delivered}*(T_{inlet} - T_{outlet})}{\dot{m}_{inlet}*(T_{inlet} - T_{dew\ pt.})} = F*\varepsilon_T \tag{3.3.14}$$

The temperature effectiveness, Eq. (3.3.13), provides a measure of how close the inlet air can be cooled towards the inlet air dew point temperature. This value ranges from 0 to 1. The cooling capacity effectiveness, Eq. (3.3.14), provides a measure of how much of the inlet air can be cooled and to what extent it can be cooled. The cooling capacity effectiveness is therefore an energy effectiveness. This effectiveness also ranges from 0 to 1 where the maximum value of 1 corresponds to cooling all of the air all of the way to its dew point temperature. The air flow through an IEC can only approach the wet bulb temperature so the above effectivenesses will always be less then 1.

Graphs of temperature and cooling capacity effectiveness for variable fraction delivered values are shown in Figs. 3.3.5 through 3.3.8 for a constant inlet state of 30°C and 0.009 kg/kg absolute humidity ratio. Figures 3.3.5 and 3.3.6 are for a constant evapora-

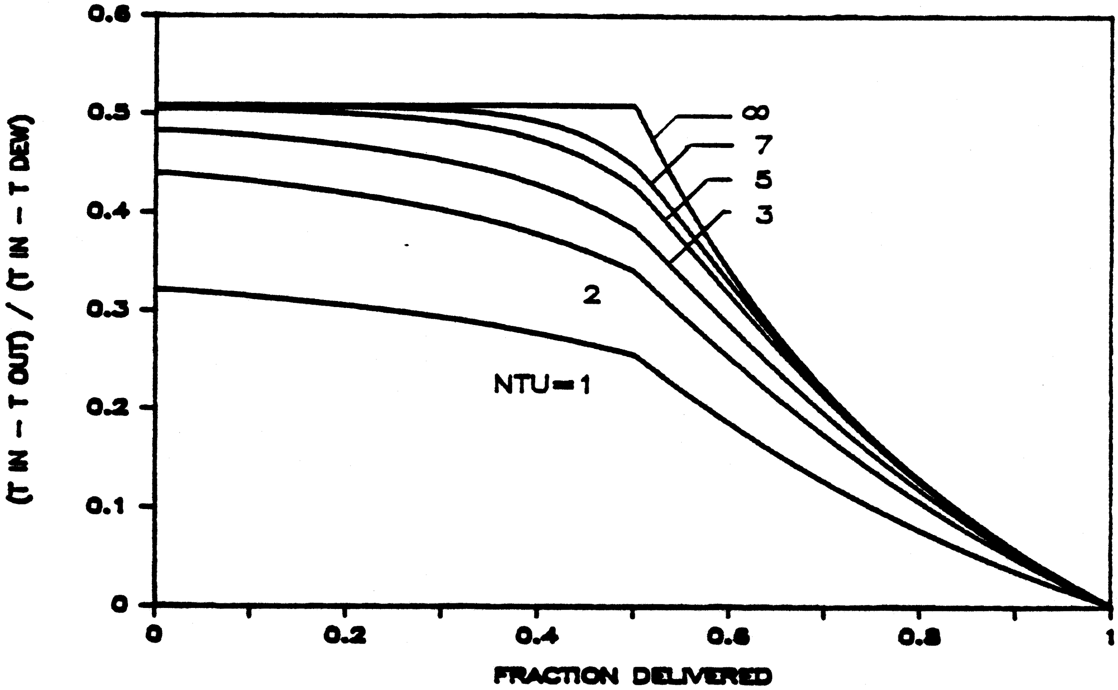

Figure 3.3.5 Temperature effectiveness vs fraction delivered for single-stage IEC. ec=0.8, T inlet=30C, W inlet=0.009 kg/kg

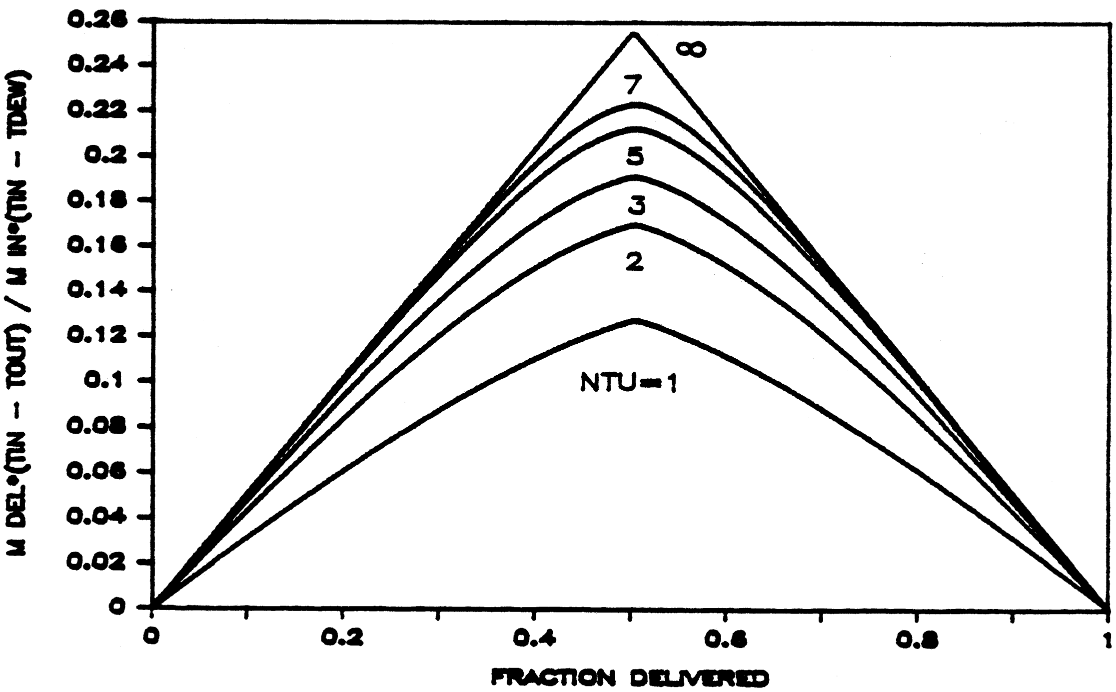

Figure 3.3.6 Cooling capacity effectiveness vs fraction delivered for single-stage IEC. ec=0.8, T inlet=30C, W inlet=0.009 kg/kg

tive cooler effectiveness of 0.8 and heat exchanger sizes ranging from 1 to infinite NTU. Figure 3.3.5 illustrates that the best and worst temperature effectivenesses occur at fractions delivered of 0 and 1 respectively. At F = 0, the heat exchanger effectiveness is maximum. At F = 1, no flow is diverted to the wet stream side of the heat exchanger and hence the heat exchanger has no cold stream heat sink. Figure 3.3.6, the graph of cooling capacity effectiveness, is seen to be symmetric about the optimum operating F of 0.5. An optimum cooling capacity effectiveness exists since the relative mass flow ratio, $\dot{m}_{delvr}/\dot{m}_{inlet}$, is zero at F = 0 and the temperature effectiveness is zero at F = 1.

Figures 3.3.7 and 3.3.8 show how both temperature and cooling capacity effectiveness vary with different evaporative cooler effectiveness for a given inlet state and for infinite NTU. It is seen that both temperature and cooling capacity effectiveness increase in proportion with the increase in the evaporative cooler effectiveness. This is true for two reasons. First, the inlet air temperature on the wet side of the heat exchanger is a linear function of the evaporative cooler effectiveness and second, the heat transfer rate across the heat exchanger is a linear function of the maximum temperature difference across the two flow streams. To indicate how the performance of a single-stage IEC varies as the inlet state changes, it is instructive to turn to the psychrometric chart. Figure 3.3.9 is a plot of constant air outlet temperatures for an IEC sized with a heat exchanger NTU of 3, an evaporative cooler effectiveness of 0.8 and a

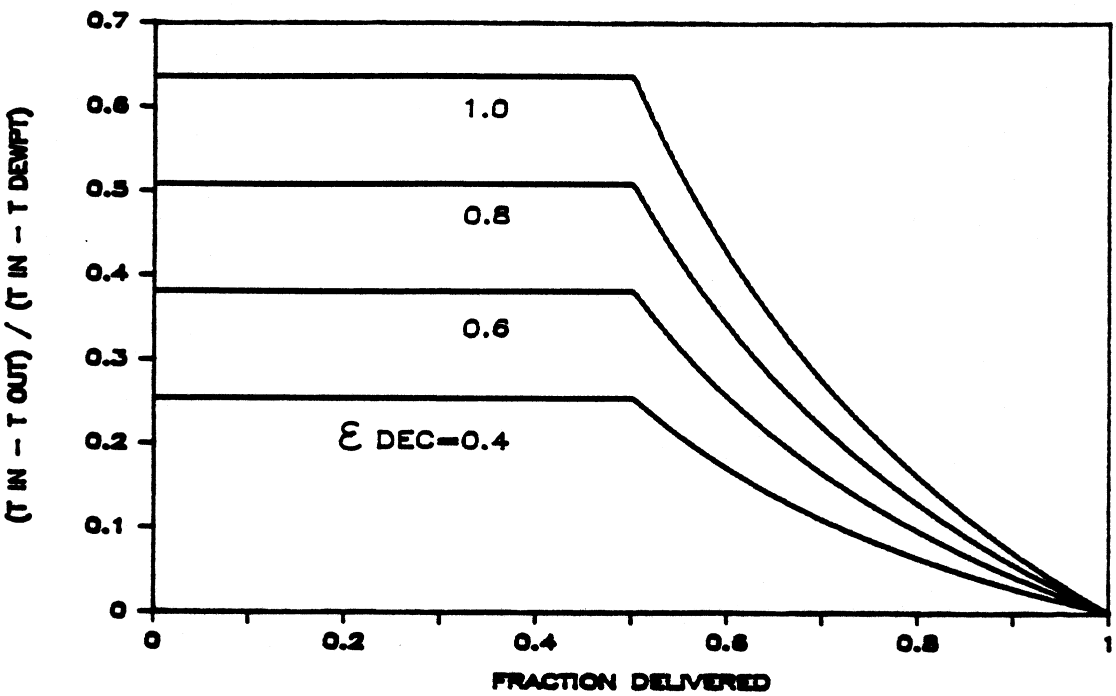

Figure 3.3.7 Temperature effectiveness vs fraction delivered for single-stage IEC, Infinite NTU, T inlet=30C, W inlet=0.009 kg/kg

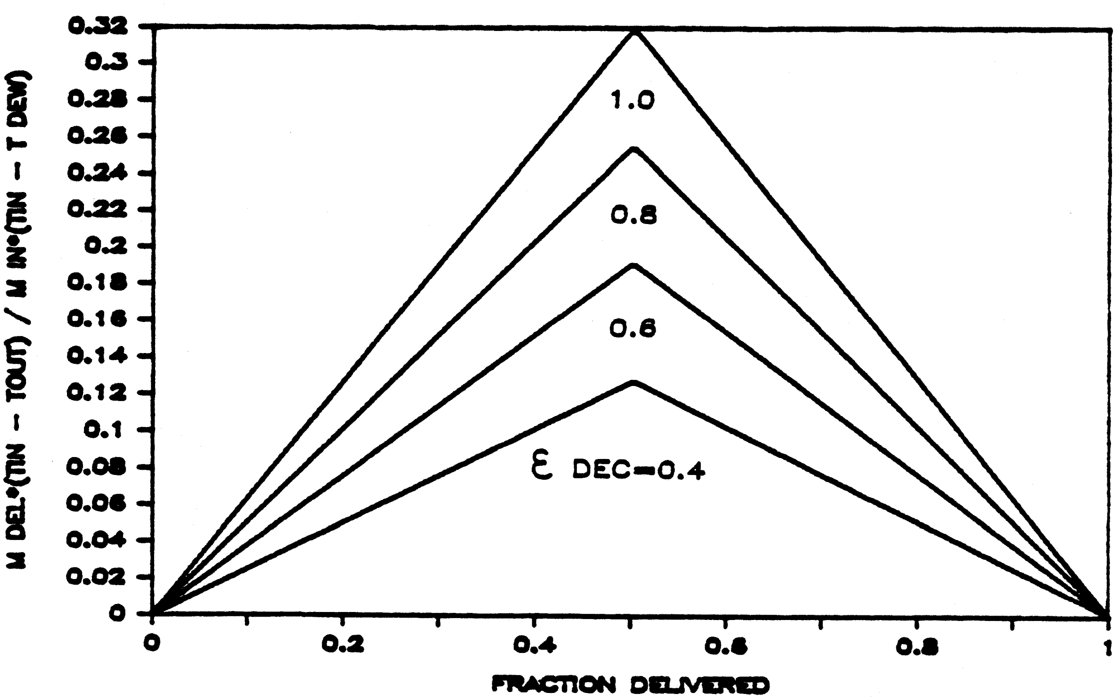

Figure 3.3.8 Cooling Capacity Effectiveness vs fraction delivered for single-stage IEC. Infinite NTU, T inlet=30C, W inlet=0.009 kg/kg

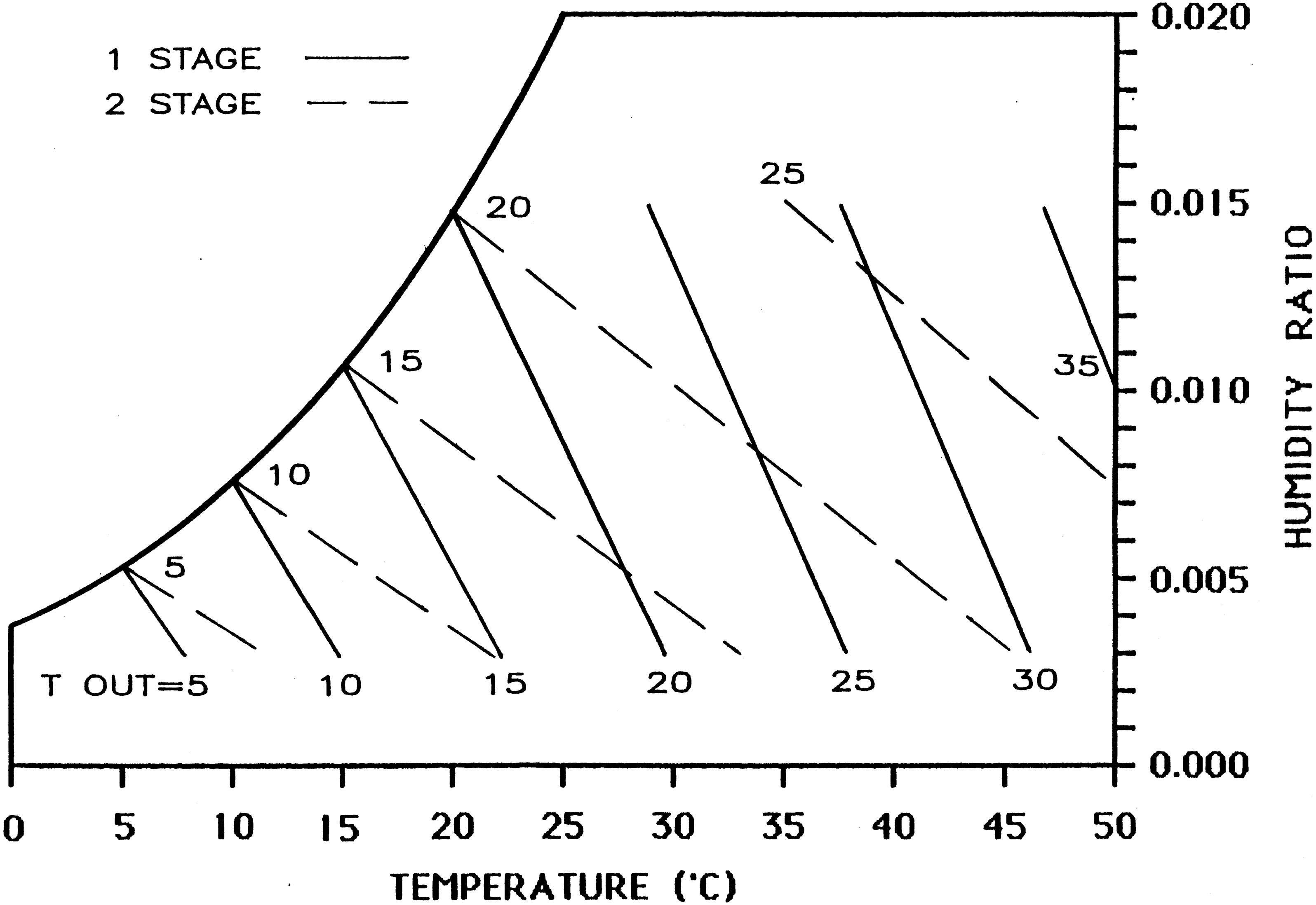

Figure 3.3.9 Lines of constant outlet temperature for single-stage and two-stage indirect evaporative cooler. ec=0.8, NTU=3.0, fraction split per stage=0.5

constant fraction delivered value of 0.5. Any combination of temperature and humidity ratio that intersects one of the solid lines results in an exiting air temperature as indicated. As an example, air entering the single stage cooler at 25°C and 0.009 kg/kg would exit at a temperature of 20°C. These lines of constant outlet temperature are straight on a psychrometric chart and resemble constant wet bulb temperature lines. All of these constant outlet temperature lines intercept the saturation curve at the value of the constant temperature line. As expected, when following along a constant dry bulb line to regions of lower absolute humidity ratio, the outlet temperature from the IEC decreases. Moving to higher dry bulb temperatures along a given humidity ratio produces higher temperatures at the exit of the IEC, however the temperature drop across the IEC is larger at warmer inlet states. In other words, the temperature effectiveness of a single-stage IEC increases as one moves to dryer and warmer states on the psychrometric chart.

Section 3.4: Multi-Staged Indirect Evaporative Coolers

A single-stage indirect evaporative cooler, as stated in Section 3.3, is limited in its ability to cool air below the inlet air wet bulb temperature. Because the wet, cool stream can be cooled no further than its wet bulb temperature in the evaporative cooling process, the delivered process air, likewise, can at best be cooled to that wet bulb temperature. In certain instances, however, it may be desirable to chill the process air below its wet bulb temperature.

Staging a succession of indirect evaporative coolers in a series configuration has the potential for cooling the inlet air to near its dew point temperature.

A schematic of such a system is illustrated in Fig. 3.4.1 along with the process representation on a psychrometric chart. Each individual stage behaves as a single-stage IEC as described in Section 3.3. The overall performance of the multiple-stage IEC is dependent on the effectiveness of each individual evaporative cooling and heat exchange process. In the limit, for an infinite number of stages, the air introduced at the inlet to the first stage can be cooled to its dew point temperature with no addition of moisture to the delivered process stream.

As in the case of a single-stage indirect evaporative cooler, again there are limitations to this process. To operate any one of the above stages at its optimum cooling capacity and COP, half of the air delivered from the last stage must be used as the wet stream cold sink. The overall fraction delivered for an n-staged IEC is therefore:

$$F_{n\text{-staged IEC}} = \left(\frac{1}{2}\right)^n \qquad (3.4.1)$$

If two stages of cooling were used at their optimum operating conditions, for example, only 25% of the inlet air to the first stage would ultimately be delivered as cooled process air at the exit of the second stage. Sacrificing a large portion of the inlet process

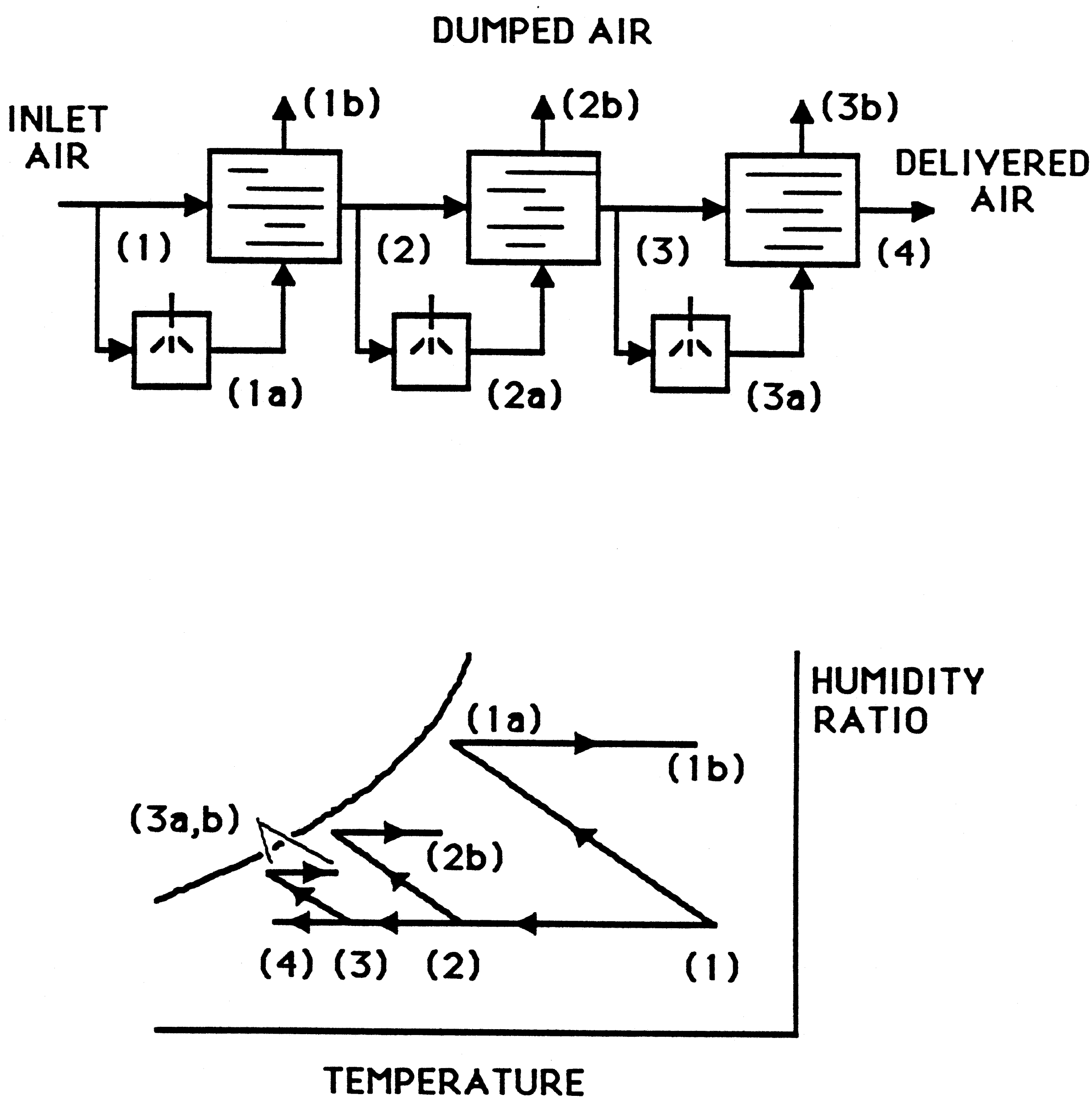

Figure 3.4.1 Schematic diagram and process representation of a three-stage indirect evaporative cooler

stream may be an expensive proposition. Depending on the origin of the air, the added advantage of the extra cooling from multiple stages may be offset by the large loss of inlet air to the ambient.

To further quantify the advantages and disadvantages of a multi-staged IEC, the temperature and cooling capacity effectivenesses defined in Section 3.3 will be used. Figures 3.4.2 and 3.4.3 are graphs of these effectivenesses for up to five stages of chilling for a constant inlet state of 30°C and 0.009 kg/kg absolute humidity ratio. These figures were generated assuming an evaporative cooler effectiveness of 0.8 and heat exchanger NTU values ranging from 1 to infinity.

Several points can be drawn from these two plots. First, it is observed that the temperature effectiveness does indeed increase toward 1 as the number of stages increase. Also, it is seen that the largest increase in temperature effectiveness occurs in going from one to two stages of cooling. The additional benefits of further staging diminishes greatly after the second stage of cooling. The cooling capacity effectiveness continually decreases despite the increasing cooling effect brought about by additional cooling stages. The drastic decrease in the delivered air flow rate dominates the cooling capacity effectiveness.

Practically speaking, the maximum number of cooling stages would probably be 2. The equipment size and first cost would become excessive as the number of stages increased beyond two stages.

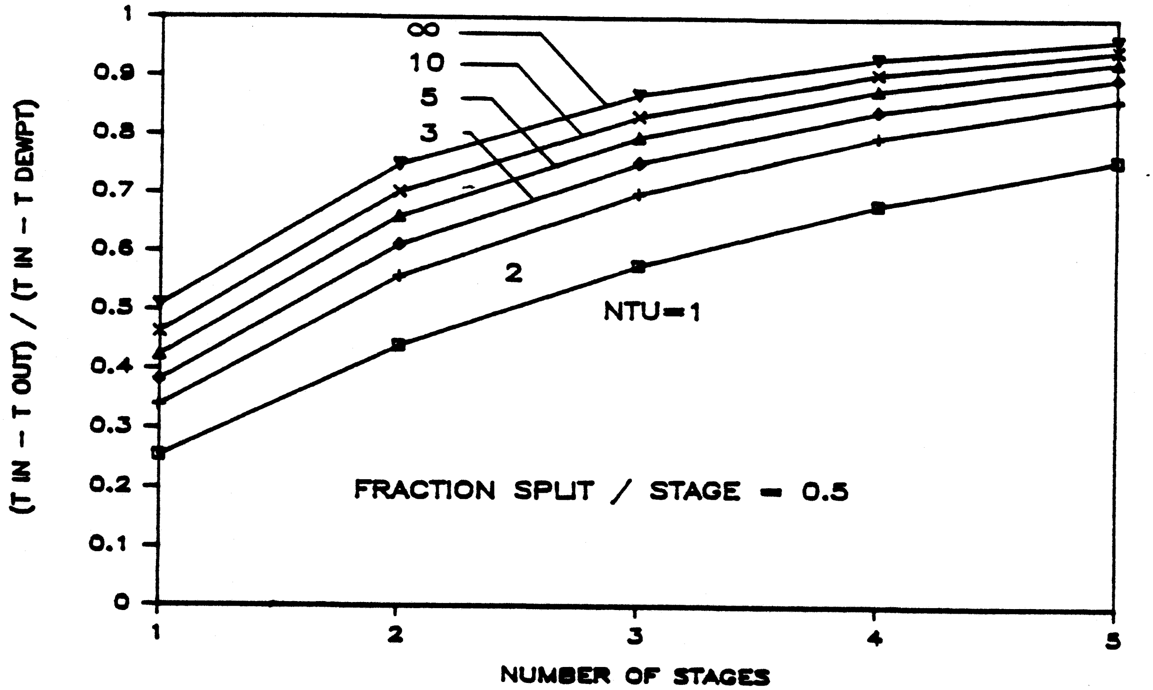

Figure 3.4.2 Temperature effectiveness for multi-staged indirect evaporative cooler. ec=0.8, T inlet=30C, W inlet=0.009kg/kg

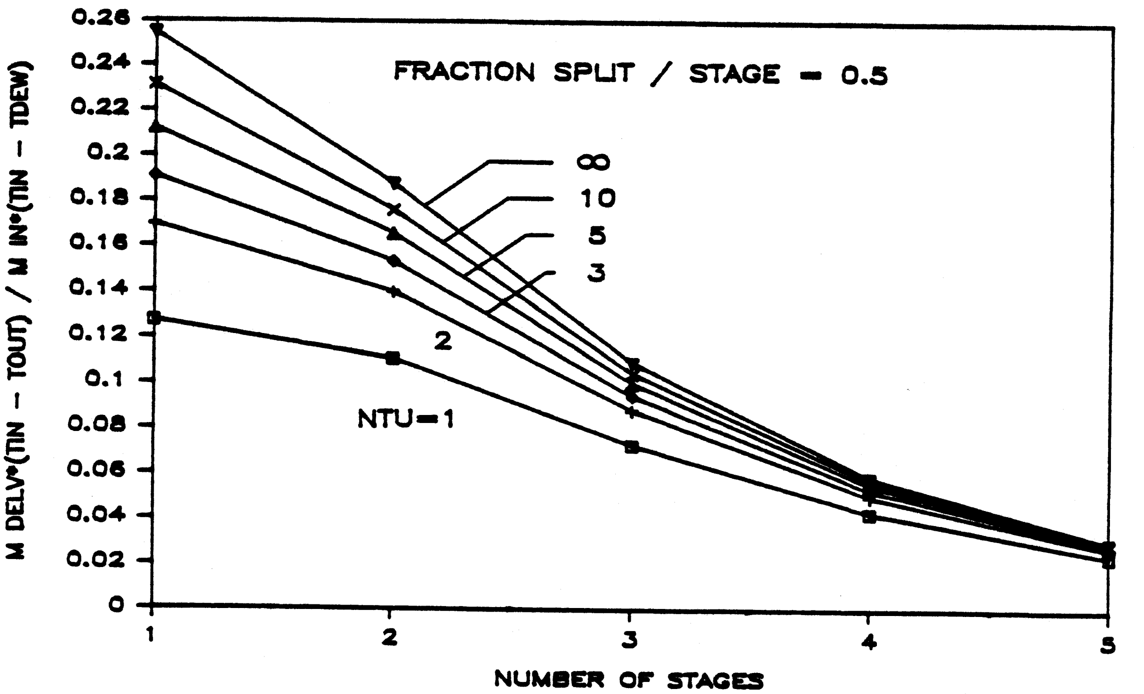

Figure 3.4.3 Cooling capacity effectiveness for multi-staged indirect evaporative cooler. ec=0.8, T inlet=30C, W inlet=0.009 kg/kg

To indicate how the performance of a two-stage IEC varies with changes in the inlet air state, lines of constant air outlet temperature are plotted on the psychrometric coordinates of Fig. 3.3.9. The trends observed in this plot are the same as those for a single-stage IEC. Performance increases as the inlet air becomes drier and warmer. It is also observed that the lines of constant outlet temperature for a 2 stage IEC are less steep than those for a single-stage IEC. If more than two stages of cooling are used, these lines would become even more flat until, theoretically, when infinite stages are used, the constant outlet temperature lines would be horizontal and numerically equal to the dew point temperature of the inlet air.

Lines of constant COP may also be plotted on a psychrometric chart for a two-stage IEC. Such a plot is shown in Fig. 3.4.4 for a cooler using the optimum fraction delivered of 0.5 per stage, a pressure drop of 125 Pa and a heat exchanger NTU of 3.0. These lines resemble the constant COP lines for a single-stage IEC and follow the shape of the saturation line. In the region of the psychrometric chart of interest for air conditioning practice, the COP's for the two-stage IEC are approximately half of those for the single-stage IEC.

Section 3.5: Heat Exchanger/Evaporative Cooler

Another air cooling device similar to a single-stage IEC may be developed by combining evaporative cooling with a single sensible

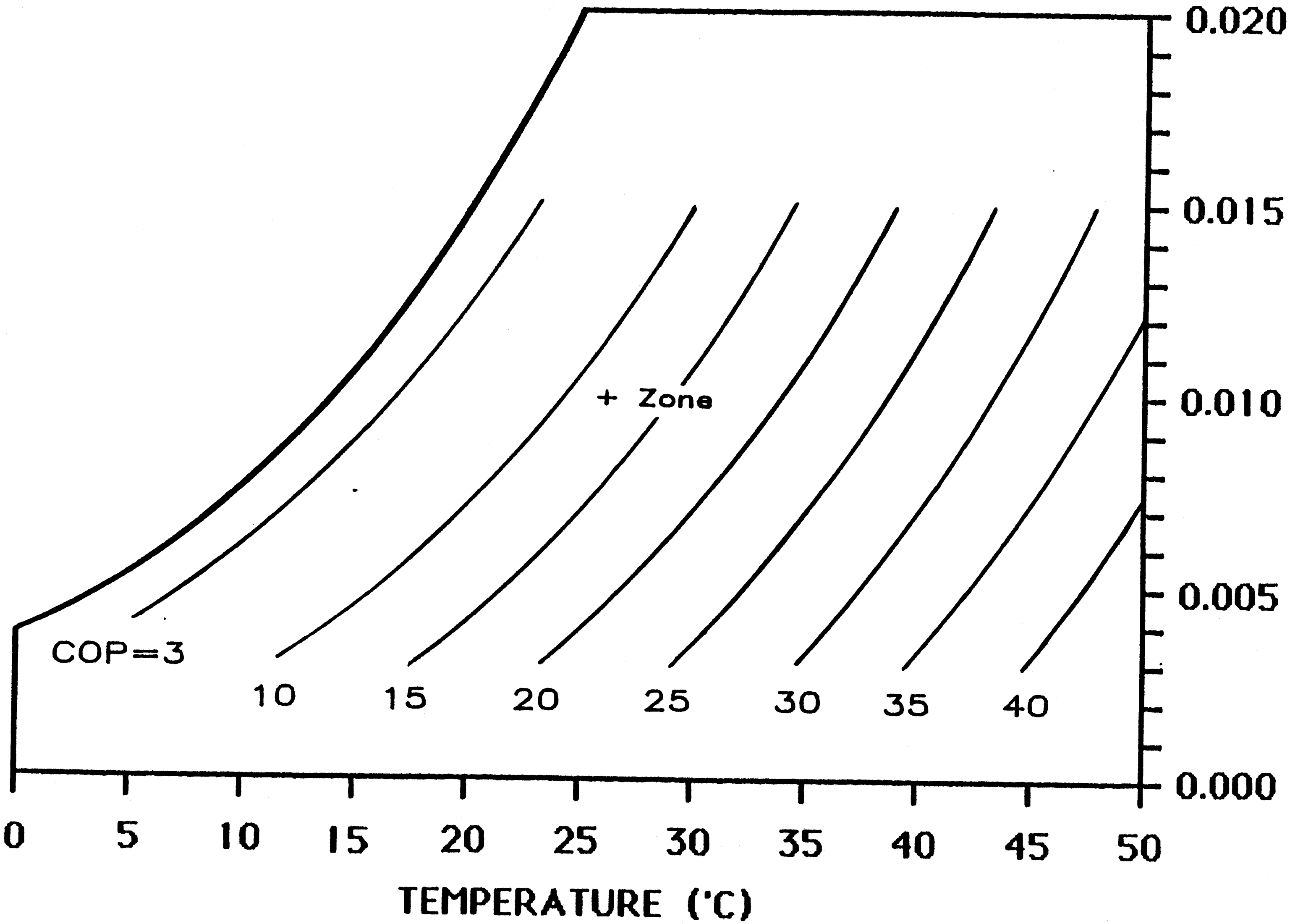

Figure 3.4.4 Lines of constant COP for two-stage IEC. ec=0.8, NTU=3.0, pressure drop=125 Pa

heat exchanger. Such a device is schematically represented in Fig. 3.5.1 and will be referred to as a Heat Exchanger/Evaporative Cooler (HX/EC). The only difference between this air cooler and a single-stage IEC is the location of where the inlet process air stream is split. With a single-stage IEC, splitting occurs before the process stream is sensibly cooled. In the cooling unit of Fig. 3.5.1, air is diverted after the process stream exits the heat exchanger.

The following equations may be written to describe how this system works.

$$\varepsilon_{HX} = \frac{q}{q_{max}} = \frac{C_{inlet}*(T_1 - T_2)}{C_{min}*(T_1 - T_3)} \tag{3.5.1}$$

$$\varepsilon_{DEC} = \frac{T_2 - T_3}{T_2 - T_{wb@2}} \tag{3.5.2}$$

Equations (3.5.1) and (3.5.2) are the definitions of the effectiveness for a heat exchanger and a direct evaporative cooler. For a given fraction delivered, the relative flow rates, capacitance rates and component effectivenesses are all known values. The temperature of the air exiting the heat exchanger, T_2, and the evaporative cooler, T_3, are unknown. Eliminating T_3 from the two equations yields:

$$\begin{aligned} &C_{min}*\varepsilon_{DEC}*\varepsilon_{HX}*(T_2 - T_{wb@2}) \\ &\quad - (T_1 - T_2)*(C_{inlet} - \varepsilon_{HX}*C_{min}) = 0 \end{aligned} \tag{3.5.3}$$

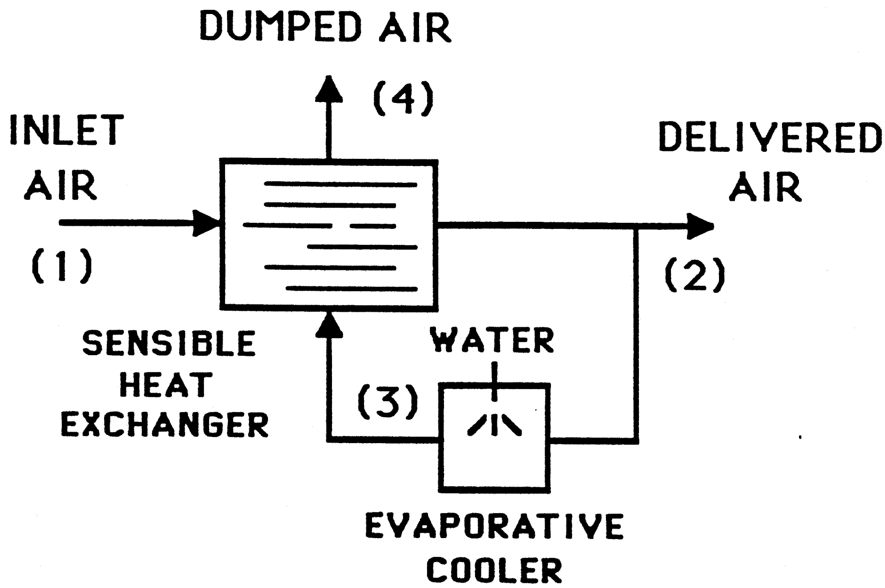

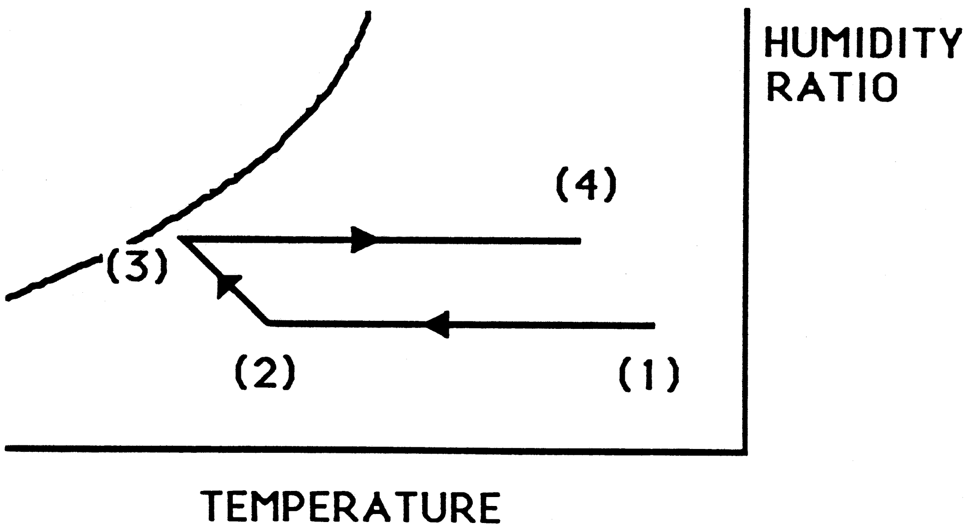

Figure 3.5.1 Schematic diagram and process representation of a heat exchanger/ evaporative cooler

The only unknowns in Eq. (3.5.3) are now the dry and wet bulb temperatures of the air exiting the sensible heat exchanger. Because there is no simple equation relating these two temperatures, Eq. (3.5.3) must be solved with a trial and success technique.

The solution of Eq. (3.5.3) is plotted in Figs. 3.5.2 and 3.5.3 in the form of temperature and cooling capacity effectivenesses. For these performance curves, a constant inlet air state of 30°C and 0.009 kg/kg absolute humidity ratio was used. The evaporative cooling effectiveness was assumed equal to 0.8 and the heat exchanger size was varied from 1 to infinite NTU.

Many observations may be drawn from these figures. First, it is possible to chill air below the inlet air wet bulb temperature without staging. In the limit of using a perfect heat exchanger, it is possible to chill the air to its dew point temperature. At this extreme condition, however, the fraction of inlet air delivered to the building zone is zero. The benefit of operating at this condition, of course, is zero as illustrated in Fig. 3.5.3. This cooler, likewise, provides zero benefit at a fraction delivered of 1.0 since at this operating point there is no temperature reducing effect. An optimum fraction delivered value therefore exists and is seen to vary from 0.4 to 0.5 for the NTU's shown.

Lines of constant COP and outlet temperature may be mapped on a psychrometric chart just as they were for the other evaporative coolers discussed in this chapter. Such a plot is shown in Fig. 3.5.4 for a cooling unit with an NTU of 3.0, an evaporative cooler

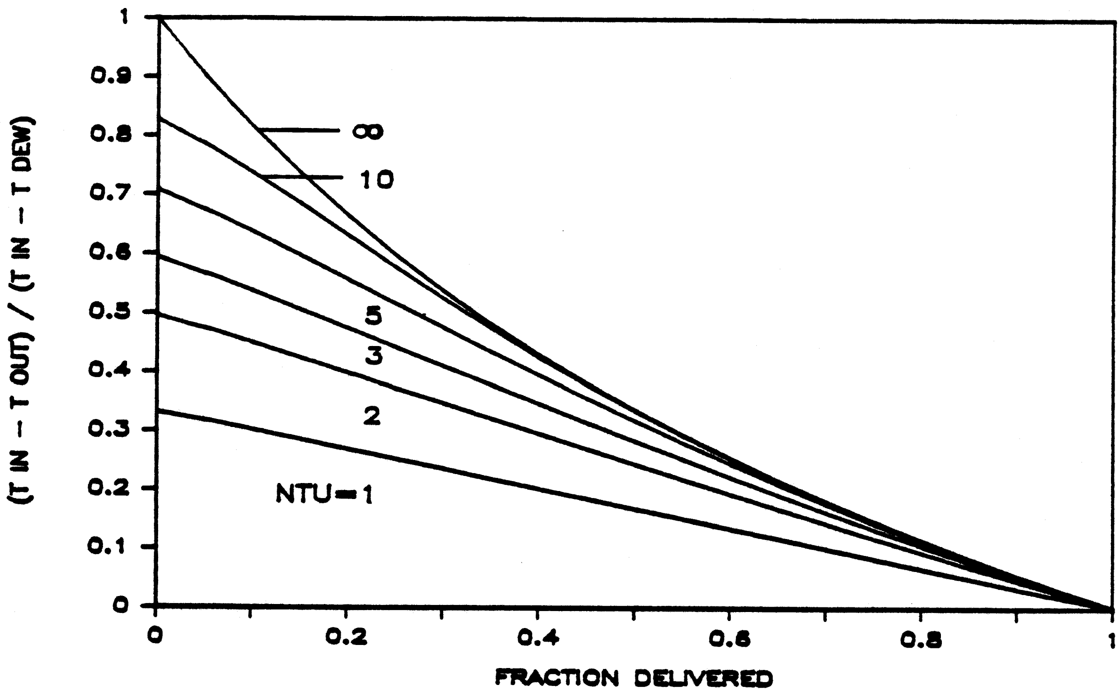

Figure 3.5.2 Temperature effectiveness vs fraction delivered for heat exchanger/ evap. cooler. ec=0.8, T inlet=30C, W inlet=0.009 kg/kg

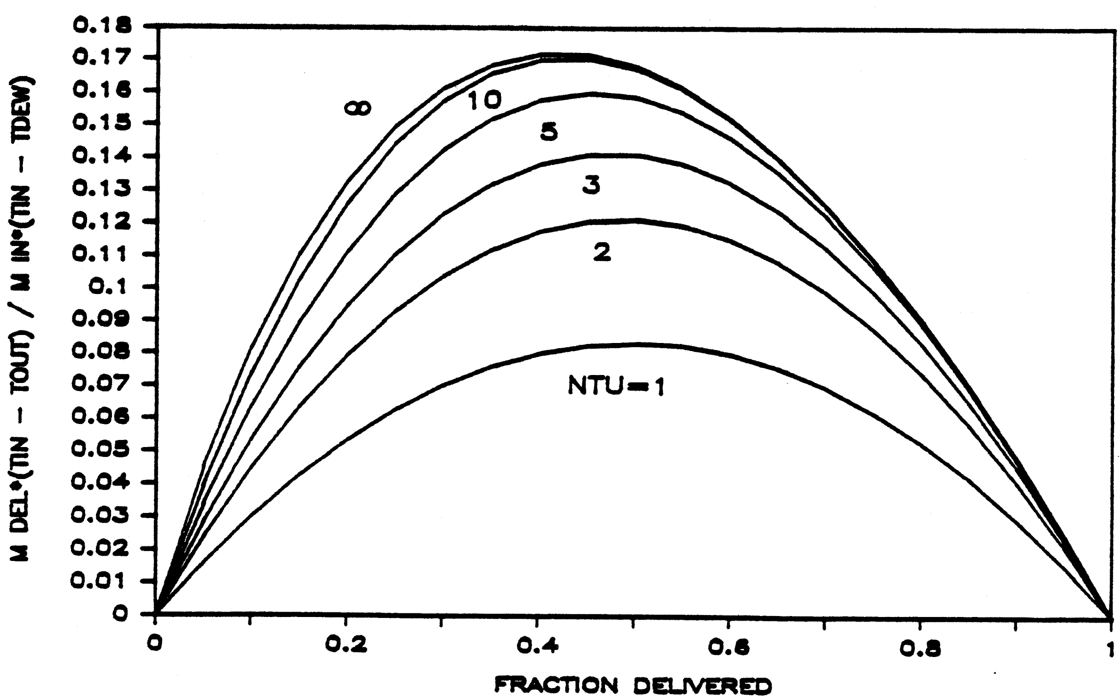

Figure 3.5.3 Cooling capacity effectiveness vs fraction delivered for heat exchanger/ evap. cooler. ec=0.8, T inlet=30C, W inlet=0.009 kg/kg

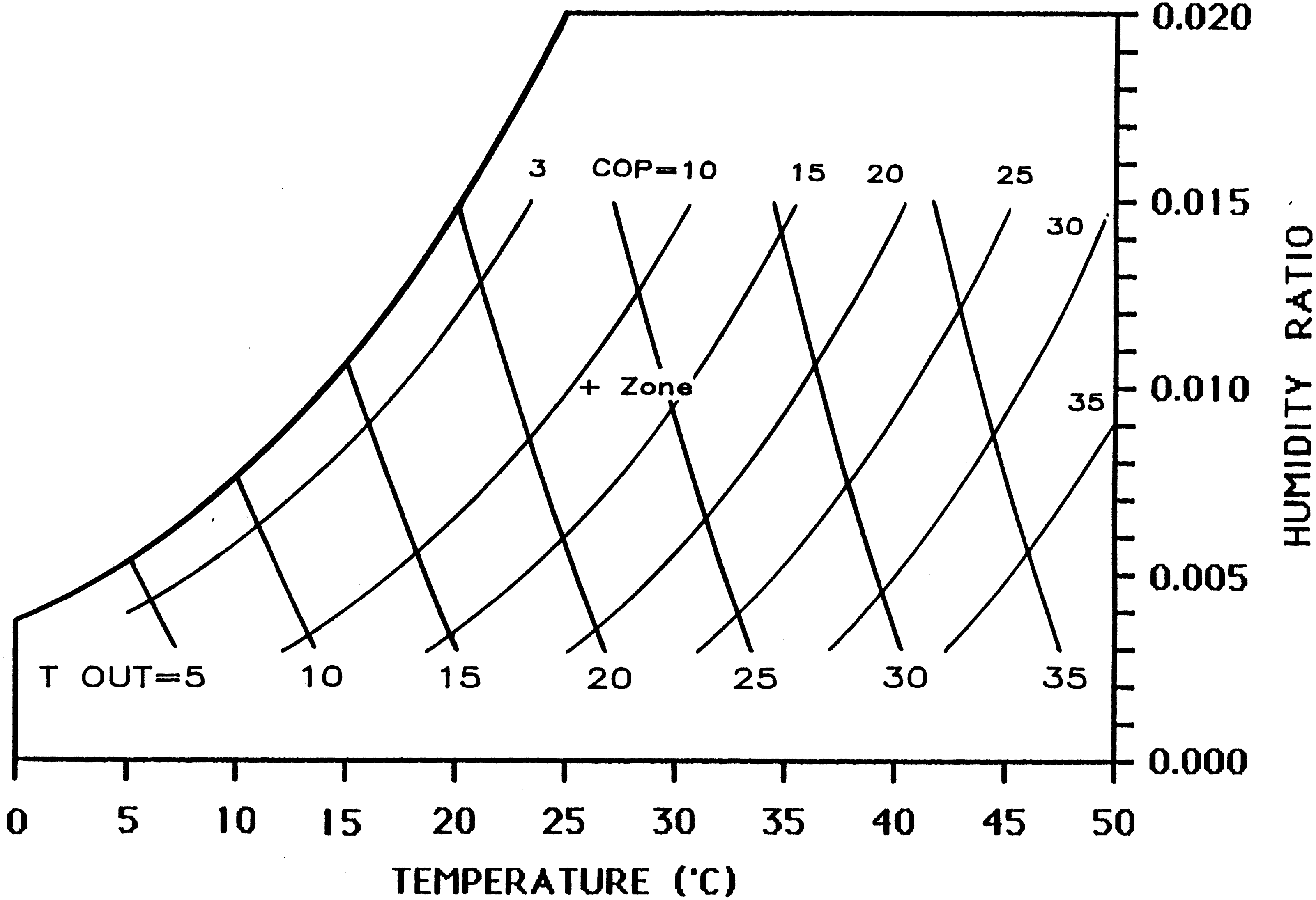

Figure 3.5.4 Lines of constant COP and outlet temperature for heat exchanger/ evap. cooler. ε_{ec}=0.8, NTU=3.0, fraction delivered=0.5

effectiveness of 0.8, a pressure drop across each component of 125 Pa and a fraction delivered of 0.5. The trends observed in this plot are the same as those for the single and multistaged evaporative coolers. The constant outlet temperature lines are nearly linear and intersect the saturation line at the temperature of the constant temperature line. At the optimum fraction delivered chosen for this plot, the constant outlet temperature lines are even more steep than those for the single-stage IEC. The constant COP lines have the same shape as the saturation curve and for a fraction delivered of 0.5 are approximately the same size as the COP's for the two-stage IEC.

It is instructive to further compare this cooling unit with the single-stage IEC of Section 3.3. The first observation is that the HX/EC can cool inlet air to a greater degree then the single-stage IEC. In their respective limits, the IEC can cool air to its wet bulb temperature, whereas the HX/EC can cool to the dew point temperature. The maximum cooling capacity for the HX/EC is approximately half of that for the single-stage IEC. It is also observed that the cooling capacity curves for the HX/EC are not symmetric about a fraction delivered of 0.5. The optimum fraction decreases toward F = 0.4 as the heat exchanger size increases. The cooling capacity curves for the IEC were symmetric about F = 0.5 regardless of the heat exchanger size. As in the case of both the single and multistaged IEC, the HX/EC unit could not be used to dehumidify the inlet process air. To meet an air conditioning load that is partly latent, this unit must be coupled to some sort of dehumidification device.

The HX/EC would appear to work well for applications where a high degree of sensible cooling is required.

Section 3.6: Cooling Tower/Heat Exchanger Air Cooler (CT/HX)

Another air cooling device can be developed by coupling a cooling tower with a sensible air/water heat exchanger. This device was first proposed and analyzed by Maclaine-cross [1985] and Kang and Maclaine-cross [1985] as a possible air chiller for use in desiccant cycles.

A system schematic and process representation of this cooler is shown in Fig. 6.1. In this process, the inlet air at state 1 is sensibly cooled to state 2 while at the same time, the chilled tower water is warmed from state W_1 to W_2. The air at state 2 is split into two streams. One is delivered as conditioned air to the building zone and the other is routed through the cooling tower. The portion of the inlet air that is channeled through the cooling tower is humidified and warmed to state 3 and then dumped to the ambient. The cooling tower receives water at state W_2 and returns it chilled to the heat exchanger at state W_1.

The model used in analyzing the coupled heat and mass transfer in the cooling tower is based on an analogy to sensible heat transfer in dry heat exchangers. This method of analyzing wet surface heat exchangers was first suggested by Maclaine-cross and Banks [1983]. A brief outline on the development of the resulting model equations

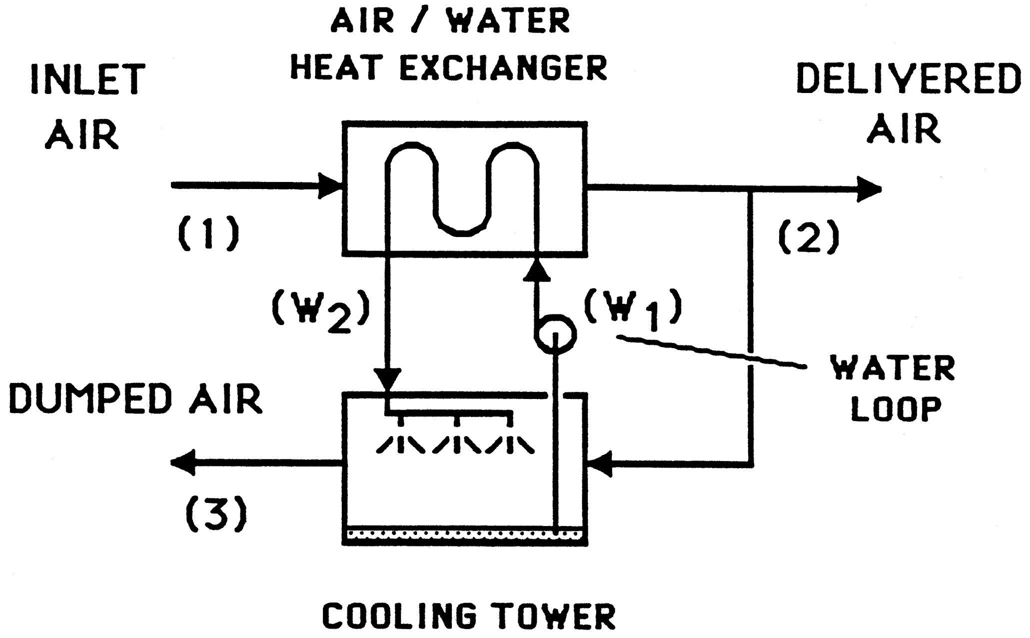

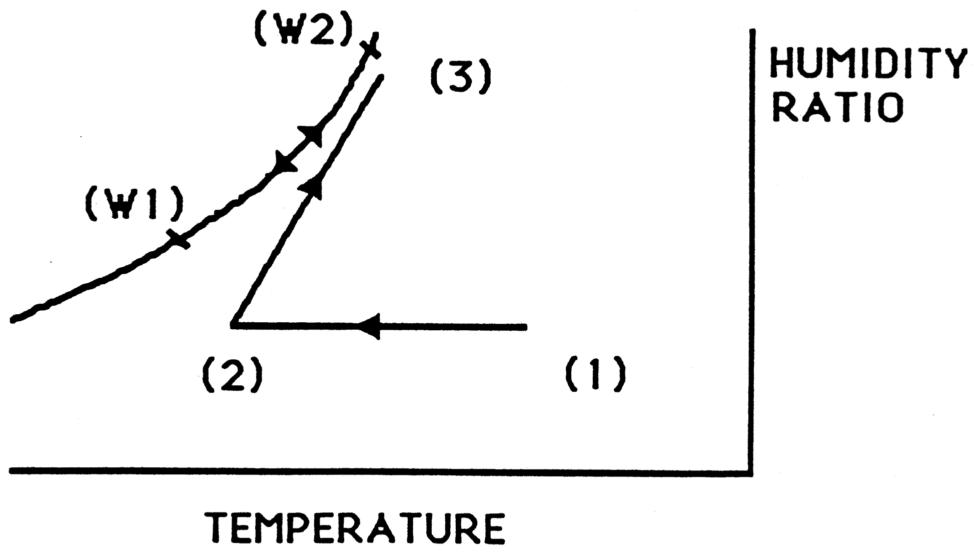

Figure 3.6.1 Schematic diagram and process representation of a cooling tower/ heat exchanger air cooler

follows. For a more complete derivation of the resulting equations, see Appendix A.

An energy balance on the fluid stream in Fig. 3.6.2 yields:

$$\dot{m}_f c_{p,f} \frac{dT_f}{dx} = UW(T_w - T_f) \tag{3.6.1}$$

An energy balance on the air/water interface yields:

$$h_{ca}(T_a - T_w) + h_D h_{fg}(\omega_a - \omega_w) + U(T_f - T_w) = 0 \tag{3.6.2}$$

Likewise, a mass and energy balance on the air stream yields Eqs. (3.6.3) and (3.6.4) respectively.

$$\dot{m}_a \frac{d\omega_a}{dy} = h_D W(\omega_w - \omega_a) \tag{3.6.3}$$

$$\dot{m}_a \frac{dh_a}{dy} = h_{ca} W(T_w - T_a) + h_D h_g W(\omega_w - \omega_a) \tag{3.6.4}$$

Two assumptions are now made to simplify the cooling tower model. The first is that the Lewis Number is unity and the second is that the saturation curve is linear in the range of temperatures and humidity ratios experienced by the cooling tower. With these assumptions, it is possible to manipulate Eqs. (3.6.1) through (3.6.4) to solve for the wet bulb depression of the air stream as it passes through the cooling tower.

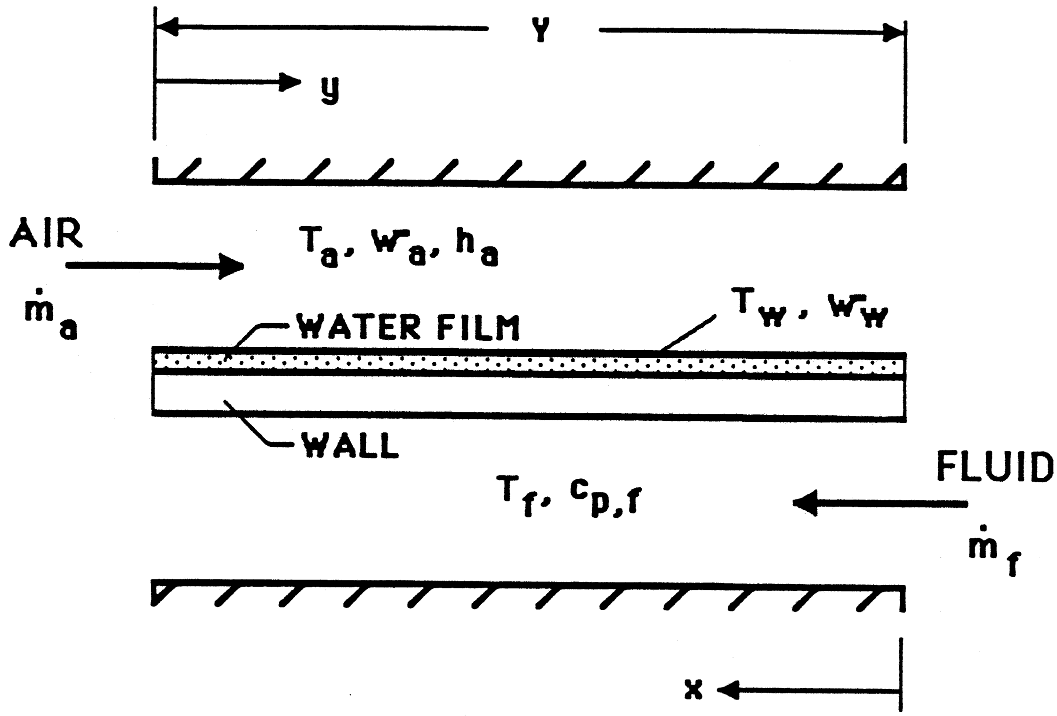

Figure 3.6.2 Mathematical model schematic of wet surface heat exchanger used in analysis of cooling tower

$$T_{a,out} - T'_{a,out} = (T_{a,in} - T'_{a,in}) * \exp(-\frac{h_c A_a}{\dot{m}_a c_{P,da}}) \quad (3.6.5)$$

The solution is analogous to the solution of the temperature variation of a fluid flowing past an isothermal surface in a sensible heat exchanger. The expression in the exponent parentheses is the cooling tower NTU. It combines the air-side heat transfer coefficient, tower surface area along with the specific heat and mass flow rate of the air.

With further algebraic manipulation, it is possible to simplify Eq. (3.6.2) to:

$$h_{wb}(T'_a - T_w) + U(T_f - T_w) = 0 \quad (3.6.6)$$

by defining a wet-bulb heat transfer coefficient as:

$$h_{wb} = h_c*(1.0 + e h_{fg}/c_{P,da}) \quad (3.6.7)$$

where e is the slope of the assumed linear saturation line. It is also possible to simplify Eq. (3.6.4) to:

$$\dot{m}_a c_{wb} \frac{dT'_a}{dy} = h_{wb} W(T_w - T'_a) \quad (3.6.8)$$

by defining a wet-bulb specific heat as:

$$c_{wb} = c_{P,da} * (1.0 + eh_{fg}/c_{P,da}) \tag{3.6.9}$$

The resulting Eqs. (3.6.1), (3.6.6) and (3.6.8) are of the same form as the equations encountered in sensible heat exchanger theory. These have been solved previously and the solutions result in the familiar effectiveness-NTU equations for counter and parallel flow heat exchanger configurations [Kays and London, 1984]. Equation (3.6.9) may be written in terms of air mixture enthalpies and humidity ratios as:

$$c_{wb} = \frac{h'_{a,out} - h'_{a,in} - (\omega'_{out} - \omega'_{in}) * h_f}{(T'_{out} - T'_{in})} \tag{3.6.10}$$

Equation (3.6.10) allows for the calculation of the capacitance rates for the cooling tower air and water streams. By choosing a tower NTU, the exiting air wet bulb temperature can be calculated with standard heat exchanger effectiveness equations. Equation (3.6.3) may then be used to solve for the wet bulb depression of the tower air and, when used with the previously calculated exiting wet bulb temperature, fixes the state of the air exiting the cooling tower.

The air/water sensible heat exchanger is modeled with the effectiveness-NTU method as detailed by Kays and London [1984].

A double iteration procedure is required to determine all of the equilibrium state points for the entire cooling unit. To begin the convergence procedure, a water temperature at the inlet to the heat exchanger is assumed. With this assumed water temperature and the known air inlet state and mass flow rates, exiting heat exchanger temperatures for both the air and water may be calculated. Next, the wet bulb temperature of the air exiting the cooling tower is assumed. This guessed wet bulb temperature is used with Eq. (3.6.10) to calculate the wet bulb specific heat and the air stream capacitance rate. With this information, an exiting wet bulb temperature may be calculated and compared with the assumed wet bulb temperature. If these two temperatures are not in close enough agreement, a new wet bulb temperature is assumed and this process is repeated. When convergence does occur, the water temperature exiting the cooling tower may be calculated and compared with the assumed water temperature entering the air/water heat exchanger. If the two water temperatures are equal, then the system is in equilibrium. If they are not the same, then a new initial water temperature must be assumed and the entire process repeated.

The procedure just outlined may be carried out for a range of delivered fractions and water mass flow rates. Figures 3.6.3 and 3.6.4 show how the system performance varies with changes in these two variables. As a measure of performance, the temperature and cooling capacity effectivenesses defined in Section 3.3 are used as the ordinates of the two plots. Figures 3.6.3 and 3.6.4 are for a cooling unit with NTU = 3 and an air inlet state of 30°C and 0.009 kg/kg absolute humidity ratio. A family of curves are found to exist that describe how the system performs. For any one given fraction

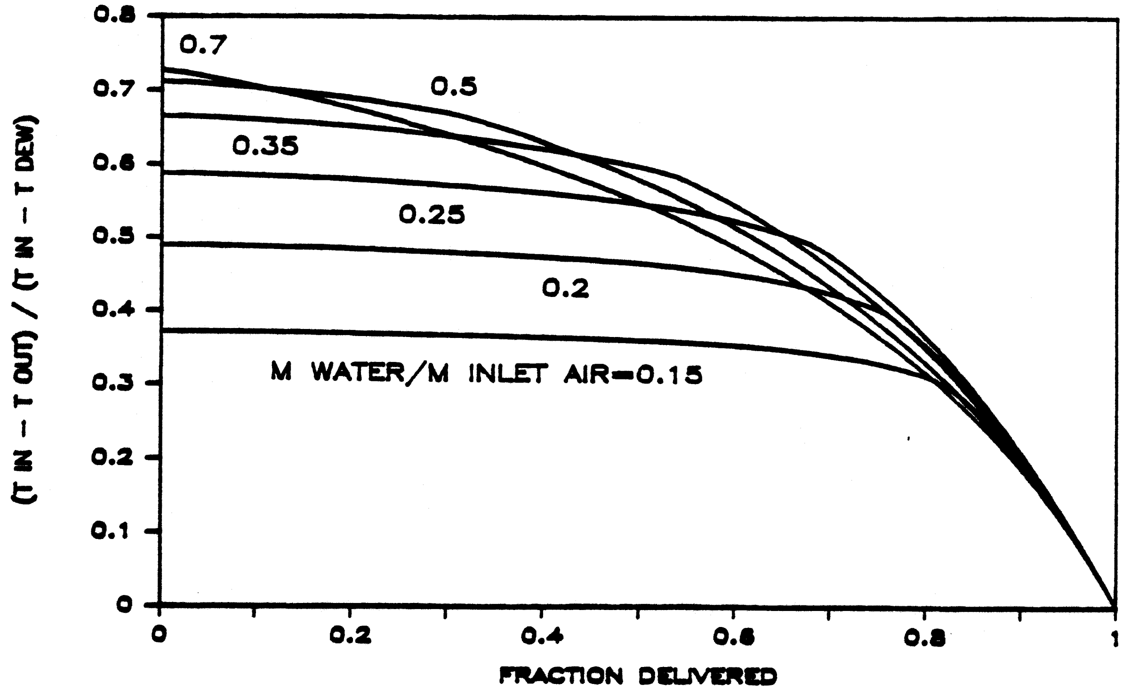

Figure 3.6.3 Temperature effectiveness curves for cooling tower/ heat exchanger. Variable water flow rates. T inlet=30C, W inlet=0.009 kg/kg

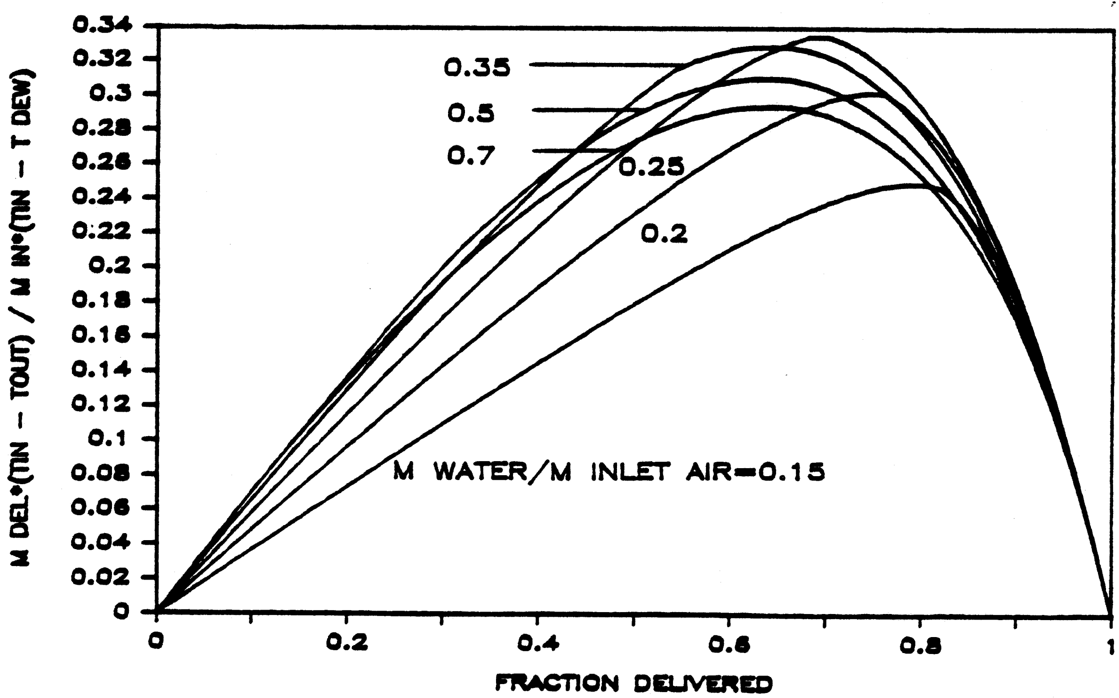

Figure 3.6.4 Cooling capacity effectiveness curves for cooling tower/ heat exchanger. Variable water flow rates. T inlet=30C, W inlet=0.009 kg/kg

delivered, there are as many system equilibrium points as there are water flow rates. It is observed, however, that there is one optimum water flow rate that maximizes the system performance. At a fraction delivered of 0.7, for example, the optimum water flow rate would be approximately 25% of the inlet air flow rate.

The optimum water flow rate is not constant as the system operating point shifts to higher or lower fractions delivered. As the fraction delivered value decreases, the optimum water flow rate increases. Figures 3.6.5 and 3.6.6 better illustrate how system performance varies with water flow rate for two cooling units with heat exchanger and cooling tower NTU's of 3 and 10. These plots compare temperature effectiveness with the water flow rate for constant values of fraction delivered. In the larger cooling unit, the maximum in the performance curve is more pronounced then it is for the smaller cooler.

The trends observed in Figs. 3.6.3 through 3.6.6 remain similar as the air inlet state changes to different conditions.

Figure 3.6.7 helps to explain why a maximum exists in the performance curves of Figs. 3.6.5 and 3.6.6. At very low water flows, the water circulating loop is the minimum capacitance stream for both the heat exchanger and the cooling tower. The water, in passing through the cooling tower, will therefore take a large temperature decrease and approach the wet bulb temperature of the air at state 2. However, the air passing through the heat exchanger will have a capacitance rate far greater then the water and will not be able to

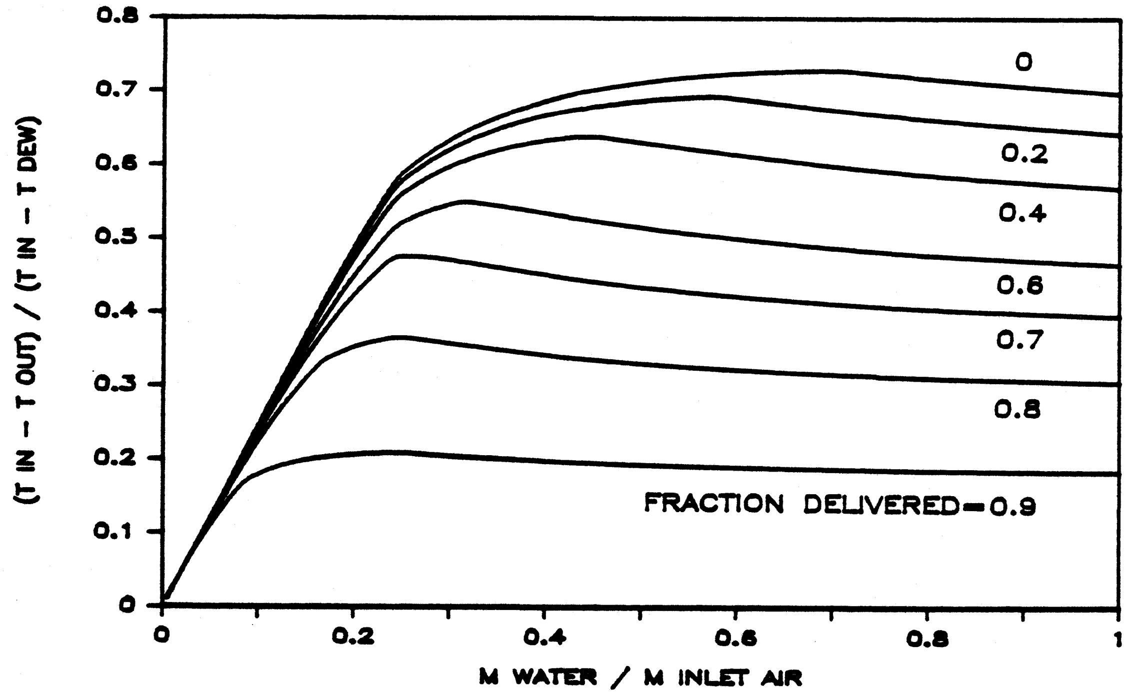

Figure 3.6.5 Temperature effectiveness vs water flow rate for cooling tower/ heat exchanger. NTU=3.0, T inlet=30C, W inlet=0.009 kg/kg

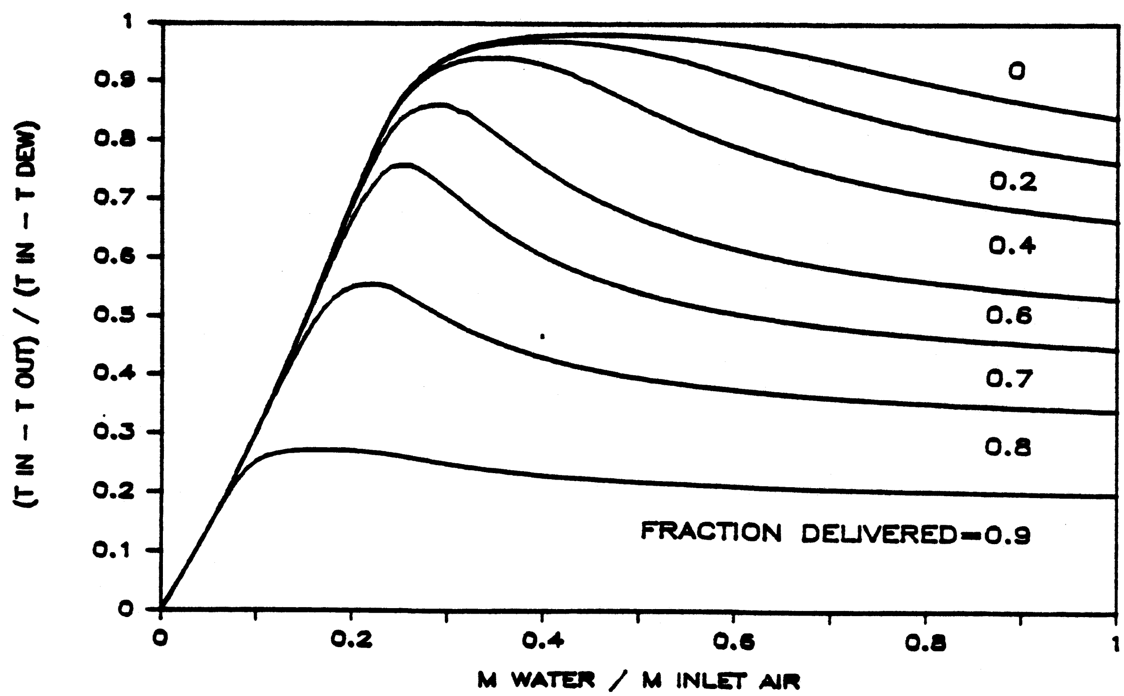

Figure 3.6.6 Temperature effectiveness vs water flow rate for cooling tower/ heat exchanger. NTU=10.0, T inlet=30C, W inlet=0.009 kg/kg

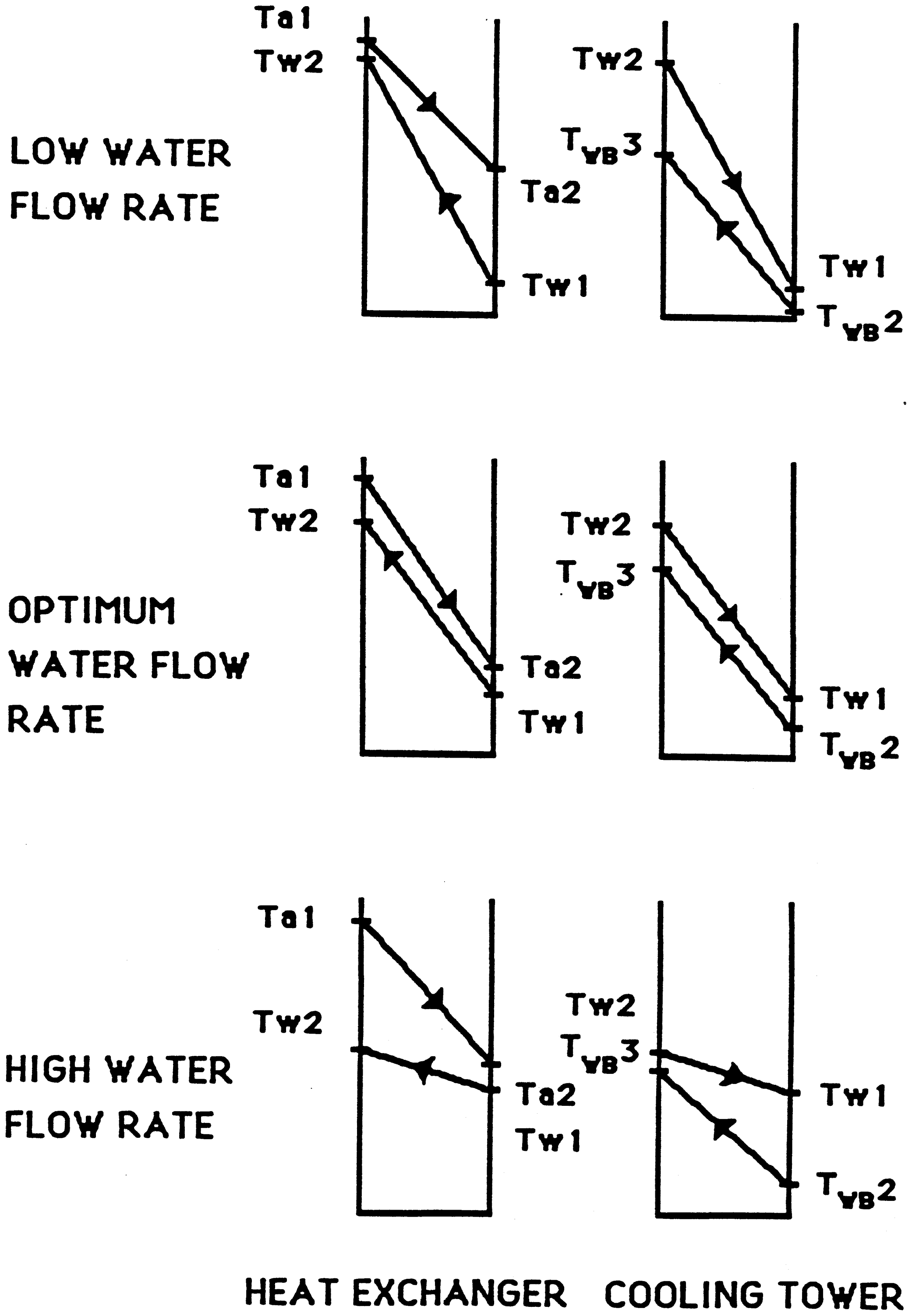

Figure 3.6.7 Temperature distributions through the two components of the cooling tower/heat exchanger air cooler for different water flow rates

approach the cold water temperature offered by the cooling tower. At the other extreme, at high water flow rates, the air in the heat exchanger and the cooling tower will become the minimum capacitance streams. The water passing through the cooling tower will have a smaller temperature change than the air and exit at a temperature substantially warmer than the wet bulb temperature of the air at state 2. In the heat exchanger, the air will have the larger temperature change and exit at a temperature close to the warm inlet water temperature. Stated more simply, at low water flow rates, the cooling tower is better able to cool the water loop but the heat exchanger is less able to use the cold water to cool the process air. At high water flow rates, the heat exchanger is better able to cool the process air closer to the water inlet temperature but the tower can not provide the heat exchanger with as cold of water. Operating the system at a flow rate between the two flow rate extremes will therefore optimize the system performance.

Further examination of Figs. 3.6.5 and 3.6.6 reveals that the best system performance, for fractions delivered ranging from 0.6 to 1.0, occurs when the water flow rate is approximately 25% of the inlet air flow rate. Since the specific heat of water is approximately four times that of air, this flow rate ratio corresponds to nearly equivalent capacitance rates in the heat exchanger. This point is further illustrated in the middle schematic of Fig. 3.6.7.

It is also observed that a reduction in system performance is more pronounced as the flow rate moves away from the optimum flow rate toward lower flow rates than toward higher flow rates. In actual operation, where it may be difficult to control the water flow rate to always obtain the optimum system performance, it would be recommended to fix the water flow rate slightly greater then 25% of the inlet air flow rate.

If the optimum water flow rate is chosen for all of the fractions delivered, the family of curves in Figs. 3.6.3 and 3.6.4 would be enclosed by one curve that characterizes the best system performance for all possible operating points. Figure 3.6.8 and 3.6.9 show the outer envelope of the temperature and cooling capacity effectiveness curves for cooling units with NTU's ranging from 1 to infinity and an inlet state of 30°C and 0.009 kg/kg absolute humidity ratio. A one-dimensional optimization routine was used to determine the best water flow rate for each particular system operating point.

With the best possible cooling unit (infinite NTU), it is possible to chill the inlet air to the dew point temperature and still deliver approximately 70% of the inlet air to the building zone. The best chiller unit of Section 3.4, the multistaged indirect evaporative cooler, could only approach the dew point temperature after diverting 100% of the inlet stream to the ambient and delivering none to the conditioned space.

As in the case of the other air coolers studied in this chapter, it is useful to see how the CT/HX Air Cooler performance varies with the inlet air state. In Fig. 3.6.10, lines of constant outlet temperature for a CT/HX with NTU of 3 and a fraction delivered of

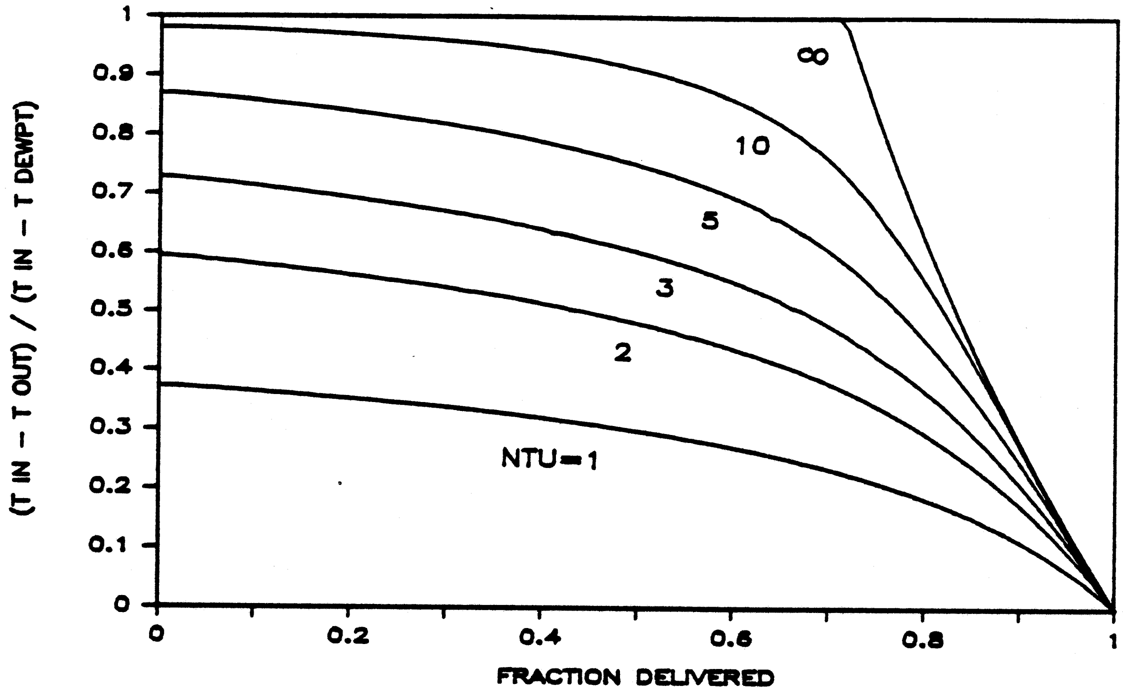

Figure 3.6.8 Optimum temperature effectiveness curves for cooling tower/ heat exchanger. Ntu=3.0, T inlet=30C, W inlet=0.009 kg/kg

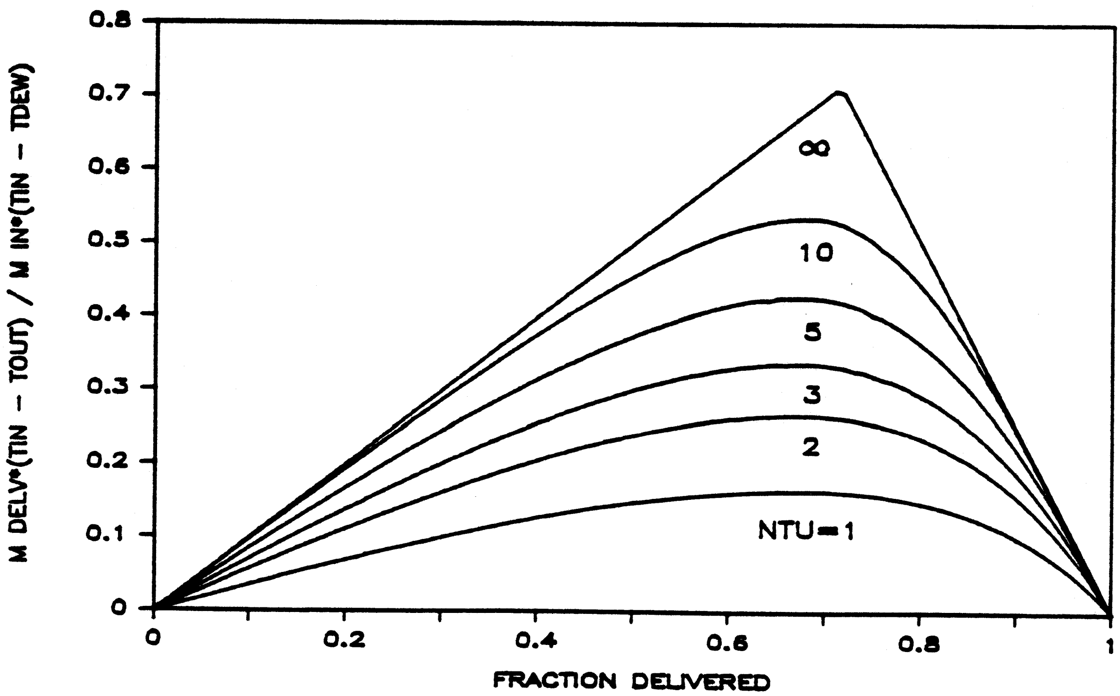

Figure 3.6.9 Optimum cooling capacity effectiveness curves for cooling tower/ heat exchanger. Ntu=3.0, T inlet=30C, W inlet=0.009 kg/kg

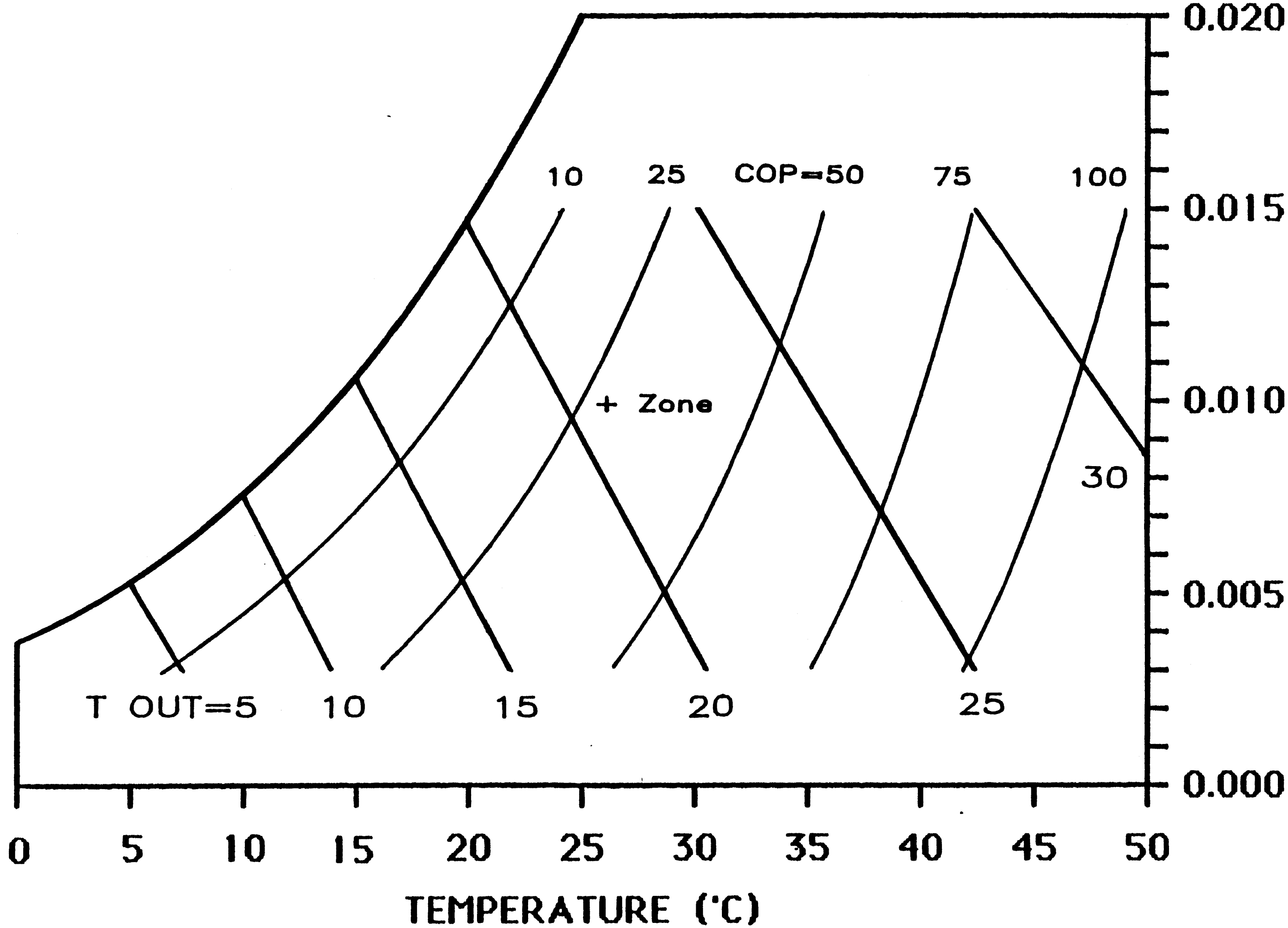

Figure 3.6.10 Lines of constant COP and outlet air temperature for cooling tower/ heat exchanger air cooler. NTU=3.0, fraction delivered=0.75, pressure drop=125 Pa

0.75 are mapped. The fraction of 0.75 was chosen since this is an operating point near the maximum in the cooling capacity effectiveness curves. The lines of constant outlet temperature resemble those for a single and multistaged IEC. They are linear lines that intercept the saturation curve at a temperature equal to the value of the constant temperature line. If the CT/HX NTU's were to increase, these lines would become flatter and, in the limit of infinite NTU, would be horizontal.

Figure 3.6.10 also illustrates how the COP for the CT/HX varies with changes in its inlet air state. These lines of constant COP were generated for a fraction delivered value of 0.75, a pressure drop of 125 Pa, and a heat exchanger and cooling tower NTU of 3.0. As in the case of the single and multistaged IEC's, these lines have the same shape as the saturation curve. In the range of air conditioning practice, the COP's ranges from 10 to 75.

The Cooling Tower/Heat Exchanger air cooler clearly has great potential for air conditioning applications. Of all of the cooling devices studied in this chapter, it has superior temperature reducing and cooling capacity effectivenesses for any value of fraction delivered. The only possible drawback to this system, in comparison to the other evaporative coolers, is its complexity. This cooler uses a cooling tower instead of an evaporative cooler. It also requires a water circulating loop to couple the two components. As is indicated by Figs. 3.6.5 and 3.6.6, the performance of this cooler is sensitive to the water flow rate. A smart control system would be required to maintain the cooler near its optimum operating point. One further caution regarding this cooler is that even though the temperature effectivenesses are very high, this cooler is still not able to dehumidify the inlet air stream and would have to be used in conjunction with a dehumidifier to successfully meet a total air conditioning load.

CHAPTER 4. ADVANCED DESICCANT AIR CONDITIONING SYSTEMS

Four air cooling devices that may be used to sensibly cool process air were introduced in Chapter 3. The two most promising were the two-stage indirect evaporative cooler (IEC) and the cooling tower/heat exchanger. These devices are capable of cooling air below the inlet air wet bulb temperature. The substitution of these coolers in place of the direct evaporative coolers, used in the classical desiccant cycle, should improve the overall cycle performance. By using sensible air coolers, it is no longer necessary to over-dry the process air in the dehumidifier to compensate for the direct evaporative cooling process. This chapter studies the use of these air coolers in the standard ventilation and recirculation cycles and analyzes the effects of these coolers at one ambient and room condition.

Section 4.1: Two-Stage IEC Desiccant Air Conditioning Cycle

A schematic diagram of a two-stage IEC desiccant air conditioning cycle in a ventilation mode is shown in Fig. 4.1.1. The corresponding process representation on psychrometric coordinates is illustrated in Fig. 4.1.2. In comparison with the classical ventilation cycle, the left portion of the new cycle in Fig. 4.1.1 remains unchanged. Fresh air is introduced at the inlet to the dehumidifier and is dried and heated from state 1 to state 2. Air at state 2 then

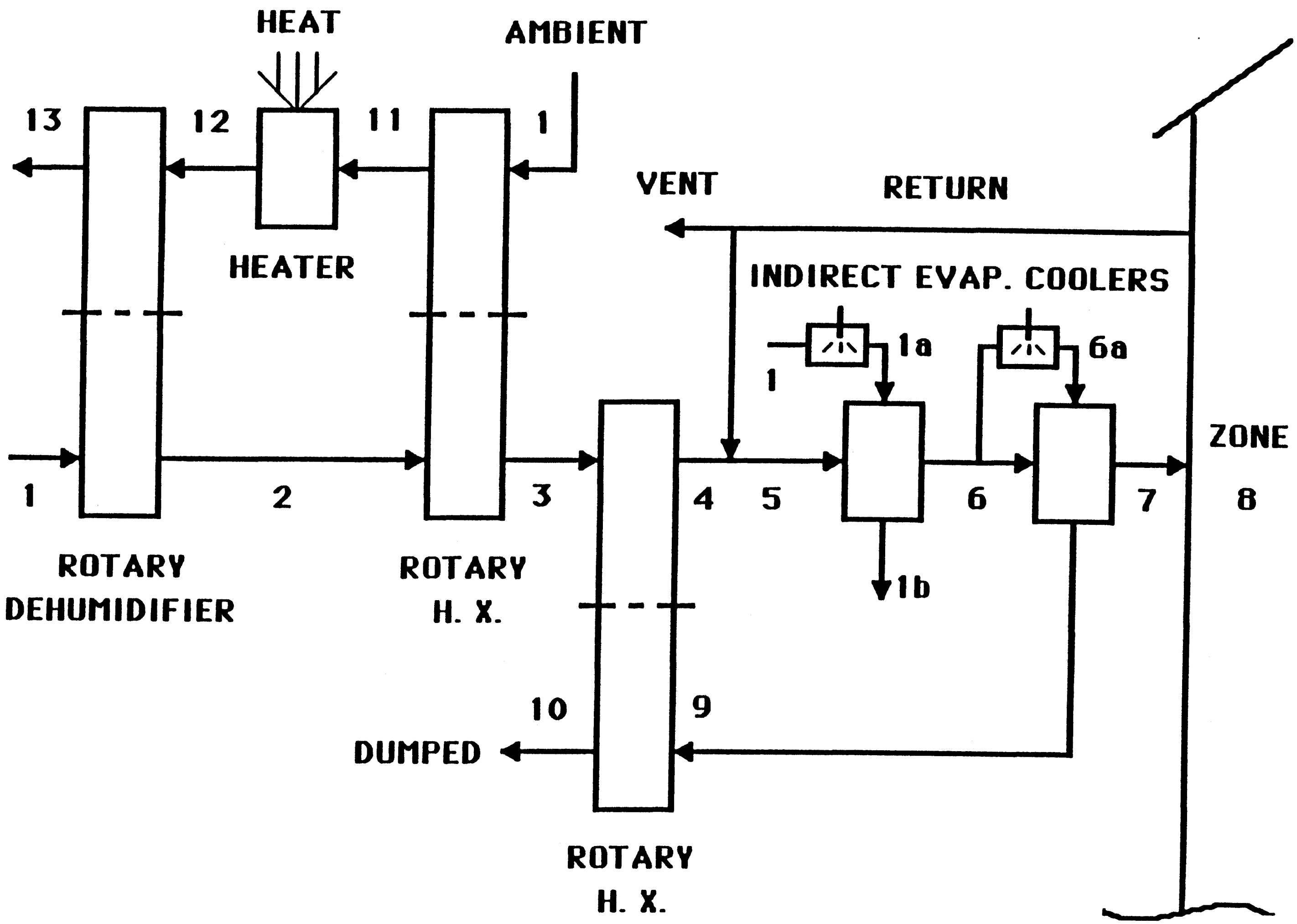

Figure 4.1.1 Schematic diagram of ventilation Two-stage IEC desiccant air conditioning cycle

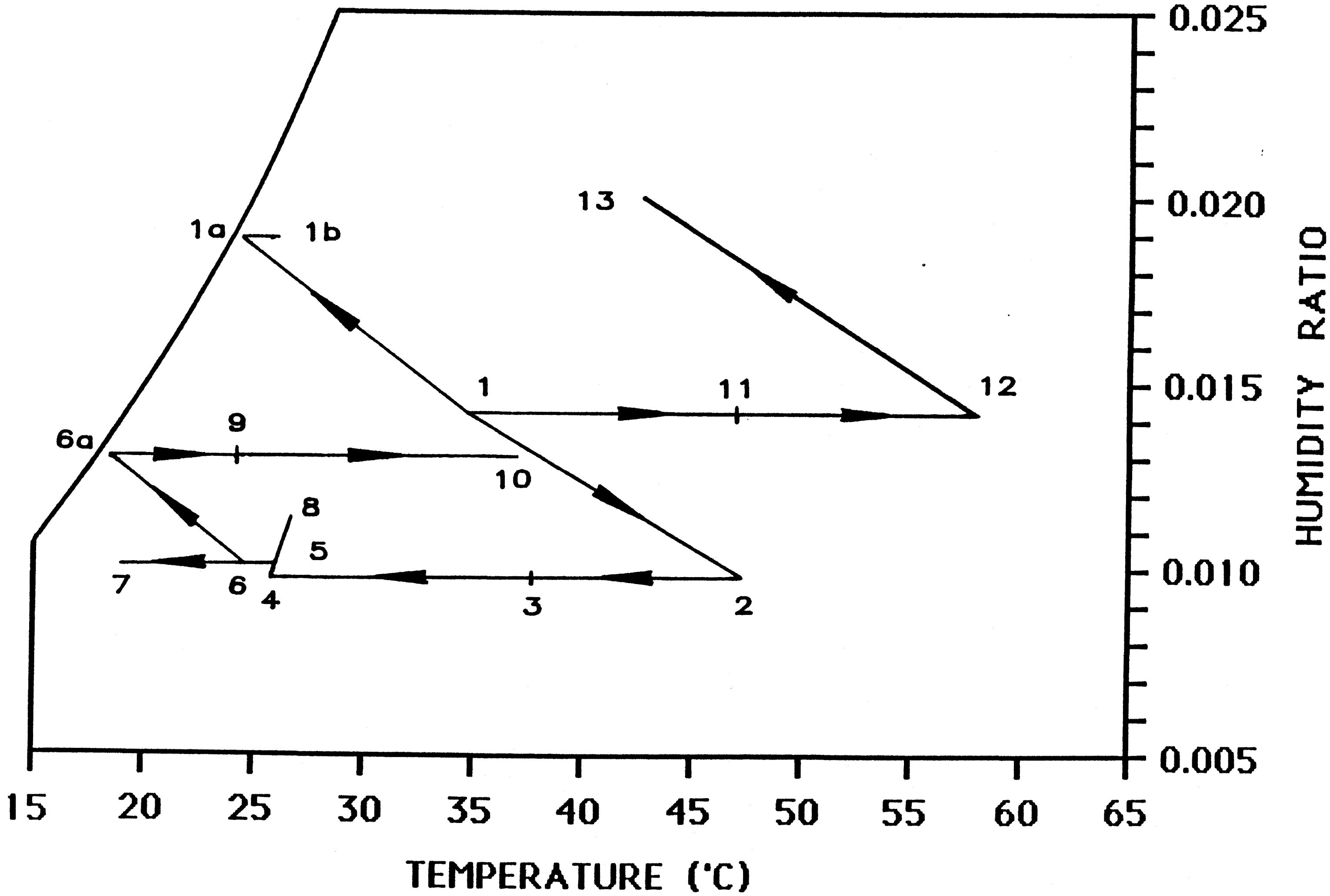

Figure 4.1.2 Process representation of ventilation two-stage IEC desiccant air conditioning cycle, ARI design conditions, 20% LLR, 10% ventilation, NTU's=9.0

sensibly exchanges heat with the ambient and is delivered to the new cooling portion of this cycle at state 3.

The staged indirect evaporative cooler employs a second rotary heat exchanger to precool the entering process air to state 4. This rotary heat exchanger uses the exhaust from the second stage cooler at state 9 as the heat sink for the process stream. The process air then mixes with return zone air and passes through the first of two stages of sensible cooling. The first stage is an indirect evaporative cooler that uses the ambient as the wet stream cold sink for the warmer process air. The second stage is a single-staged indirect evaporative cooler (See Section 3.3). The single-stage IEC diverts a portion of the air at state 6 for use as the wet stream heat sink in the air/air heat exchanger. Air exits from the second stage at the supply state, 7. The ability to divert any portion of the process air in the second stage for use as a heat sink provides the control necessary for varying the temperature at the supply state.

There is a fundamental difference between this ventilation cycle and the classical ventilation cycle of Fig. 2.3.1. In the classical ventilation cycle, the entire supply air stream comes from the ambient and is processed through the dehumidifier; there is no mixing of ventilation air with the return air. However, the ventilation cycle of Fig. 4.1.1 mixes return air with the dehumidifier outlet air. This is done for two reasons. First, by dehumidifying only the required ventilation air and the air which is ultimately exhausted from the air chiller, the dehumidifier unit can be much smaller than a dehumidifier that is designed to dehumidify the entire supply air stream. Second, the zone air is often drier then the ambient. In this case, it is more favorable, from an energy standpoint, to reuse the drier zone air then it is to introduce wet ambient air through the dehumidifier.

There are three main points that should be made regarding the controls used in the cycles to be discussed in this and following chapters. First, for all simulations conducted in this study, a constant enthalpy difference across the supply and zone states of 10 kJ/kg is used. This implies that at low latent load ratios, a larger proportion of the zone cooling load is attributed to sensible cooling then it is to latent cooling. The change in supply state with latent load ratio is further illustrated in Fig. 4.1.3.

The second point regarding the controls is that as more sensible cooling is required, a higher portion of supply air must be exhausted from the chillers (See Sections 3.3 and 3.6). To make up for this lost air flow, an equal amount of fresh air must be introduced to the inlet to the dehumidifier and originates from the warmer and more moist ambient. In addition to the exhausted air, ambient air must also be supplied in an amount equal to the ventilated zone air. As an example, if the total air conditioning load on the zone is 1000 kJ/second then the supply air flow rate is 100 kg/second. If the required ventilation rate for that particular zone is 10%, then 10 kg/second of ambient air must be processed through the dehumidifier and mixed with the return zone air.

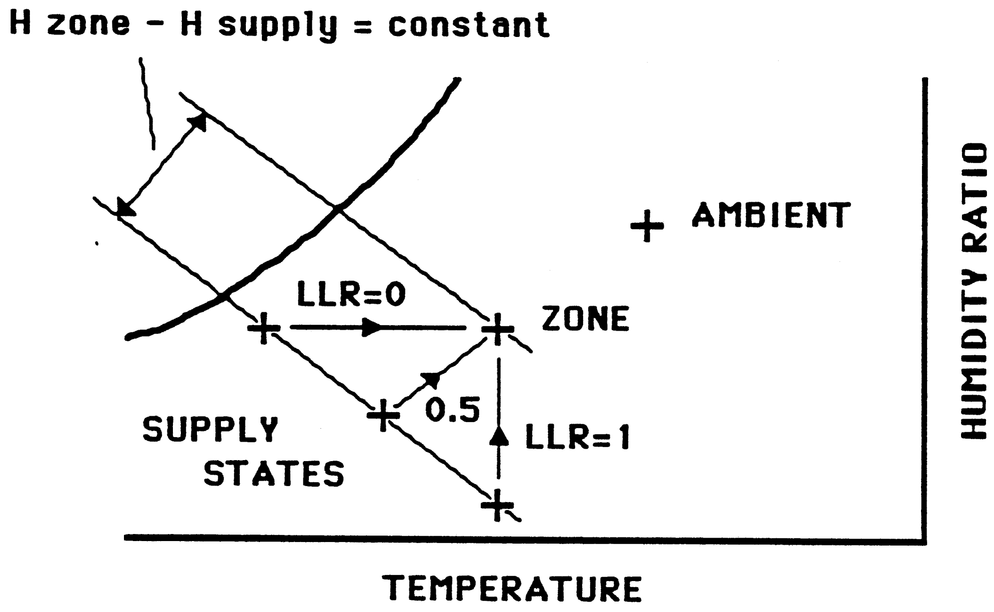

Figure 4.1.3 Illustration of how the supply state varies with latent load ratio for a constant enthalpy difference across the supply and return air

A further control mechanism is employed if the flow through the dehumidifier is too low and the amount of moisture in the air stream available for removal is insufficient to allow the latent load on the zone to be met. In instances where this situation holds (namely high fractions delivered and low required ventilation rates) one of two responses is taken. If the zone air is drier then the ambient, then return air is recirculated and mixed with the inlet air to the dehumidifier. If the ambient air is the drier air stream, then more ventilation air is introduced to the inlet to the dehumidifier.

The example illustrated in Fig. 4.1.2 is for American Refrigeration Institute (ARI) design conditions (Ambient: 35°C, 0.0142 kg/kg; Zone: 26.7°C, 0.0111 kg/kg), a 10 percent zone ventilation rate, a 20% zone latent load ratio and all cycle component NTU's equal to 9.0. To meet both the sensible and latent cooling load on the zone, 51.5% of the inlet air to the cooler must be exhausted to the ambient. The resultant thermal COP (zone cooling load/ energy input to heater) for ARI conditions is 0.96.

Figure 4.1.4 shows the fraction (F) of the inlet air to the cooler that is delivered to the space as a function of the zone latent load ratio. There are three distinct regions in this curve. The first region lies between latent load ratios of 0 and 0.2 and is characterized by fraction delivered values less then 0.5. To understand why these delivered fractions are so low, one must recall the performance characteristics of the single-stage IEC discussed in Section 3.3. The temperature effectiveness curve for a single-stage

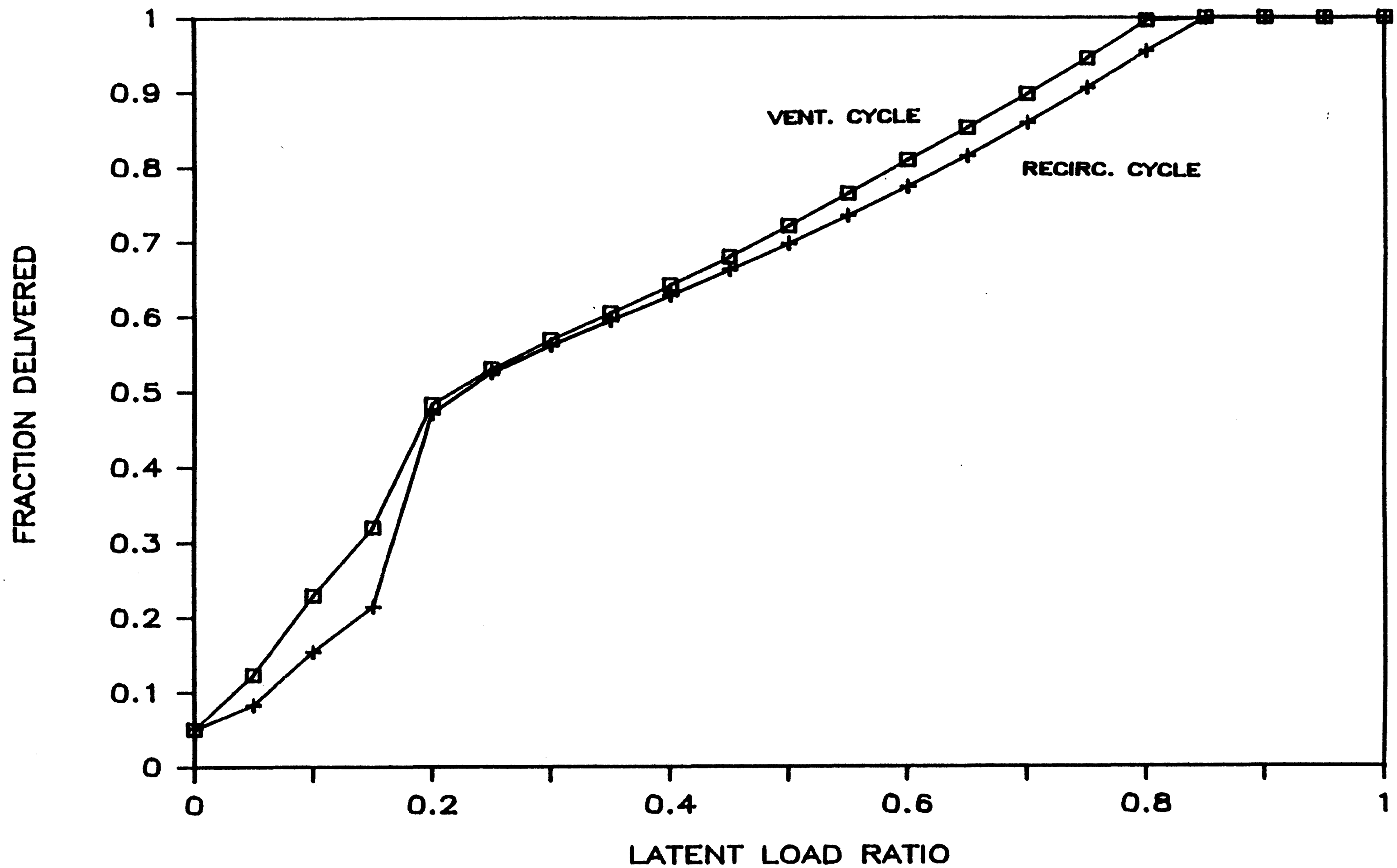

Figure 4.1.4 Fraction delivered vs latent load ratio for two-stage IEC cycle. ARI conditions, 10% ventilation, NTU=9.0

IEC is not continuous but rather has two segments that meet in a knee at a fraction delivered of 0.5 (See Fig. 3.3.5). For delivered fractions between 0 and 0.5 there is not much effect on the outlet air temperature. At fractions greater than 0.5, that is, operating to the right of the knee in the temperature effectiveness curve, there is good response in temperature reduction to changes in fraction delivered. For this particular ARI design example, at the lower latent load ratios, there is enough demand for sensible cooling that the required fraction delivered values lie to the left of the knee in the temperature effectiveness curve.

At latent load ratios greater than 0.2, the cooler operates to the right of the knee in the temperature effectiveness curve and resultant fractions are greater than 0.5. Operating the system in Fig. 4.1.1 at latent load ratios increasing past 0.2 therefore results in a continuous increase in the required fraction delivered values.

The third segment in Fig. 4.1.4 lies between latent load ratios of 0.8 and 1.0. In this portion of the curve, the load is mainly latent and the supply state is not required to be as cold as it is at lower latent load ratios (See Fig. 4.1.3). At latent load ratios greater than 0.8, the first stage of cooling provides sufficient temperature reduction and the second stage of cooling may be turned off so that the fraction delivered equals unity.

It is also instructive to plot the required dehumidifier regeneration temperature as a function of latent load ratio for the same ventilation system. Figure 4.1.5 provides such a plot for the same

ARI design conditions. Again, three distinct regions exist. The first region lies between latent load ratios of 0.0 and 0.6. As the latent load ratio increases, the required supply and exiting dehumidifier humidity ratio decreases. To meet this demand, the regeneration temperature must increase. Also, as the latent load ratio increases from 0.0 to 0.6, the mass flow rate of exhausted air and therefore the fresh air introduced to the dehumidifier decreases. Since there is a decreasing amount of air from which to extract moisture, the amount of moisture removed from the existing air per unit mass must increase in order to meet the zone latent load. To remove this extra moisture requires an additional increase in regeneration temperature.

The second region in the regeneration temperature curve lies between latent load ratios of 0.6 and 0.8. For this particular design point example, at a latent load ratio of 0.6, there is very little air introduced at the inlet to the dehumidifier since only a small amount of air must be exhausted from the cooler. At this point, the control scheme discussed earlier in this section is implemented and air is recirculated from the return stream and mixed with the inlet fresh air. This lowers both the inlet humidity ratio and the corresponding regeneration temperature as illustrated in Fig. 4.1.5.

The final region in the regeneration curve occurs at latent loads greater than 0.8 where the fraction delivered is equal to 1.0. In this region, the mass flow rate from the ambient is just equal to the required ventilation rate. This decrease in flow from the ambi-

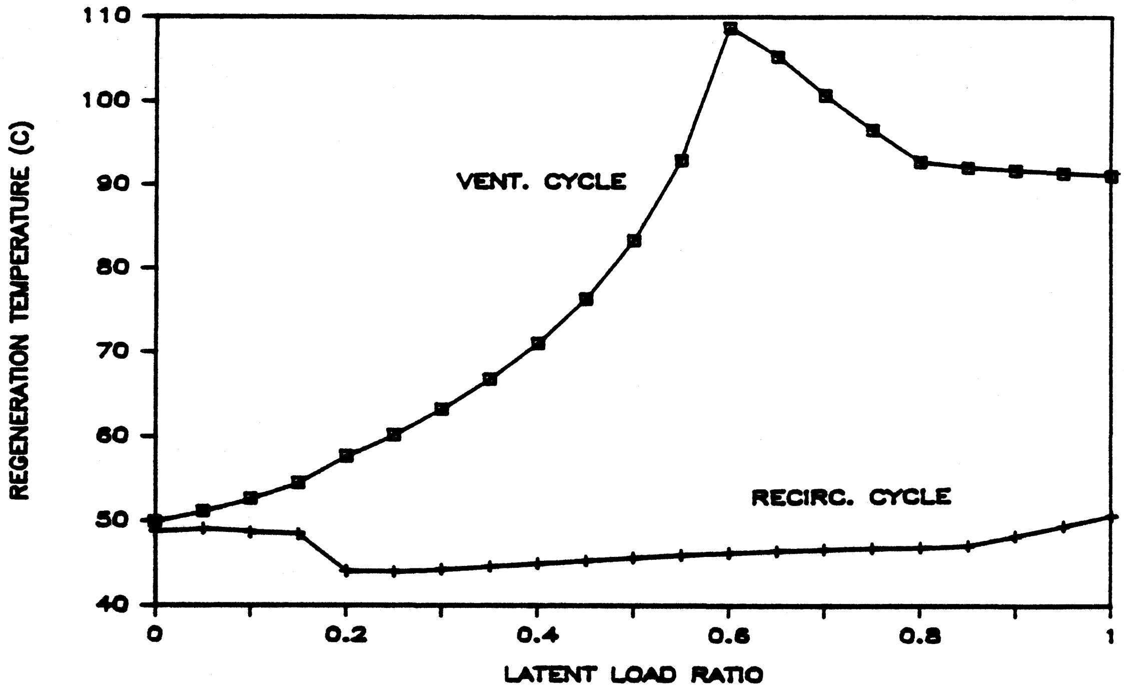

Figure 4.1.5 Regeneration temperature vs LLR for two-stage IEC cycle, ARI, 10% vent, NTU=9.0

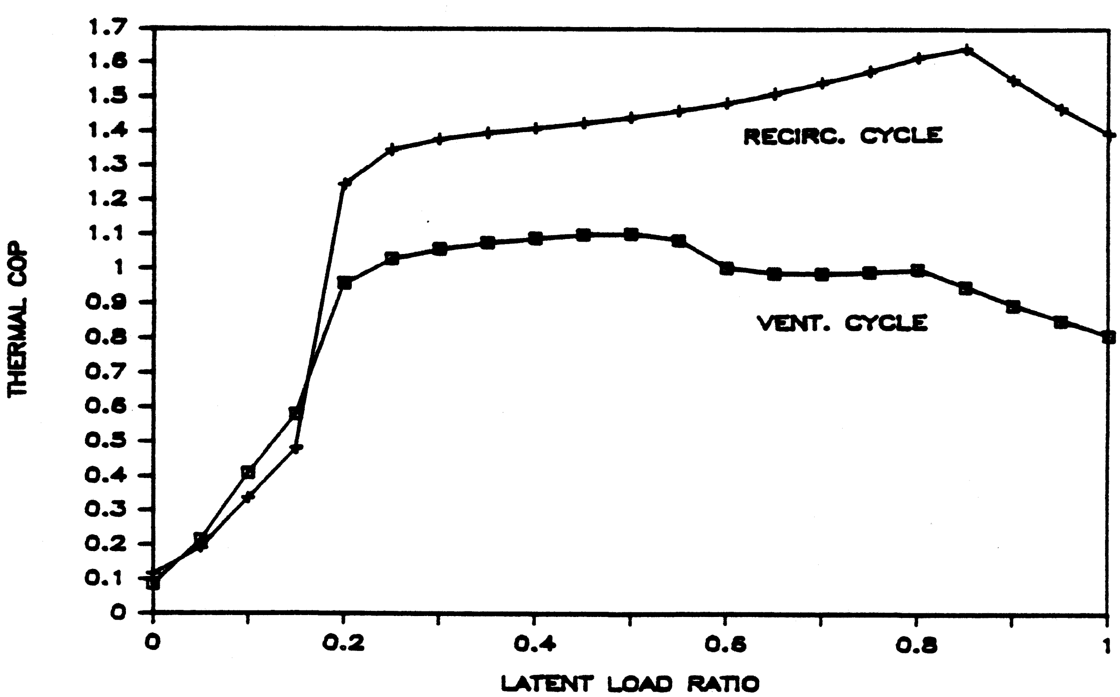

Figure 4.1.6 Thermal COP vs LLR for two-stage IEC cycle ARI conditions, 10% vent, NTU=9.0

ent and continued small increase in recirculation flow from the return air yields a slight decrease in the inlet humidity ratio and regeneration temperature.

A plot of the thermal coefficient of performance for the ventilation cycle as a function of latent load ratio is shown in Fig. 4.1.6. This figure reflects the fraction delivered curve of Fig. 4.1.5 over the entire range of latent load ratios. For latent loads up to 0.2, the coefficient of performance is very low due to the low fraction delivered. At latent loads greater than 0.2 but less than 0.6, COP increases to a maximum of 1.1. At latent load ratios greater than 0.6 but less than 0.8, return air from the zone is recirculated to the inlet of the dehumidifier and even though the inlet humidity ratio is now lower than when return air was not recirculated, the flow through the dehumidifier and heater has increased. The energy input into the heater therefore increases and the COP decreases. At latent loads greater than 0.8, the COP decreases further in proportion to the increase in recirculated air flow through the dehumidifier and heater.

To gain insight into how the performance of the staged IEC ventilation cycle varies as the amount of ventilation air changes, ARI design point simulations were run at a constant latent load ratio of 20% and variable percent ventilation. The percentage ventilation is the percentage of the supply air flow rate that is made up of fresh air introduced from the ambient. Figure 4.1.7 illustrates how the required regeneration temperature decreases as the ventilation

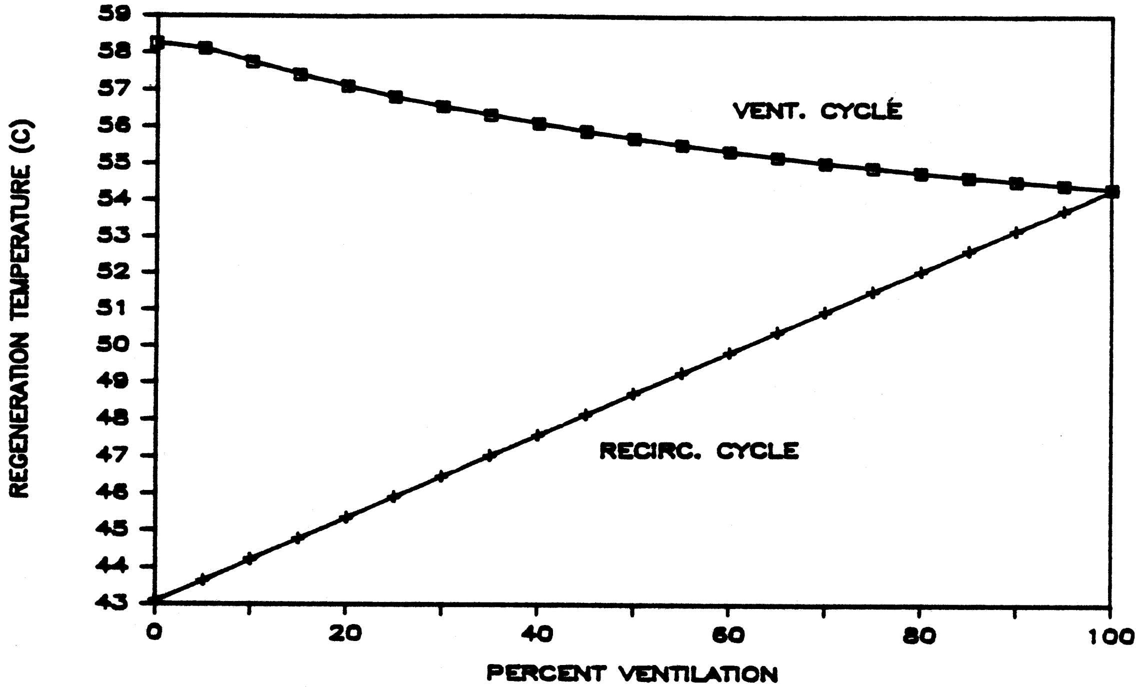

Figure 4.1.7 Regeneration temperature vs % ventilation for two-stage IEC cycle. ARI conditions, 20% LLR, NTU=9.0

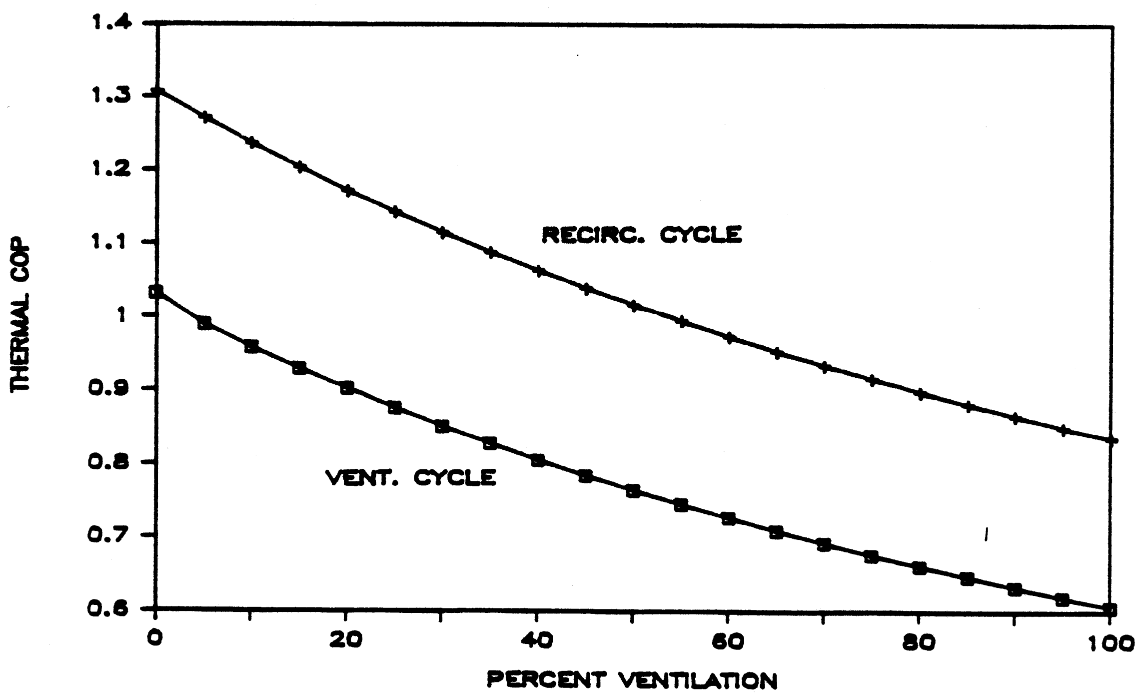

Figure 4.1.8 Thermal COP vs % ventilation for two-stage IEC cycle. ARI conditions, 20% LLR, NTU=9.0

increases. If more air is processed through the dehumidifier, then the processed air requires less moisture removal per unit air flow to meet the latent load. Since the degree of dehumidification reduces with the process air mass flow rate, the regeneration temperature decreases also. Figure 4.1.8 illustrates how the thermal COP varies with the percentage ventilation. As the percentage ventilation increases, the COP decreases 40% from 1.03 to 0.6. This decrease in COP can be attributed largely to the increase in the mass flow rate through the dehumidifier and heater.

The two stage IEC desiccant cycle may also be configured in a recirculation mode. A schematic diagram for such a system is illustrated in Fig. 4.1.8. In this cycle, fresh ambient air at state 1 is mixed with return air at the inlet to the dehumidifier. This air is then dried and heated as it passes through the dehumidifier and exits at state 3. As in the case of the ventilation cycle, the ambient air is used as a heat sink in the first rotary heat exchanger and cools the exiting dehumidifier air to state 4. At this point, the process air enters the sensible cooling portion of the cycle and is precooled to state 5 and then further chilled to state 6 with the first stage of cooling. If necessary, the air is further cooled in the second stage cooler and delivered to the conditioned space at state 7.

The recirculation cycle illustrated in Fig. 4.1.9 may also be simulated at ARI conditions, 10% ventilation rate and 20% latent load ratio. To completely meet both the sensible and the latent load on the zone, 52.8% of the air at the entrance to the cooler is exhausted

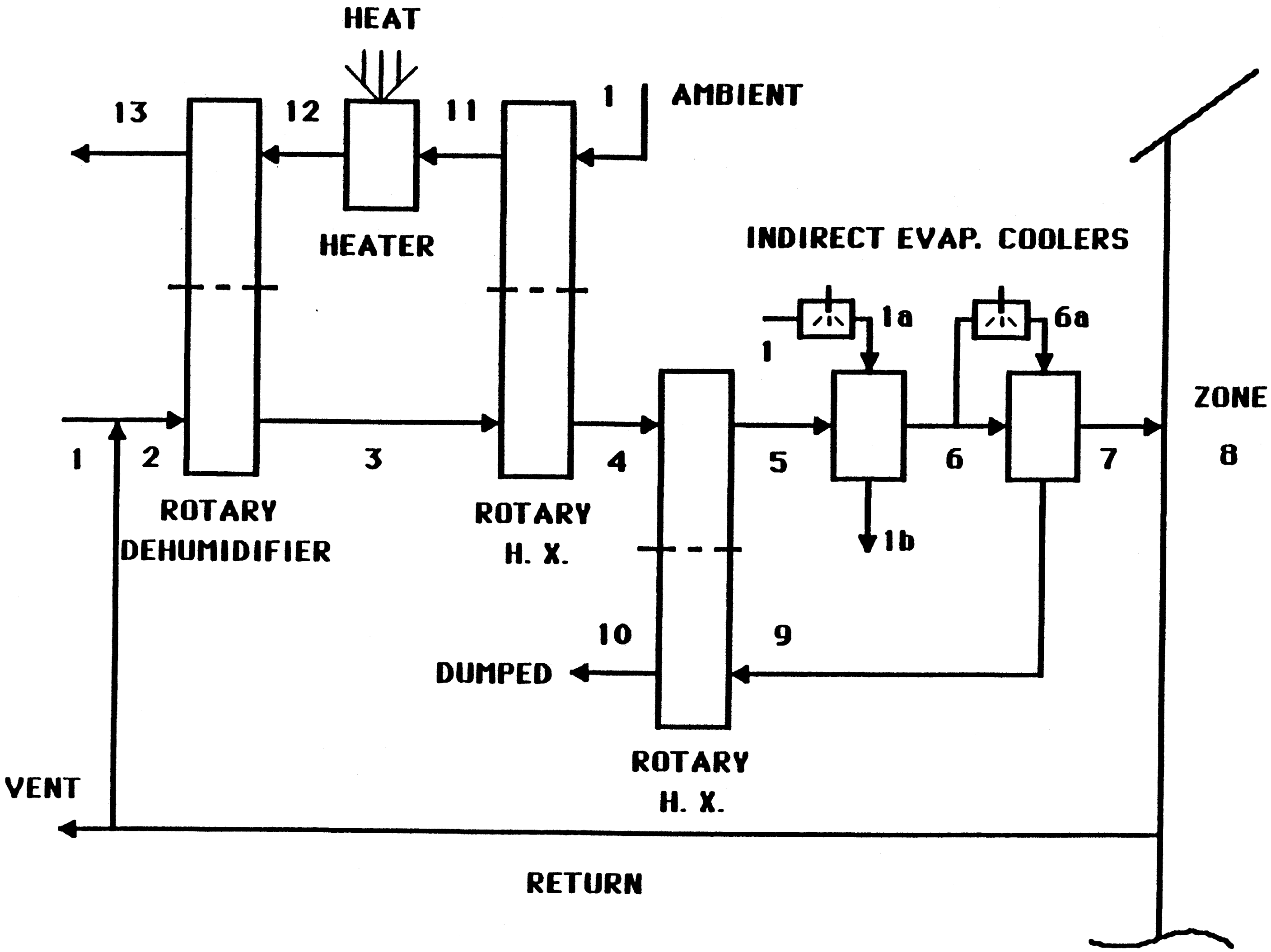

Figure 4.1.9 Schematic diagram of recirculation two-stage IEC desiccant air conditioning cycle

to the ambient. The thermal COP for this recirculation cycle is 1.17 at ARI conditions.

The recirculation two-stage IEC cycle was also simulated at ARI conditions and 10% ventilation rate for variable latent load ratios. A graph of the fraction of inlet air to the cooler that was delivered to the conditioned space is shown in Fig. 4.1.4. The trends observed for the recirculation cycle mirror those observed for the ventilation cycle. At low latent load ratios, a large sensible load must be carried by the second stage of the air cooler and the cooler operates to the left of the knee in the temperature effectiveness curve. At latent loads between 0.2 and 0.8, the cooler operates in the smoother region of the temperature effectiveness curve. In this region, the fraction delivered varies continuously between 0.5 and 1.0. At latent loads greater than 0.8, the second stage of the air cooler is not necessary and the corresponding fraction delivered is equal to 1.0.

The regeneration temperature is also illustrated in Fig. 4.1.5 for the same ARI conditions. The trends observed in this curve are different from those observed for the ventilation cycle. At low latent load ratios, the fraction delivered values are low requiring a high inlet mass flow rate from the ambient. The dehumidifier inlet humidity ratio is therefore increased and requires a higher regeneration temperature to dry the desiccant. At latent load ratios between 0.2 and 0.8, the mass flow rate of exhausted air and inlet fresh air decreases and the inlet humidity ratio therefore also drops. As the latent load ratio increases, however, the required outlet humidity ratio also drops and offsets the benefit of the decreased flow through the dehumidifier. At latent load ratios higher than 0.85 the fraction delivered equals 1.0 (Fig. 4.1.4) and the inlet humidity ratio no longer decreases. From this point on, the regeneration temperature continues to increase.

The thermal coefficient of performance for the recirculation cycle is plotted in Fig. 4.1.6. This curve has the same shape as that of the ventilation cycle. At lower latent load ratios, the COP is low due to the high flow rates through the dehumidifier and heater. At latent loads between 0.2 and 0.85, the fraction delivered is between 0.5 and 1.0 and the decreased mass flow rate through the dehumidifier and heater increases the COP. At latent loads greater than 0.85, the fraction delivered is 1.0 and the inlet state to the desiccant is now constant. The required outlet humidity ratio continues to decrease, however, and the resulting increase in regeneration temperature reduces the COP.

Figure 4.1.7 and 4.1.8 illustrates how the regeneration temperature and cycle COP vary with the ventilation rate at constant ARI conditions and 20% latent load ratio. At zero ventilation rate, the inlet to the dehumidifier is the return zone air. As the amount of ventilation increases, the inlet to the desiccant becomes more humid and the required regeneration temperature gradually increases. The coefficient of performance decreases since more energy is required to increase the regeneration temperature at the higher ventilation rates.

Section 4.2: Cooling Tower/Heat Exchange Desiccant Cycles

As an alternative to the indirect evaporative cooler of the previous section, the standard direct evaporative cooler of the classical ventilation cycle can be replaced with a cooling tower/ heat exchanger air cooler. A system diagram and corresponding process representation on a psychrometric diagram for such a cycle is illustrated in Figs. 4.2.1 and 4.2.2. As in the two-stage IEC cycle presented in Section 4.1, the left hand portion of this cycle remains the same as the classical ventilation cycle. Air is dried and heated as it passes through the dehumidifier to state 2 and then sensibly cooled with the first rotary heat exchanger. A second rotary heat exchanger is used to precool the inlet air to the air/water heat exchanger and uses the cool, wet exhaust air from the cooling tower as its heat sink. After mixing with return zone air, the process air is further cooled as it passes through the air/water heat exchanger from state 5 to 6. The air at state 6 is split into two streams. One is delivered to the building zone and the second is warmed and humidified to state 8 as it passes through the cooling tower. The particular example shown in Fig. 4.2.2 is for ARI conditions, 10% ventilation rate, 20% latent load ratio and component NTU's equal to 9.0. This air conditioning cycle delivers 74.9% of the inlet air to

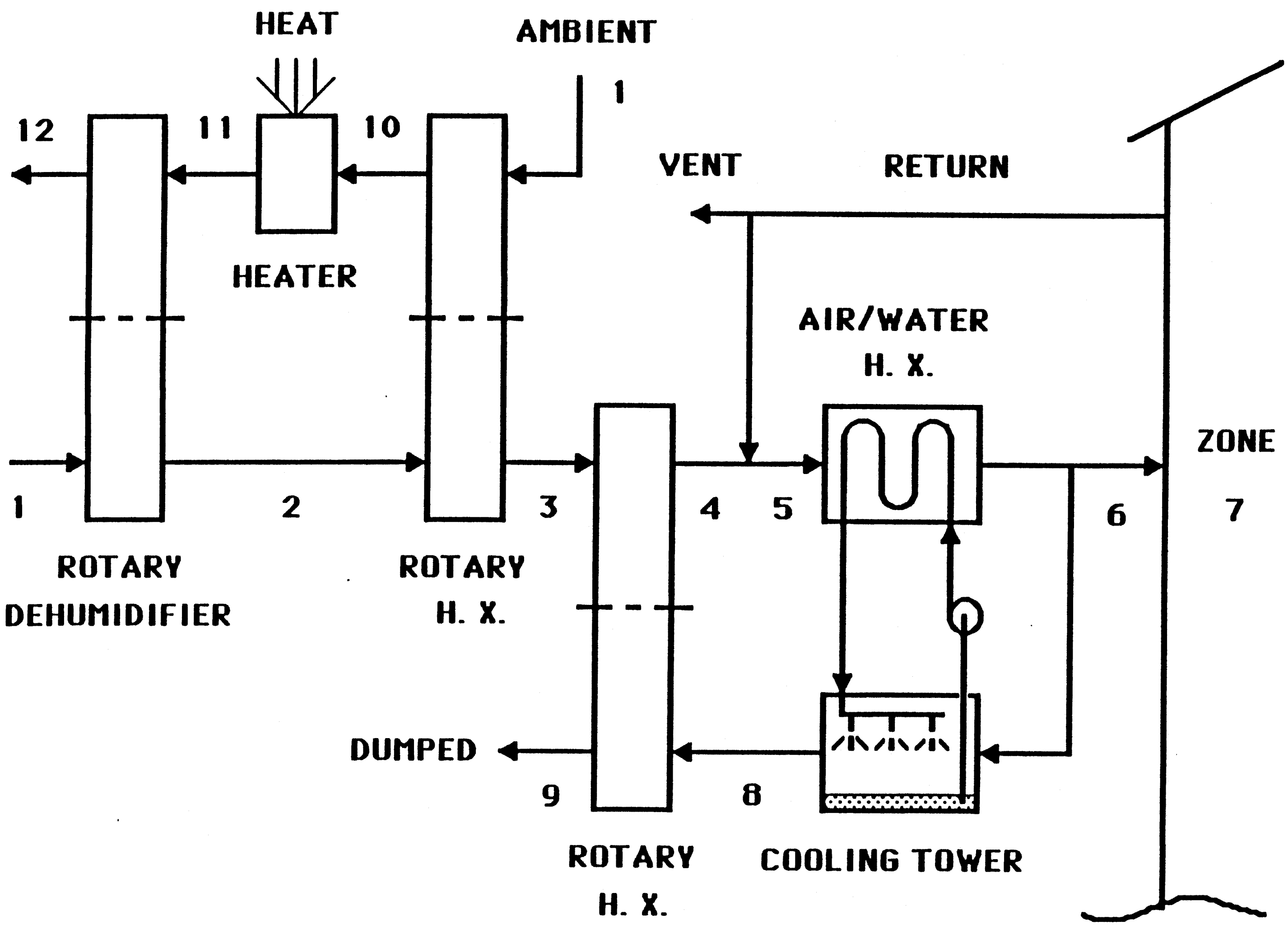

Figure 4.2.1 Schematic diagram of ventilation cooling tower/ heat exchanger desiccant air conditioning cycle

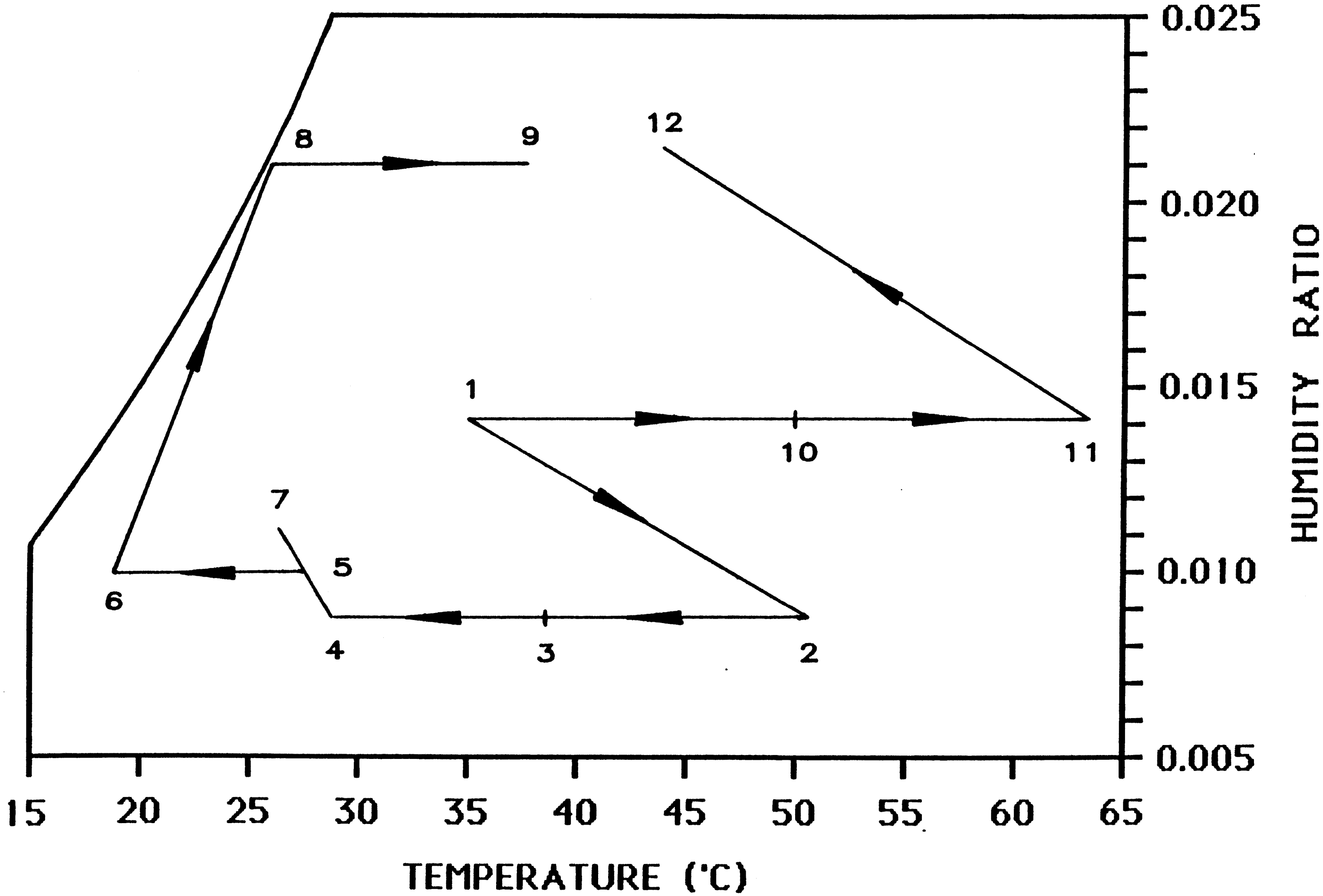

Figure 4.2.2 Process representation of ventilation cooling tower/ heat exchanger desiccant air conditioning cycle. ARI design conditions, 20% LLR, 10% ventilation, NTU's=9.0

the cooler to the conditioned space. The resultant COP based on thermal energy input is 2.08.

Figure 4.2.3 illustrates the fraction of the inlet air to the air/water heat exchanger that is delivered to the zone as a function of the latent load ratio. The fraction delivered value increases from 0.56 to 0.92 as the latent load ratio increases from 0.0 to 1.0. This curve is smooth and continuous unlike the fraction delivered values for the 2-stage IEC cycle of Section 4.1. The fraction delivered never reaches 1.0 for this design point as opposed to the 2-stage IEC where the ambient driven IEC could handle the sensible cooling at higher latent loads. The fraction delivered curve also has greatest slope at lower latent load ratios and is flatter at higher latent loads.

A plot of dehumidifier regeneration temperature as a function of latent load ratio is shown in Fig. 4.2.4 for the ventilation cycle. This curve has two distinct segments. At latent loads less than 0.5 the inlet air delivered to the dehumidifier is 100% ambient air. As the required dehumidifier outlet humidity ratio decreases, the regeneration temperature increases. At latent load ratios greater than 0.5, return zone air is recirculated and mixed with the ambient air to increase the mass flow rate through the desiccant. Since the humidity ratio after mixing the return air decreases, the required regeneration temperature also decreases.

Figure 4.2.5 illustrates how the ventilation cycle thermal COP varies with latent load ratio. This curve is seen to have a maximum

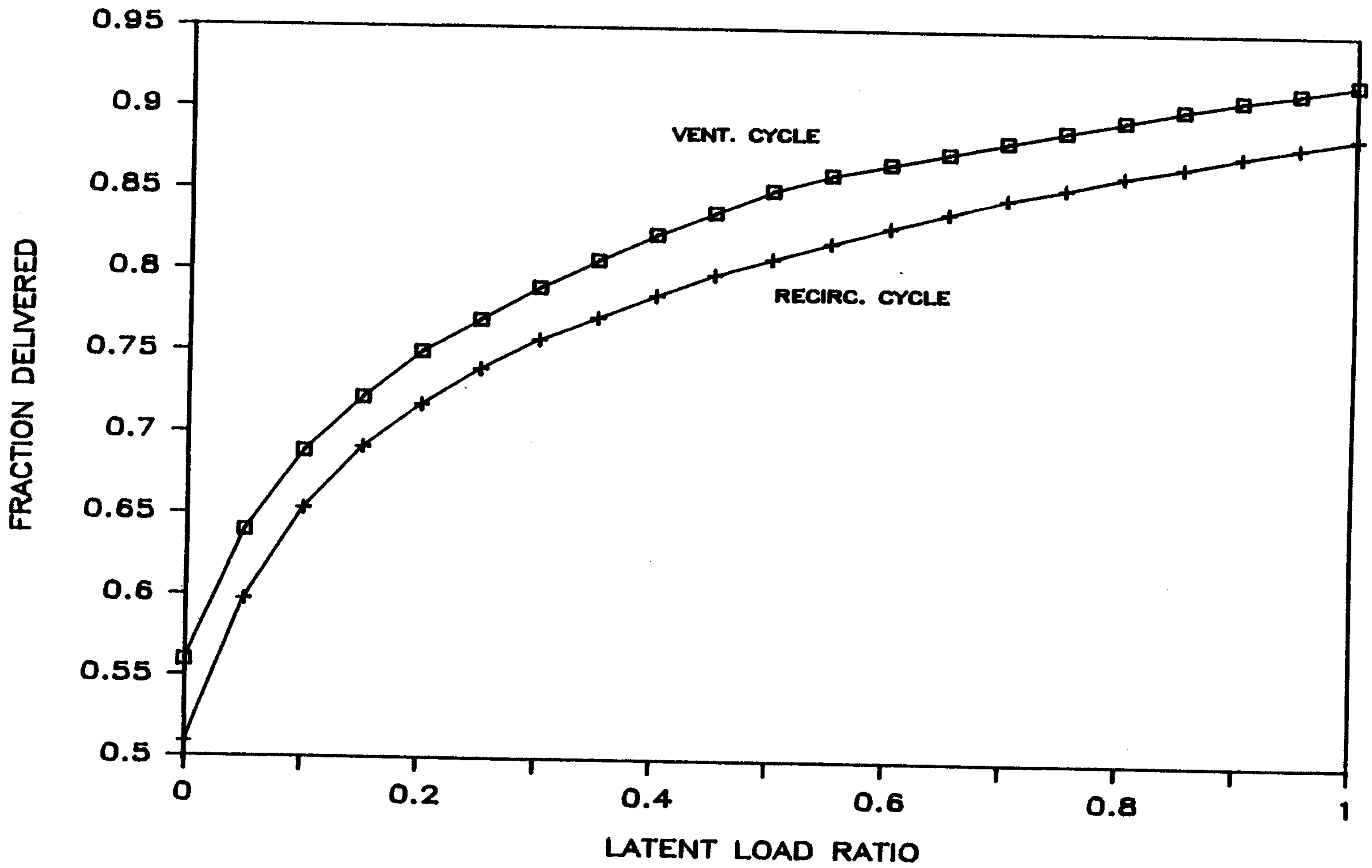

Figure 4.2.3 Fraction delivered vs latent load ratio for cooling tower/ heat exchanger cycle. ARI conditions, 10% vent., NTU=9.0

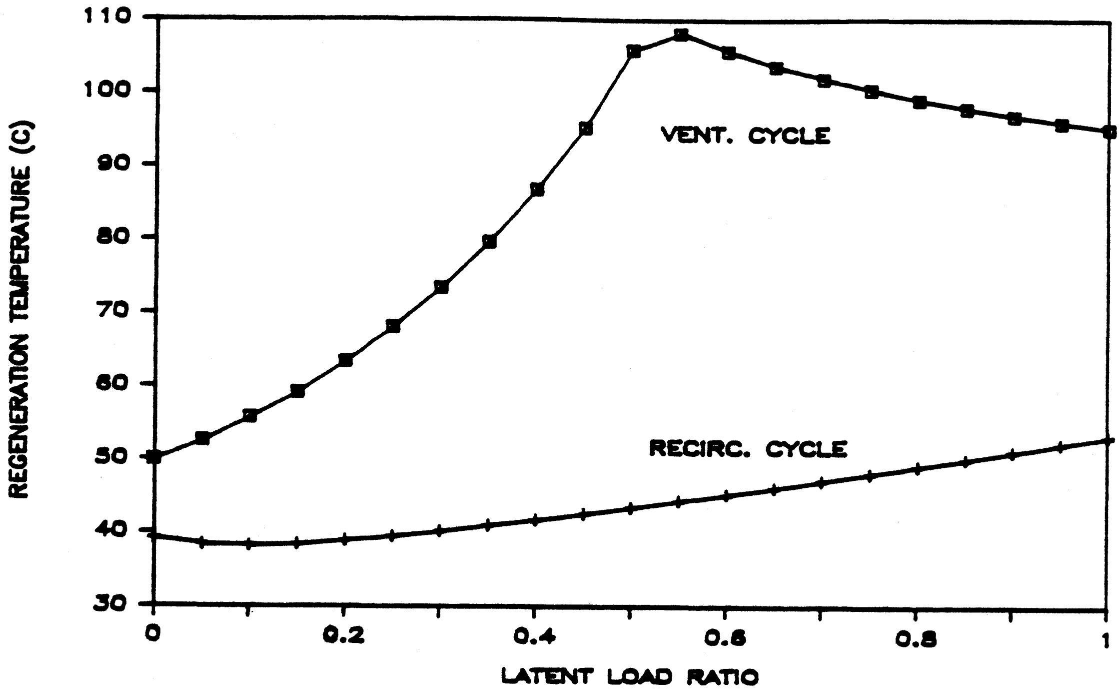

Figure 4.2.4 Regeneration temperature vs LLR for CT/HX cycle, ARI conditions, 10% vent, NTU=9.0

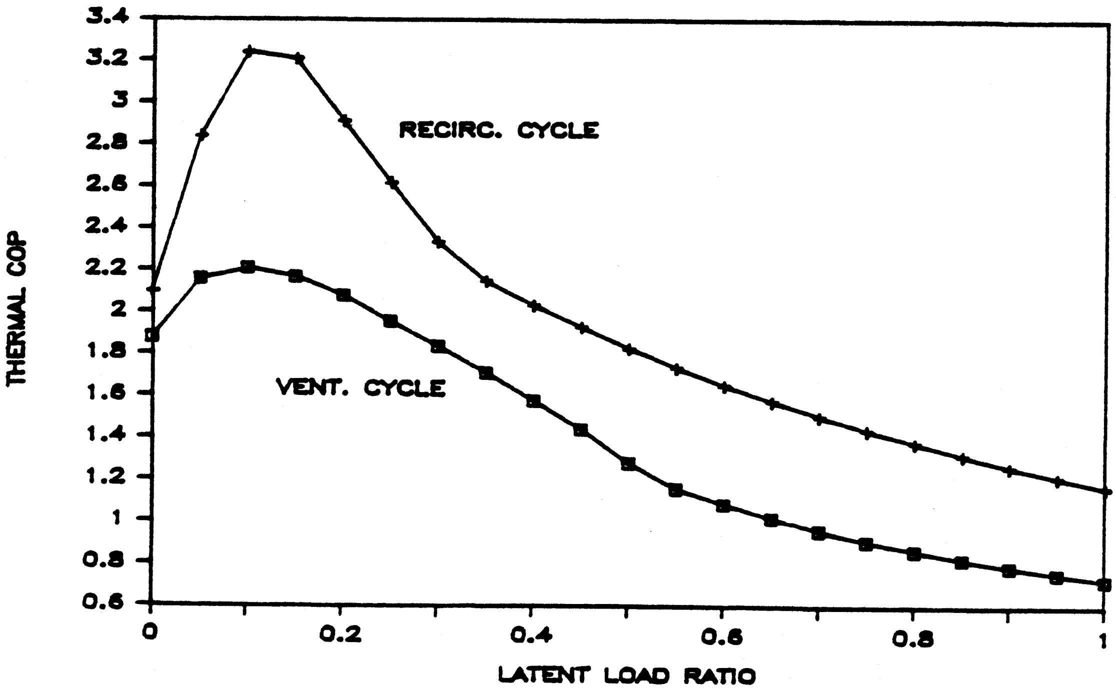

Figure 4.2.5 Thermal COP vs latent load ratio for CT/HX cycle. ARI conditions, 10% vent

COP at a latent load of 0.15. Up to a latent load 0.15, the mass flow rate of exhausted cooling tower air and hence the air through the dehumidifier and heater decreases. This decreases the energy input to the heater and boosts the thermal COP. However, at latent load ratios greater than 0.15, the required regeneration temperature continues to increase and the COP drops off gradually to 0.72 at 100% latent load.

The regeneration temperature and thermal COP for the ventilation cycle are plotted in Figs. 4.2.6 and 4.2.7 as a function of ventilation rate for a constant zone latent load ratio of 0.2. As the ventilation rate increases the regeneration temperature decreases since the mass flow through the dehumidifier increases. As mentioned earlier, to meet a given latent load, the amount of moisture reduction per unit of air increases as the mass flow rate of air through the dehumidifier decreases. The thermal COP illustrated in Fig. 4.2.7 decreases at higher ventilation rates despite this reduced regeneration temperature and is due largely to the increased mass flow rate through the dehumidifier and heater.

The cooling tower/ heat exchanger desiccant cycle may also be configured in a recirculation mode as illustrated in Fig. 4.2.8. For the same ARI conditions studied earlier, the fraction of inlet air to the air cooler that is delivered to the conditioned space is now 0.76 and the corresponding thermal COP is 2.91.

A graph of fraction delivered values for different zone latent load ratios is shown in Fig. 4.2.3 for the ventilation cycle. This

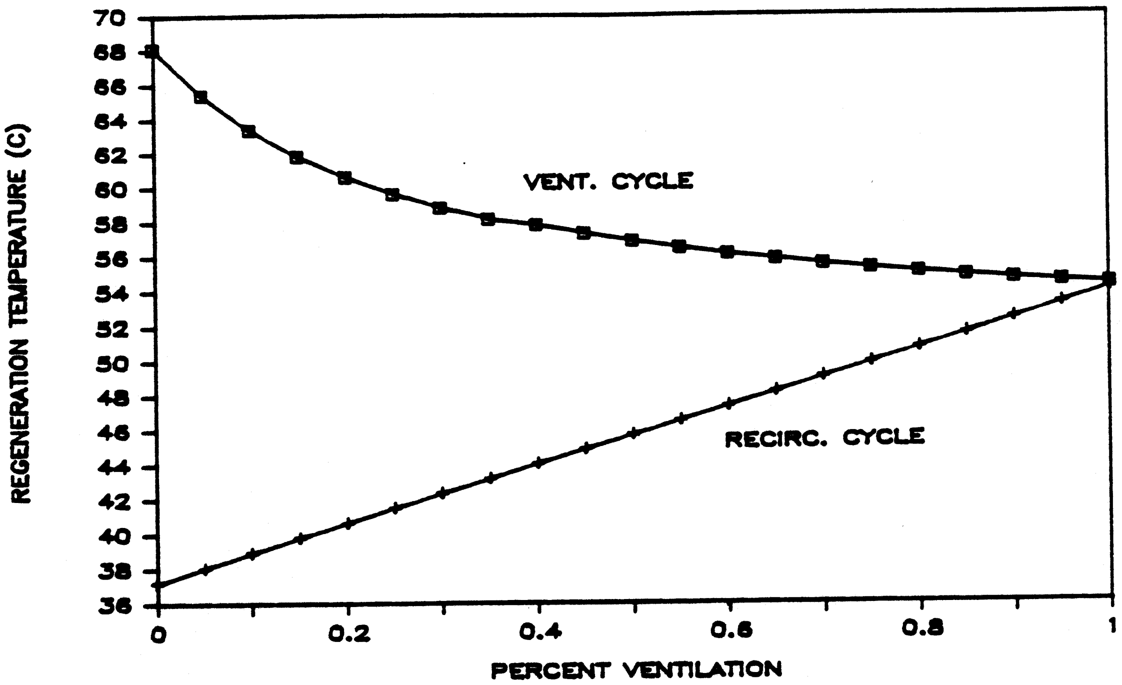

Figure 4.2.6 Regeneration temperature vs %ventilation for CT/HX cycle, ARI, 20% LLR, NTU=9.0

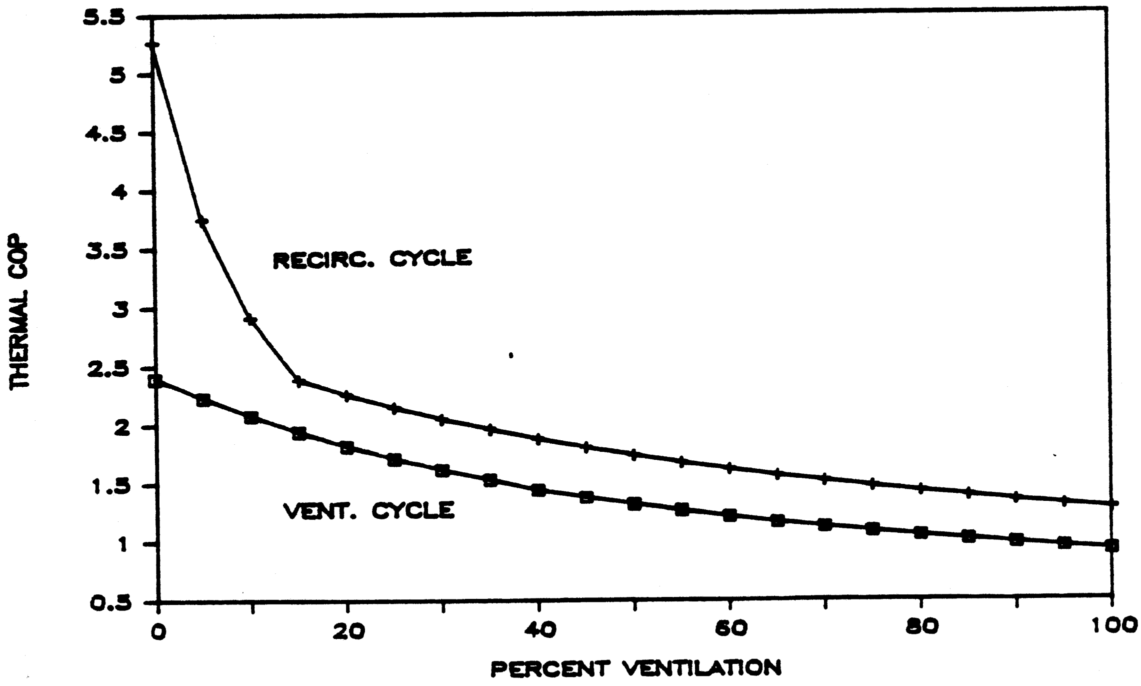

Figure 4.2.7 Thermal COP vs % ventilation for CT/HX cycle ARI conditions, 20% LLR, NTU=9.0

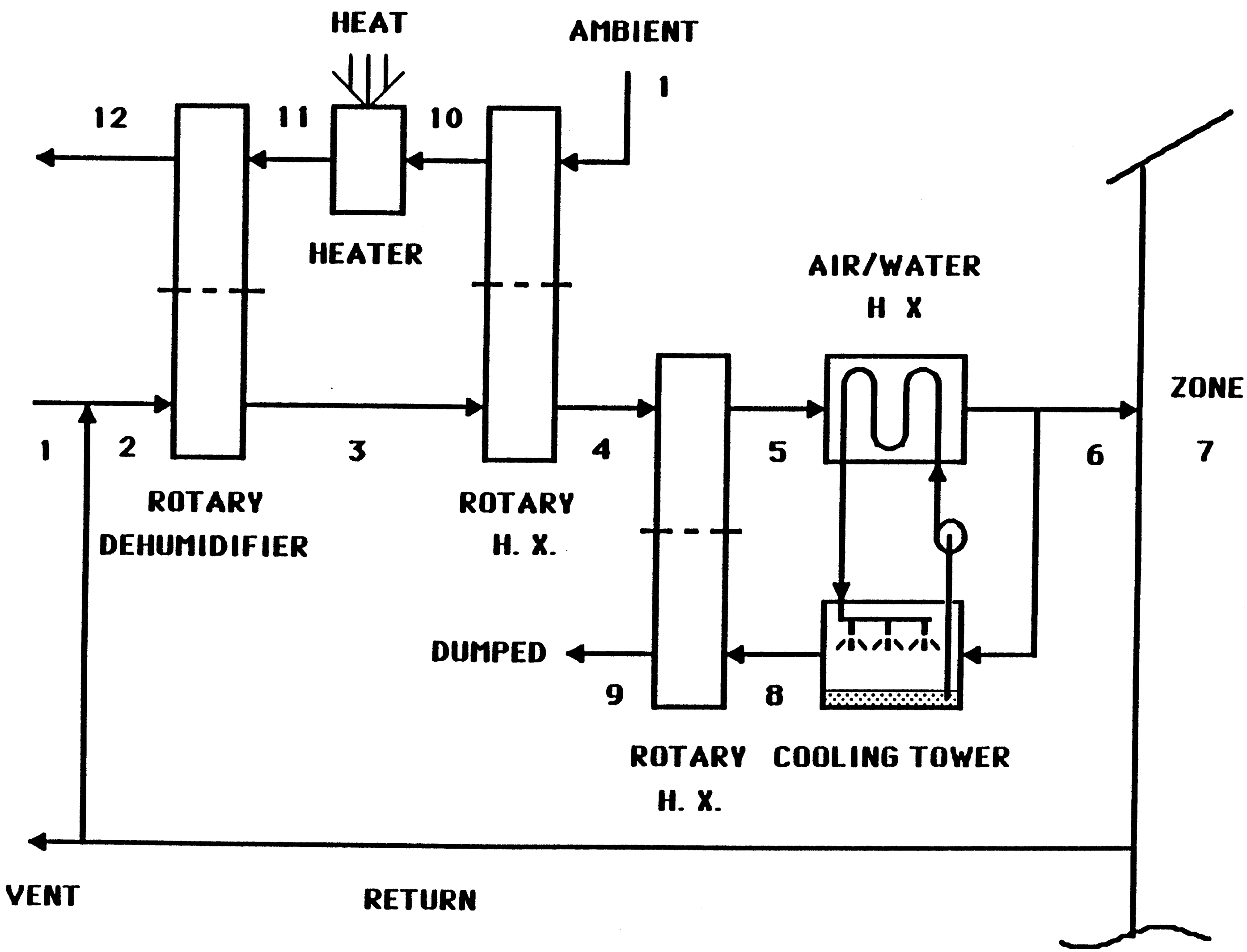

Figure 4.2.8 Schematic diagram of recirculation cooling tower/ heat exchanger desiccant air conditioning cycle

curve closely resembles the fraction delivered curve for the ventilation cycle discussed earlier in this section. The region of highest slope is at lower latent load ratios and the slope decreases as the latent load increases to 1.0. The required delivered fractions for the recirculation cycle are always slightly less then those required for the ventilation cycle.

The graph of the desiccant regeneration temperature is shown in Fig. 4.2.4 as a function of latent load ratio. A minimum exists in the regeneration temperature at low latent load ratios due to the decreasing fresh inlet air introduced to the dryer and consequent decrease in inlet humidity ratio. At latent load ratios greater than 0.2 though, the required outlet humidity ratio from the dehumidifier decreases to a greater extent then does the inlet and the resulting regeneration temperature increases slightly.

The thermal COP for the recirculation cycle is plotted in Fig. 4.2.5 along with the COP for the ventilation cycle. The recirculation COP resembles the curve for the ventilation cycle over all ranges of latent load ratio. A maximum in the COP exists at a LLR of 0.15 where the gains from the decreased heater mass flow rate outweigh the drawbacks due to the increasing regeneration temperature.

To again illustrate how the recirculation cycle performance varies with changing ventilation, a plot of dehumidifier regeneration temperature is shown in Fig. 4.2.6. The increase in regeneration temperature is nearly linear with the increase in ventilation rate.

The thermal COP is shown in Fig. 4.2.7 as a function of ventilation rate. The high COP's at low ventilation rate for this sample design point are attributed to the bypassing of the first rotary heat exchanger when the ambient temperature is greater than the exiting dehumidifier process air. At ventilation rates greater than 15%, the heat exchanger is again activated and the COP decreases gradually thereafter.

Section 4.3: Conclusions

The main difference between the recirculation and ventilation cycles for both the two-stage IEC and the cooling tower/heat exchanger air conditioning units is the location of where the return air mixes with the fresh air and the amount of air that is processed through the dehumidifier and heater. The ventilation cycle processes fresh air from the ambient through the desiccant and mixes the return air stream with the fresh air after it exits the dehumidifier. The recirculation cycle mixes return air at the entrance to the dehumidifier and dehumidifies both the fresh air and the returned zone air. The equipment in the recirculation cycles therefore tends to be larger than that found in ventilation cycles.

In comparing the two different air conditioning units discussed in this chapter several points arise. First, the cooling tower/heat exchanger (CT/HX) unit delivers higher fractions of inlet air-cooler air to the building zone then does the two-staged IEC unit. At the ARI design conditions, 20% LLR and component NTU's equal to 9.0, the

CT/HX unit and the staged IEC unit deliver 74.9% and 48.5% of the inlet air, respectively. The COP's based on thermal energy input are 2.08 and 0.96, respectively. The "fractioning" temperature control feature works well for both units, however, the CT/HX unit provides a more continuous control of outlet temperature with fraction delivered than does the staged IEC. At fractions less then 0.5, the staged IEC has limited utility for temperature control. Overall, the staged IEC may be a less complicated air conditioning unit and more technologically feasible than the CT/HX unit (See Section 3.6).

In general, both cycles present favorable changes to the classical ventilation and recirculation desiccant cycles. Replacing the direct evaporative coolers with sensible air chillers results in 25% and 170% higher COP's for the two-staged IEC and CT/HX cycle, respectively, over a thermal COP of 0.77 for the classical ventilation cycle at ARI conditions (See Section 2.3). A further advantage of using these new sensible air coolers is that a control feature has been added to the cycles. The classical desiccant cycles rely on varying heat exchanger and direct evaporative cooler effectiveness to control the supply air temperature. This control technique may be difficult to implement [Curt, 1986]. The control scheme called for in these new systems, however, relies only on the splitting of the supply stream into two parts and channeling one stream through an alternate piece of equipment. This is a common air conditioning practice which could be carried out by an adjustable dampering system placed in the ducting network.

CHAPTER 5. COMPONENT MODELS FOR CYCLE SIMULATION STUDIES

In Chapter 4, two new desiccant air conditioning cycles, entitled the staged IEC and the cooling tower/heat exchanger cycles, were studied in single design-point simulations. These simulations were for ARI ambient and zone conditions. While these design-point runs are instructive in understanding how control schemes and individual components interact with each other, they do not give information regarding how a particular system performs in a certain climitological region and under different zone loading conditions.

To get a better feel for how a system performs at different sets of conditions and loads, seasonal computer simulations must be run. Because this particular study is concerned with the performance of different desiccant systems in Wisconsin climate and because the power utility for which this work is being performed is located primarily in the center of this state, Madison weather data [Solmet, 1983] was used exclusively throughout this thesis.

TRNSYS [Klein, 1983], a transient energy system simulation program was used to study cycle performance throughout one typical meteorological cooling season. TRNSYS is a program that simulates energy systems using models of the individual components in an entire system coupled together in a networking fashion. With this modular configuration, separate pieces of information, such as mass flow rates or temperatures, may be passed between subsystems within the total system. During a simulation, information is exchanged between components until total system convergence is achieved.

For the research conducted in this thesis, each individually studied cycle is formulated in a TRNSYS compatible form as one complete component. This one component contains all subsystem models and numerical convergence is calculated within this one component. Although this is not the way TRNSYS is typically used, there are several advantages to running TRNSYS in this form. First, if all of the program iterations are conducted in one component, then convergence is much faster then if TRNSYS iterates between all of the possible system components. Because seasonal simulations can be time consuming, any reduction in computational effort is important. A second advantage in modeling an entire system with one component is that any zone may be combined with that one component for quick comparison studies.

This chapter gives information on the specific models used to describe the individual components within a single cycle. This chapter will also describe the convergence techniques and control hierarchy used to arrive at steady state operating points at every simulation time step.

Section 5.1: Silica Gel Rotary Dehumidifier

The dehumidifier model used throughout this thesis predicts the performance of a rotary wheel silica gel dehumidifier. This model uses an effectiveness-NTU model developed by Van den Bulk, Mitchell and Klein [1985] to compare the performance of an ideal dehumidifier with infinite heat and mass transfer coefficients to a real dehumidifier with finite resistance to heat and mass transfer.

The performance of the rotary dehumidifier depends on many variables. The inlet regeneration and process air states, as well as physical design parameters such as dehumidifier wheel speed and the relative mass flow rate of the process and regeneration streams combine to yield widely different dehumidifier performance.

In the general theory of regenerators, a dimensionless capacitance rate parameter, Γ_p, is defined as:

$$\Gamma_p = \frac{\text{mass of desiccant/time in rotation}}{\text{mass flow rate of process air}} \tag{5.1.1}$$

This parameter compares the mass of the desiccant and the time for the wheel to turn through one full cycle with the mass flow rate of the air through the process side of the wheel. From optimization studies, Van den Bulck, Mitchell and Klein [1986] have shown that for cycles operating in ventilation modes near ARI ambient conditions, the optimum Γ_p value is 0.15 and the regeneration air mass flow rate is 0.8 times that of the process stream. For cycles operating in a recirculation mode near ARI zone conditions, Γ_p equals 0.1 and the regeneration flow rate is 0.6 times the process air mass flow rate. The optimum parameters vary with regeneration temperature and the inlet humidity ratio.

Two effectivenesses are also defined to fix the outlet process air stream state.

$$\varepsilon_\omega = \frac{\omega_{in} - \omega_{out}}{\omega_{in} - \omega_{out,ideal}} \tag{5.1.2}$$

$$\varepsilon_h = \frac{h_{in} - h_{out}}{h_{in} - h_{out,ideal}} \tag{5.1.3}$$

These effectivenesses compare the actual outlet air humidity ratio and enthalpy with the ideal outlet air state that would result if there were infinite heat and mass transfer coefficients between the air and the desiccant. Figure 5.1.1 shows ε_ω as a function of the overall number of transfer units with C^* as a parameter for a Lewis number of unity. C^* is a dimensionless ratio analogous to the ratio of capacitance rates seen in general heat exchanger theory. C^* may be written as:

$$C^* = \frac{\Gamma_P}{\Gamma_{P,R}} \tag{5.1.4}$$

where $\Gamma_{P,R}$ is the optimal flow rate parameter which minimizes the dehumidifier outlet humidity for given inlet states, wheel rotational speed, and infinite transfer coefficients.

For the sake of computational simplicity, Eq. (5.1.2) is used in a slightly modified form as:

$$\varepsilon_m = \frac{\omega_{in} - \omega_{out}}{\omega_{in} - \omega_{out,int}} \tag{5.1.5}$$

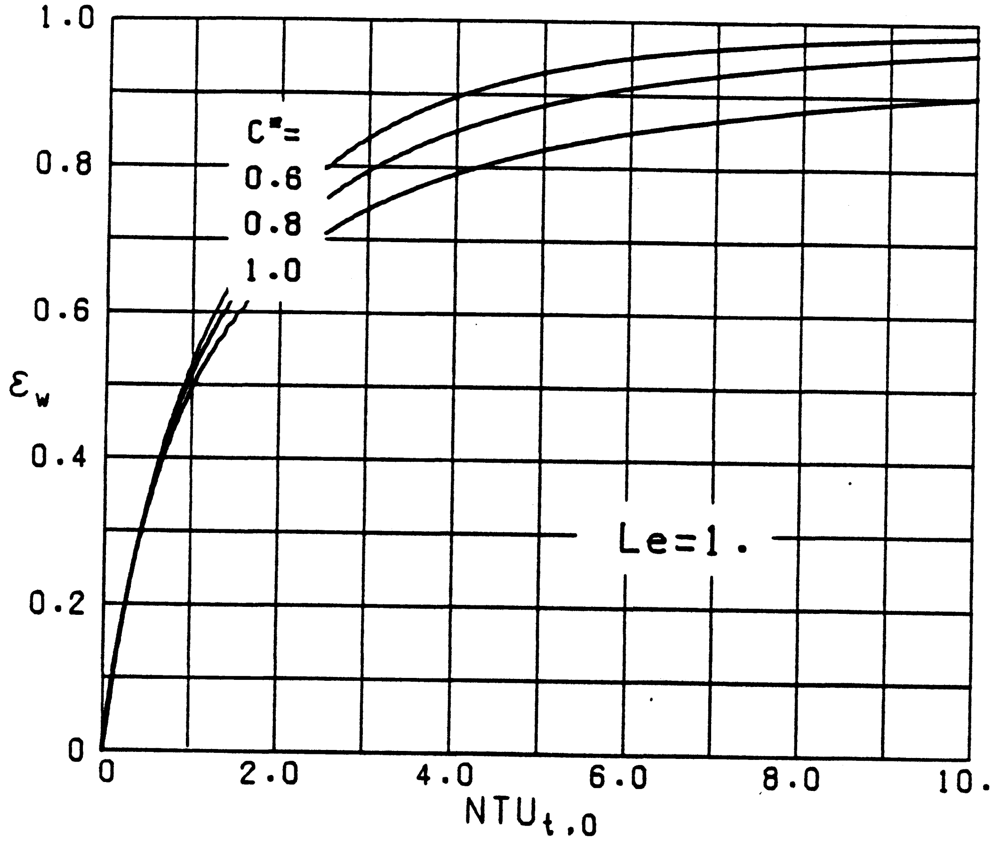

Figure 5.1.1 Moisture effectiveness for various C^*s at Le=1.0. From Van den Bulck, et al, 1985.

C^*	$W_{out,ideal}$	$\varepsilon_w / \varepsilon_m$	ε_w	ε_m
0.6	4.03 g/kg	0.90	0.97	0.87
0.8	3.72	0.92	0.93	0.86
1.0	3.52	0.94	0.88	0.82

$\overline{\varepsilon_w} = 0.93$ $\overline{\varepsilon_m} = 0.85$

Table 5.1.1 Comparison of ε_w and ε_m for various C^*s at an inlet state of 25C, 15g/kg and 85C regeneration temperature. Wout,int=2.75 g/kg.

where $W_{out,int}$ is the ideal process air outlet humidity ratio predicted by the intersection point method [Maclain-cross, 1972]. The calculations required to obtain $W_{out,int}$ are less involved than those required to calculate $W_{out,ideal}$. The outlet air state predicted by the intersection point method, however, overpredicts the degree of dehumidification performed by the desiccant when compared to the outlet state predicted by the effectiveness-NTU model. In an attempt to quantify the degree of over-prediction, a typical inlet state and regeneration temperature of 25°C and 0.015 kg/kg and 85°C, respectively, was investigated for C^*'s ranging from 0.6 to 1.0. Table 5.1.1 lists some of these results. Column 2 of this table lists the ideal outlet dehumidifier state as predicted by the effectiveness-NTU model and column 3 lists the ratio of the moisture effectivenesses, $\varepsilon_\omega/\varepsilon_m$, as determined from Eqs. (5.1.2) and (5.1.5). From Fig. 5.1.1, at an overall dehumidifier NTU of 7.5, ε_ω values may be obtained and the corresponding ε_m of column 5 may be calculated. From these numbers, ε_m can be expressed in terms of ε_ω by means of a correction factor:

$$\varepsilon_m \approx 0.93 * \varepsilon_\omega \tag{5.1.6}$$

For an overall NTU of 7.5, and a Lewis number of 1.0, the average ε_ω from Table 5.1.1 is 0.93 and the corrected average ε_m is 0.85. It has been shown that the corresponding enthalpy effectiveness (Eq. (5.1.3)) may be assumed unity and is held constant for all of the simulations conducted in this study [Van den Bulck, Mitchell, Klein, 1985].

In generalizing Eq. (5.1.6) for inlet states near the above average state, it is believed that representative and acceptable predicted outlet states will result through its use.

A "smart" control system must be employed to operate the rotary dehumidifier near its optimum operating point. To obtain the optimum performance, sensors would have to detect both the process air inlet state and mass flow rate. With this information, the controller would then continuously adjust the wheel speed and regeneration air mass flow rate to minimize the process air outlet humidity.

Section 5.2: Cooling Tower/Heat Exchanger Air Cooler

The cooling tower/heat exchanger air cooler was discussed in Section 3.6. The mathematical model used to analyze this cooler has been previously outlined in Section 3.6 and is further described in Appendix A. To arrive at the steady-state solution for any possible inlet air state requires two nested iteration loops. To converge at solutions is therefore a lengthy and inefficient process for use in seasonal simulations. To facilitate long running simulations, a different scheme was therefore devised to hasten the convergence process. A program was written that optimizes the cooling tower/heat exchanger air cooler performance and then was used to simulate the cooling unit over a broad range of temperatures, humidity ratios and fractions delivered. The performance data from this program was then stored in files for later retrieval. An interpolating subroutine retrieves this performance data during simulations when given the air states and fraction delivered value. This interpolating scheme is fast and saves much computing time. A copy of the program source code used to generate and retrieve the required chiller information is listed in Appendix B.

Section 5.3: Heat Exchangers

The heat exchangers used in all of the cycles investigated in this thesis are modeled with standard effectiveness-NTU equations for a counterflow configuration. The effectiveness for the heat exchanger may be calculated with Eq. (5.3.1) when the NTU for the heat exchanger is specified.

$$\varepsilon_{CFHX} = \frac{1 - \exp(-NTU*(1 - C_{min}/C_{max}))}{1 - (C_{min}/C_{max})*\exp(-NTU*(1 - C_{min}/C_{max}))} \qquad (5.3.1)$$

The capacitance rate for each flow stream is then calculated and the heat transfer rate for each stream may be determined from Eq. (5.3.2) as

$$q = \varepsilon_{CFHX}*(\dot{m}c_p)|_{min} * \Delta T_{max} \qquad (5.3.2)$$

where $\dot{m}*c_p|_{min}$ is the minimum capacitance rate flow stream and ΔT_{max} is the maximum temperature difference across the heat exchanger.

Section 5.4: Fan Work and Pumping Power

The cycles discussed in chapter 6 need fans to move the air through the system components. The energy input to these fans may be calculated with Eq. (5.4.1).

$$\dot{W} = \dot{m}\Delta p/(\rho*\eta_f) \tag{5.4.1}$$

The efficiency term, η_f, in Eq. (5.4.1) takes into account the inefficiencies in both the motor and the fan. A value of 0.50 is used exclusively throughout this thesis as a representative value of η_f.

Because the pressure drop is a function of the air mass flow rate, Eq. (5.4.2) corrects the pressure drop term with standard fan laws.

$$\Delta p = \Delta p_{base}*(\dot{m}/\dot{m}_{base})^2 \tag{5.4.2}$$

The flow rate, $\dot{m}_{base}$, is the air mass flow rate which corresponds with the base pressure drop, ΔP_{base}. Substituting Eq. (5.4.2) into Eq. (5.4.1) for the fan pressure drop yields Eq. (5.4.3).

$$\dot{W} = \frac{\Delta p_{base}}{\rho*\eta_f} * \frac{\dot{m}^3}{\dot{m}^2_{base}} \tag{5.4.3}$$

Section 5.5: Simple Zone Model

To simulate how a certain air conditioning system operates under different loading conditions, it is necessary to develop a TRNSYS compatible zone model. A simple model was therefore written to output both the sensible and latent cooling loads once given certain specified inputs. These inputs include the zone overall heat transfer conductance-area product, UA, the solar thermal energy load, $\dot{Q}_{solar}$, as well as information regarding the time dependent internal instantaneous sensible gains, $\dot{G}$, and moisture generation rate, $\dot{m}_{gen}$. The total instantaneous sensible gains to the zone are calculated with Eq. (5.5.1).

$$\dot{Q}_{sensible,total} = \dot{G} + \dot{Q}_{UA} + \dot{Q}_{solar} + \dot{Q}_{infil} \qquad (5.5.1)$$

where the gains due to infiltration may be expressed as:

$$\dot{Q}_{infil} = \dot{m}_{infil} c_{pa} * (T_{ambient} - T_{zone}) \qquad (5.5.2)$$

The total latent load is calculated with Eq. (5.5.3).

$$\dot{Q}_{latent,total} = h_{fg} * (\dot{m}_{gen} + \dot{m}_{infil}(\omega_{ambient} - \omega_{zone})) \qquad (5.5.3)$$

This model is quite simple in its structure and does not take into account any building heat or moisture capacitance. The loads that are output every time step therefore are due strictly to instantaneous gains; there is no contribution to the zone load due to the release or storage of sensible or latent energy. The fundamental reason for ignoring the building capacitance is to simplify the analysis of the results generated from the various cycle models. Adding capacitance to the zone would only serve to confuse the issue of what zone attributes contribute to the observed cycle performance.

Because the zone model does not include capacitance affects, the zone air state is kept constant and is not allowed to float. For this study, the zone was maintained at ARI conditions (26.7°C and 0.0111 kg/kg). The internal sensible gains and moisture generation is simulated and passed to the zone model as an output from TRNSYS forcing functions.

Section 5.6: Cycle Convergence Procedure

For any of the desiccant air conditioning cycles introduced in Chapter 4 to come to steady-state conditions, a series of systematic steps must be taken. Because both of the proposed cycles discussed in Chapter 4 rely on dumping part of the cooled process air to the ambient, the convergence mechanism must center around choosing the correct fraction of the air entering the chiller that is delivered to the zone. To start the convergence procedure, a guess is therefore made at the value of the fraction delivered. From this one guess, a series of calculations are made to determine flow rates and state points around the cycle. The first calculation that is made determines the required ambient fresh air mass flow rate.

$$\dot{m}_{ambient} = \dot{m}_{vent} + \dot{m}_{supply}*((1.0/F) - 1.0) \qquad (5.6.1)$$

Here $\dot{m}_{vent}$ equals the required ventilation rate and F is the fraction of air cooled in the air chiller that is delivered to the zone.

For the recirculation cycles, the required outlet humidity ratio from the dehumidifier is equal to the supply humidity ratio calculated by Eq. (2.0.1). The ventilation cycles, however, mix return zone air with the air exiting the dehumidifier. Equation (5.6.2) therefore calculates the humidity ratio required at the outlet of the dehumidifier for the ventilation cycles.

$$\omega_{deh,o} = ((\dot{m}_{deh,i} + \dot{m}_{return})*\omega_{supply} - \dot{m}_{return}*\omega_{zone})/\dot{m}_{deh,i} \qquad (5.6.2)$$

Here $\dot{m}_{deh,i}$ equals the inlet mass flow rate to the dehumidifier and $\dot{m}_{return}$ equals the supply air mass flow rate less the required ventilation rate. Once given the exiting dehumidifier humidity ratio, the corresponding regeneration temperature is chosen that will delivere this required humidity reduction.

The next step at arriving at the steady-state conditions is to determine the temperature of the air entering the air cooler. If the air conditioning cycle uses the cooling tower/heat exchanger unit, then this temperature is passed back from the interpolating subroutine discussed in Section 5.2. If the air conditioning cycle uses the staged IEC's, then a separate iteration is required to determine the correct temperature at the entrance to the first IEC that will yield the correct supply temperature with the guessed value of fraction delivered. A final calculation is made to determine the temperature of the air exiting the second rotary heat exchanger. This calculation can only be made after the inlet state to the air cooler is found since the air chiller exhaust acts as the heat sink for the heat exchanger. Once the temperature exiting the second rotary heat exchanger is known, a comparison of this temperature is made with the temperature calculated earlier as the inlet to the air chilling unit. In the ventilation cycle, an intermediate mixing calculation is required before this comparison can be made. When the guessed fraction delivered value is correct, then, depending on whether the cycle is in the ventilation or recirculation mode, the inlet temperature to the air chilling unit will equal either the temperature leaving the mixer or the second rotary heat exchanger, respectively. If the two temperatures are not in close enough agreement, then a new fraction delivered value is assumed and the process is repeated.

In an actual simulation, the first guessed fraction delivered is always set to 1.0. This fraction corresponds to turning the chiller off and provides a test to determine if cooling is required at all. The second guessed fraction delivered is always equal to the last successful guess from the previous time step in the simulation. The secant method is then used to rapidly converge to the correct steady-state operating conditions.

Section 5.7: Program Controls

There are several control features built into the desiccant models studied in this thesis. The first control feature checks whether there is a load on the zone. If there is no load, and there is, at the same time, no ventilation requirements, then the entire air conditioning unit may be turned off. Under this condition, both the thermal and electric energy input to the cycle is set to zero.

If there is no load on the zone and there is a positive need for ventilation air, then the supply air state is set equal to the zone state. The convergence procedure as outlined in Section 5.6 then proceeds as usual. If, however, there is a non-zero load on the zone, then the supply states are calculated with Eqs. (5.7.1) through (5.7.3).

$$h_{supply} = h_{zone} - \Delta h_{supply} \tag{5.7.1}$$

$$\dot{m}_{supply} = (\dot{Q}_{sen,total} + \dot{Q}_{lat,total})/\Delta h_{supply} \tag{5.7.2}$$

$$\omega_{supply} = \omega_{zone} - \dot{Q}_{lat,total}/(\dot{m}_{supply} * h_{fg}) \tag{5.7.3}$$

Depending on the user determined enthalpy difference across the supply and return air streams, Δh_{supply}, the supply air stream enthalpy and mass flow rate may be calculated with Eq. (5.7.1) and (5.7.2), respectively. The supply humidity ratio is calculated with

Eq. (5.7.3). Once these supply states are determined, the convergence procedure discussed in Section 5.6 is implemented.

A further control check is made regarding the air mass flow rate through the dehumidifier. As mentioned in Section 4.1 and 4.2, a situation may arise in system operation where there is insufficient mass flow through the dehumidifier. In these cases, there is not enough moisture in this stream available for removal to meet the latent load on the zone. The occurrence of such a situation in a simulation is detected by Eq. (5.6.2). This equation calculates the required humidity ratio at the exit of the dehumidifier. If this humidity is below a predetermined minimum level, then either return air is recirculated and mixed with the inlet ambient air or more fresh ventilation air is brought in from the ambient. The amount of recirculated air or extra ventilation air is given by Eq. (5.7.4).

$$\dot{m}_{\text{vent or recirc}} = \{\dot{m}_{\text{ambient}}*(\omega_{\text{supply}} - \omega_{\text{min}}) + \dot{m}_{\text{return}}*(\omega_{\text{supply}} - \omega_{\text{zone}})\}/(\omega_{\text{min}} - \omega_{\text{zone}}) \tag{5.7.4}$$

The minimum allowable humidity ratio, ω_{min}, is a value specified by the user of the system. When air is recirculated or new air is ventilated, the outlet humidity is set equal to this minimum humidity level. The remainder of the convergence procedure outlined in Section 5.6 is then carried out.

Varying the minimum allowable dehumidifier outlet humidity ratio between 0.002 and 0.006 kg/kg produces negigible effects on the overall cycle thermal COP. Using higher ω_{min} settings does, however, decrease the required regeneration temperature at the heater outlet whenever more air is processed past the desiccant. Furthermore, using a higher value for ω_{min} will require processing more air past the desiccant more often than it is when a lower humidity ratio setting is used. For the simulations conducted in Chapters 6 and 7, ω_{min} is set to 0.004 kg/kg.

Another control feature monitors the fraction of the air entering the chiller that is delivered to the zone. If this fraction delivered value ever drops below a minimum pre-selected value, then the cooler unit is undersized for the given load. At this point, to successfully meet the sensible cooling requirements on the chiller, more air must be processed through the chiller to decrease its required temperature drop. To increase the mass flow rate of air through the cooler, a smaller enthalpy difference must be specified across the supply and return zone air streams. Whenever the air cooler is deemed too small, this enthalpy difference is decreased incrementally until the resultant temperature decrease across the chiller is sufficient to handle the cooling load. Every time it is decided that the air chiller is too small, however, the iteration scheme outlined in Section 5.6 must be restarted.

One final control mechanism monitors the temperature and humidity difference across each of the rotary components in the system.

If, for example, the air entering the dehumidifier is drier then it needs to be at the exit of the dehumidifier, the unit is turned off by stopping the wheel rotation. Also, if there is no potential for cooling across any of the rotary heat exchangers, then they too are turned off.

CHAPTER 6: SEASON SIMULATIONS OF DESICCANT AIR CONDITIONING CYCLES

In Chapter 4 the cooling tower/heat exchanger and the staged IEC advanced desiccant air conditioning cycles were studied. In Chapter 5, the idea of performing seasonal simulations with the use of TRNSYS, a transient system simulation program was then introduced. The individual components that make up entire systems were discussed and then system controls and convergence procedures were studied. In this chapter, those TRNSYS models are exercised and the results for seasonal simulations with Madison, Wisconsin weather data and a building zone that models a typical Wisconsin commercial building are presented.

Of the two new cycles studied in Chapter 4, the cooling tower/ heat exchanger cycle showed the most potential for air conditioning over the broadest range of zone latent loads. For this reason, only this cycle will be considered in this chapter. Resulting simulation histograms for regeneration temperature, energy input and fraction delivered values are shown. Finally, for comparison purposes, seasonal simulation results are shown for the same building zone when conditioned with the classical ventilation and recirculation desiccant cycles.

Section 6.1: Typical Wisconsin Commercial Building Zone

Before seasonal simulations may be run, a sample building zone must first be formulated. The zone used in this chapter is a typical three story commercial building with a total floor area of 2790 square meters. Table 6.1.1 summarizes the specific building characteristics and information about the air conditioning loads. Because this building is assumed to be occupied during the day-time hours only, the simulated internal sensible and moisture gains are scheduled such that during unoccupied hours, the loads are scaled back to 25% of that experienced during occupied hours. The required ventilation rate for a typical building is dictated by design code [DILHR, 1982]. During occupied hours, a ventilation rate of 1/2 room air changes per hour is assumed. During unoccupied hours, no fresh ventilation air is provided.

Figure 6.1.1 illustrates how the air conditioning loads on the zone vary with the hour of the day for July 19, a typical July day. Several points may be made with regard to Fig. 6.1.1. First, the scheduling of the internal gains on the zone load are very apparent. Between hours 17 and 7 (5 PM to 7 AM), the building is vacant and internal loads are low. During the day-time hours, 7 AM to 5 PM, the loads increase due to lighting, occupation, equipment usage, solar gains, etc. The peak air conditioning load occurs at hour 15 and corresponds to the peak in both the solar and the envelope conductance gains on the zone. During the day-time hours, the latent load ratio is approximately 0.10. During the unoccupied hours, the zone latent load ratio ranges from 0.5 to 1.0. These high latent loads are attributed to the negative cooling load on the building from the envelope conductance losses. A final point is that the majority of

PARAMETERS FOR SAMPLE ZONE

FLOOR AREA	2790 m^2	(30,000 ft^2)
BUILDING VOLUME	9302.5 m^3	(328,500 ft^3)
WALL AREA	1828 m^2	(19,680 ft^2)
WINDOW AREA	322 m^2	(3470 ft^2)
WALL CONDUCTANCE	1.32 $W/m^2 \cdot C$	(0.234 Btu/hr-ft^2-F)
WINDOW CONDUCTANCE	3.50 $W/m^2 \cdot C$	(0.62 Btu/hr-ft^2-F)
OVERALL CONDUCTANCE	3540 W/C	(4805 Btu/hr-F)
ZONE TEMPERATURE	26.7 C	(80 F)
ZONE HUMIDITY RATIO	0.0111 kg/kg	

	7 AM-5 PM	5 PM - 7 AM
SENSIBLE GENERATION	32.3 W/m (3 W/ft^2)	8.1 W/m^2 (0.75 W/ft^2)
MOISTURE GENERATION	5.4 kg/hr-1000m^2 (1 lb/hr-1000ft^2)	1.4 kg/hr-1000m^2 (0.25 lb/hr-1000ft^2)
VENTILATION RATE	0.5 Air change/hr (5580 kg/hr)	-0- -0-

Table 6.1.1 Zone parameters for typical Wisconsin commercial building used in season simulations

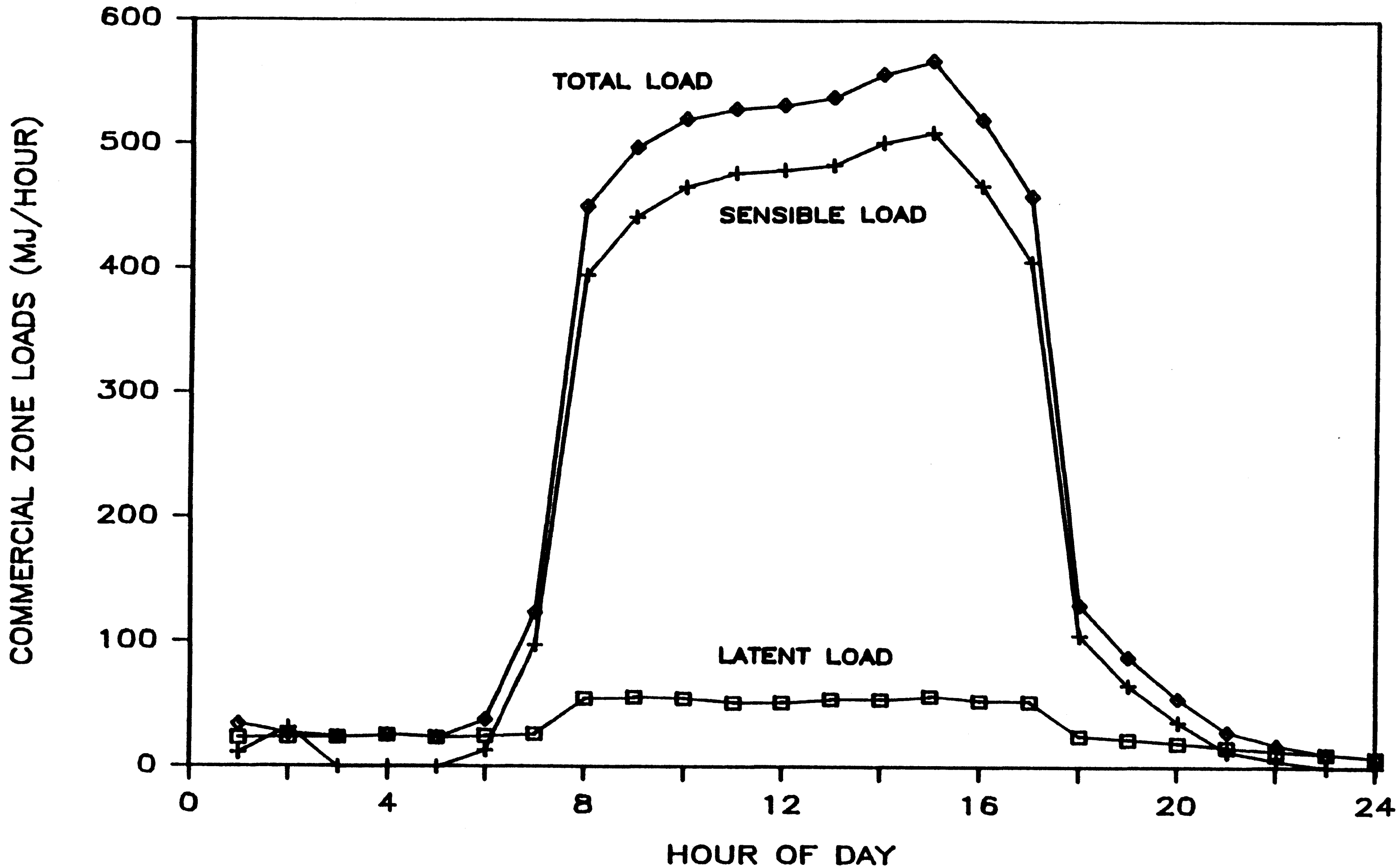

Figure 6.1.1 Air conditioning loads on typical Wisconsin commercial building for July 19

the sensible load on the zone is attributed to internal gains. The building envelope losses or gains contribute very little towards the total sensible load on the zone.

Section 6.2: July 19 Desiccant Air Conditioning Simulations

To better understand how the cooling tower/heat exchanger air conditioning unit performance varies with the time of day, the CT/HX unit is combined with the sample zone of Section 6.1 and this entire system was simulated for July 19. July 19 is both hot and humid, requiring zone dehumidification and sensible cooling. Figure 6.2.1 shows a plot of the regeneration temperature as a function of the hour of the day for a system with component NTU's equal to 9.0. For the cycle operating in the ventilation mode, regeneration temperatures range from 85°C to 50°C. During unoccupied hours, where the loads on the zone are mostly latent, higher regeneration temperatures are required then during the day-time hours when the latent load is approximately 10% of the total load.

The regeneration temperatures for the recirculation cooling tower/heat exchanger cycle are also shown in Fig. 6.2.1. These temperatures follow the same pattern as does the regeneration temperature for the ventilation cycle, however, these temperatures, on the whole, vary between 50°C and 35°C. The lower regeneration temperatures seen in the recirculation cycle are due to the lower inlet humidity ratio at the dehumidifier entrance and the reduced degree of dehumidification required across the dehumidifier.

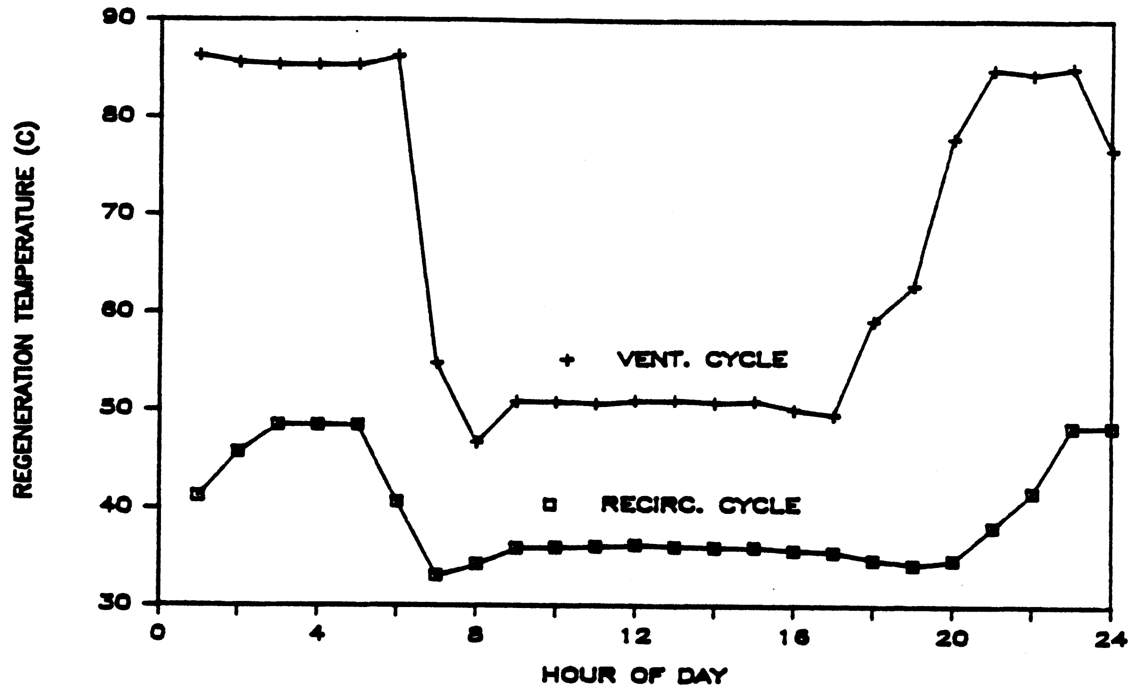

Figure 6.2.1 Regeneration temperature vs hour of day for typical Wisconsin zone, July 19, CT/HX cycle

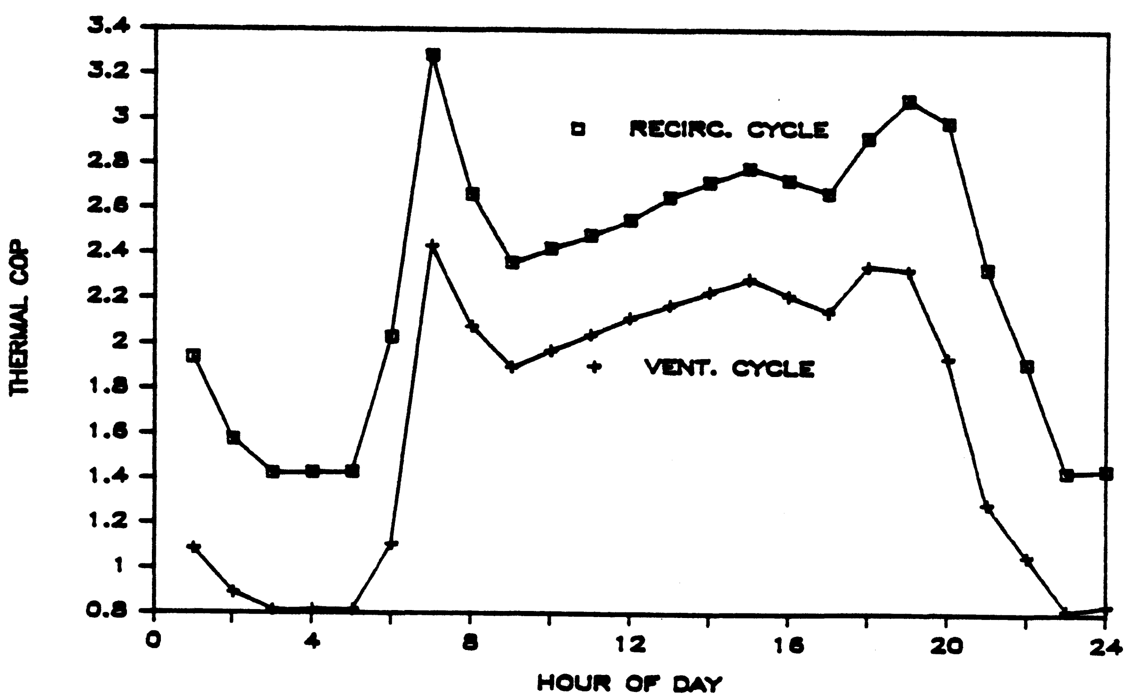

Figure 6.2.2 Thermal COP vs hour of day for typical Wisc. commercial zone, July19, CT/HX cycle

Figure 6.2.2 is a plot of the thermal coefficient of performance for both units as a function of the time of day. At early and late times of the day, when the latent loads are dominant, the coefficient of performance is lower than when the latent load ratio is lower. At all times, the COP is higher for the recirculation cycle and in the range of 1.4 to 3.2. The daily energy-averaged thermal COP for this day is 2.57 for the recirculation cycle and 2.03 for the ventilation cycle.

Figure 6.2.3 is a plot of the fraction of the air that enters the cooling tower/heat exchanger air cooler that is delivered to the zone as a function of the time of day for the ventilation cycle. This flow rate follows the same pattern as does the regeneration temperature and thermal COP. At early and late hours, the latent load is high and the supply state is not required to be as cold as it is at lower latent loads (see Fig. 4.1.1). Because not as much sensible cooling is required of the air chiller, only a small amount of air must be exhausted to the ambient and the resulting fraction delivered is near unity. At the lower latent loads, that is, in the day-time hours, the supply state must be colder then at the higher latent loads and the resulting fractions delivered decrease to near 0.7.

Figure 6.2.3 suggests that two constant fraction delivered settings may be used with this building when it is both occupied and unoccupied. The fraction delivered is a function of the latent load ratio (see Section 4.1). During occupied hours, when the latent load

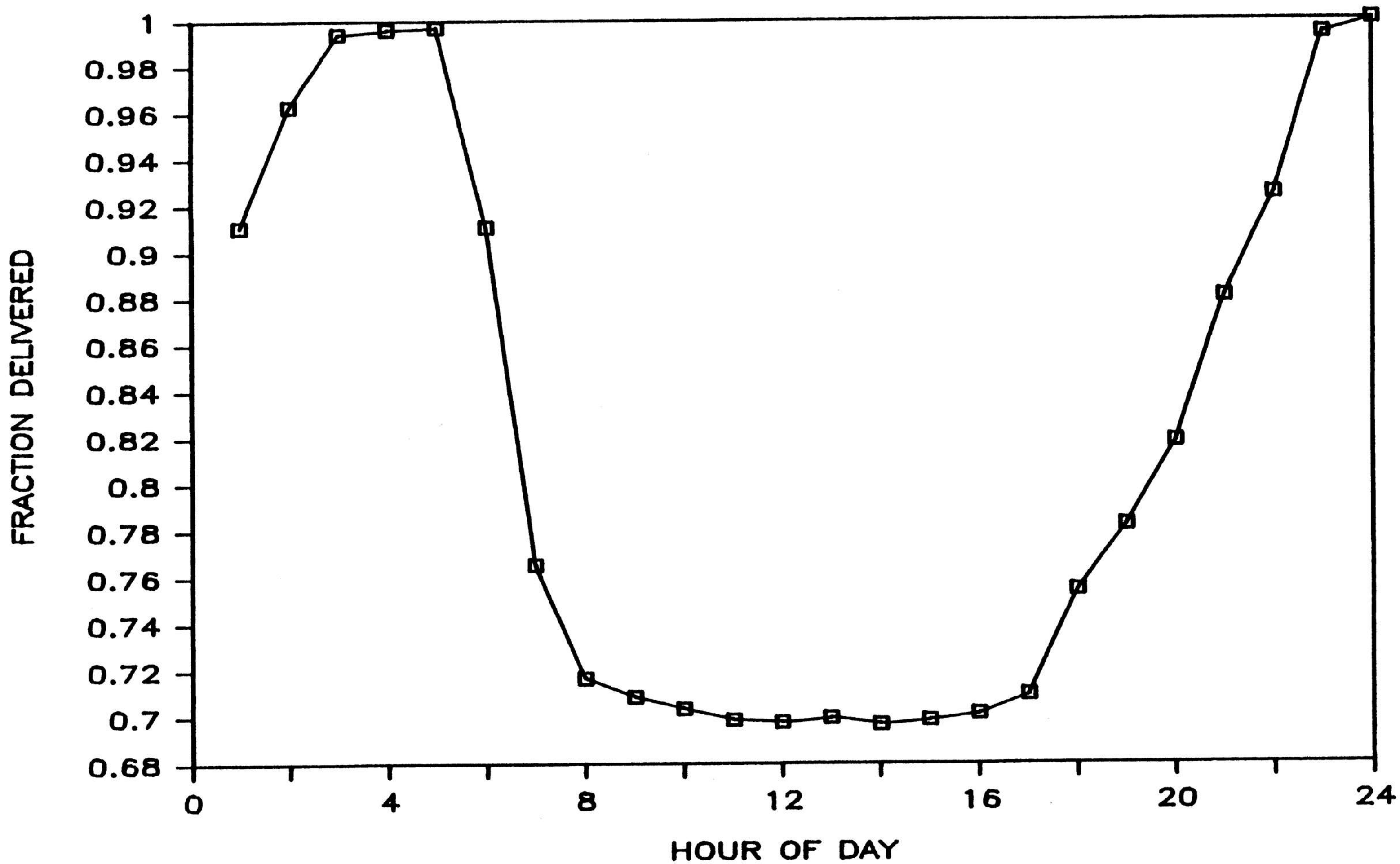

Figure 6.2.3 Fraction delivered vs hour of day for typical Wisconsin commercial zone, July 19, ventilation CT/HX cycle

is low, the fraction delivered may be set at a low value. During unoccupied hours, when the zone load is mostly latent, the fraction delivered value may be set up to a higher value. A complicated fractioning control scheme, therefore, may not be necessary to control the zone temperature. It may be possible to use a thermostat-type controller to vary the fraction delivered and, hence, the supply air temperature with the time of day.

Figure 6.2.4 is a plot of the air mass flow rates through the ventilation cooling tower/heat exchanger cycle that is coupled with the commercial zone of Section 6.1. This figure traces the cycle flow rates through each of the system components. In general, the flows through the components are highest during the day-time hours when the air conditioning load is largest. The highest flow rate through the system is through the air/water heat exchanger, which equals the sum of the required ventilation air, the return zone air and the exhausted cooling tower air. The mass flow rate of air brought in from the ambient is equal to the air ventilated from the zone plus that which is dumped through the cooling tower. As the fraction of delivered air approaches unity, the inlet mass flow rate approaches the ventilation air mass flow rate. These flow rate values illustrate the need for designs that reduce the parasitic power requirements.

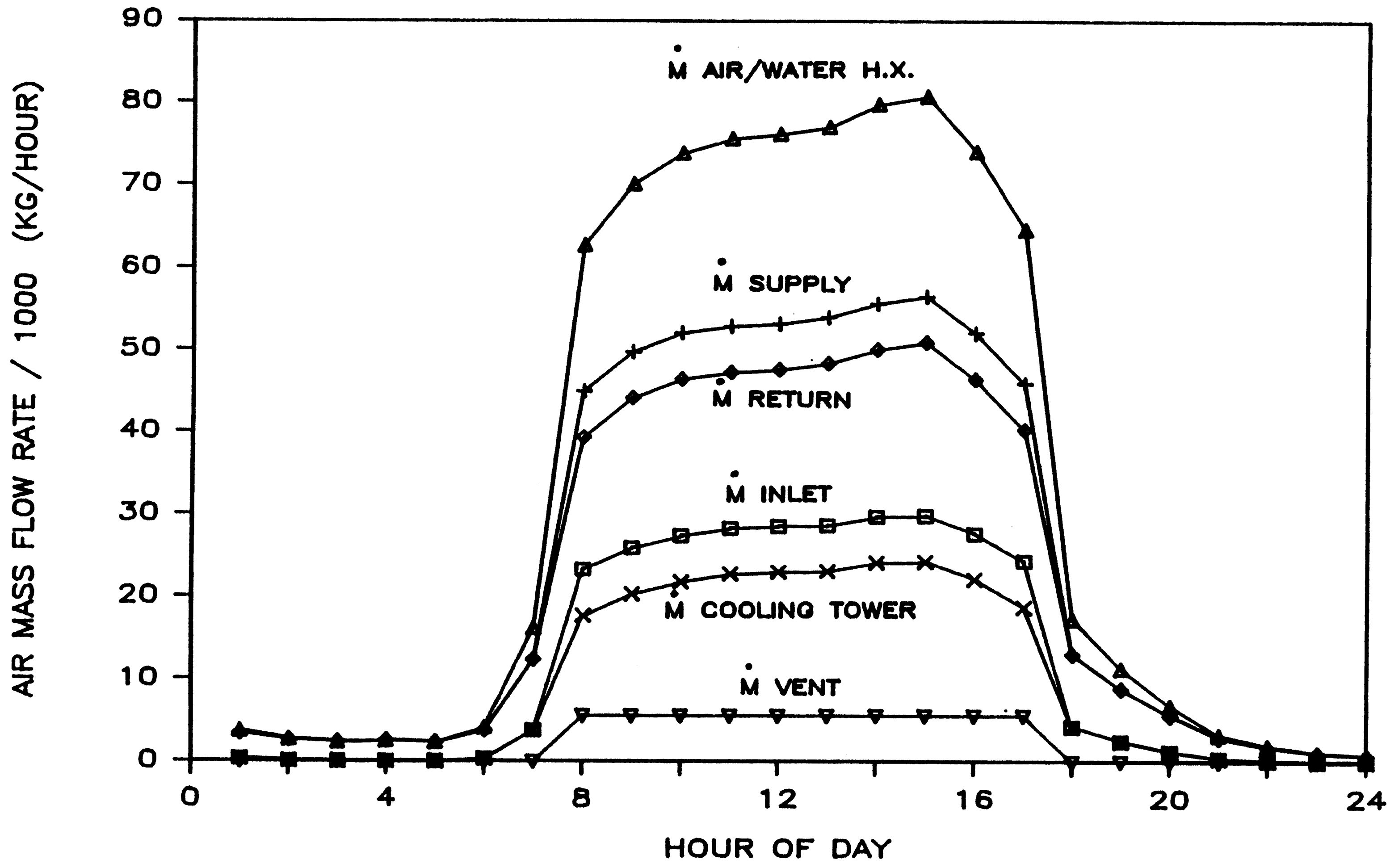

Figure 6.2.4 Air mass flow rates through the ventilation CT/HX cycle vs hour of day for typical Wisconsin commercial zone, July 19

Section 6.3: Seasonal Simulations of Cooling Tower/Heat Exchanger Air Conditioning Cycle

The cooling tower/heat exchanger air conditioning cycle was evaluated for an entire cooling season with Madison weather data while coupled to the sample zone described in Section 6.1. Simulations were conducted for both the ventilation and recirculation modes of operation with all of the component NTU's equal to 9.0 and while the zone was maintained at ARI conditions. The results for the season simulation are shown in Figs. 6.3.1 through 6.3.5. Figure 6.3.1 shows a histogram plot of the fraction of the inlet air flow to the cooler that is delivered to the zone for the entire cooling season. This plot gives the total number of hours that the unit operated at each of the fractions intervals listed. Two main points may be drawn from this histogram. First, there are two distinct fraction delivered regions; one at fractions of approximately 0.72 and the second at fractions equal to 1.0. These two regions correspond to the two times of the day when high sensible cooling is and is not required, respectively. Again, this illustrates that the cooling tower/heat exchanger air conditioning unit may be operated at two different fraction delivered control settings to meet a load on any particular zone throughout a day.

Figure 6.3.2 shows how many hours the air conditioning unit operates at each regeneration temperature interval when operating in the ventilation mode. For this particular sample zone, the cycle operates at a mean regeneration temperature of 55°C. There is also a

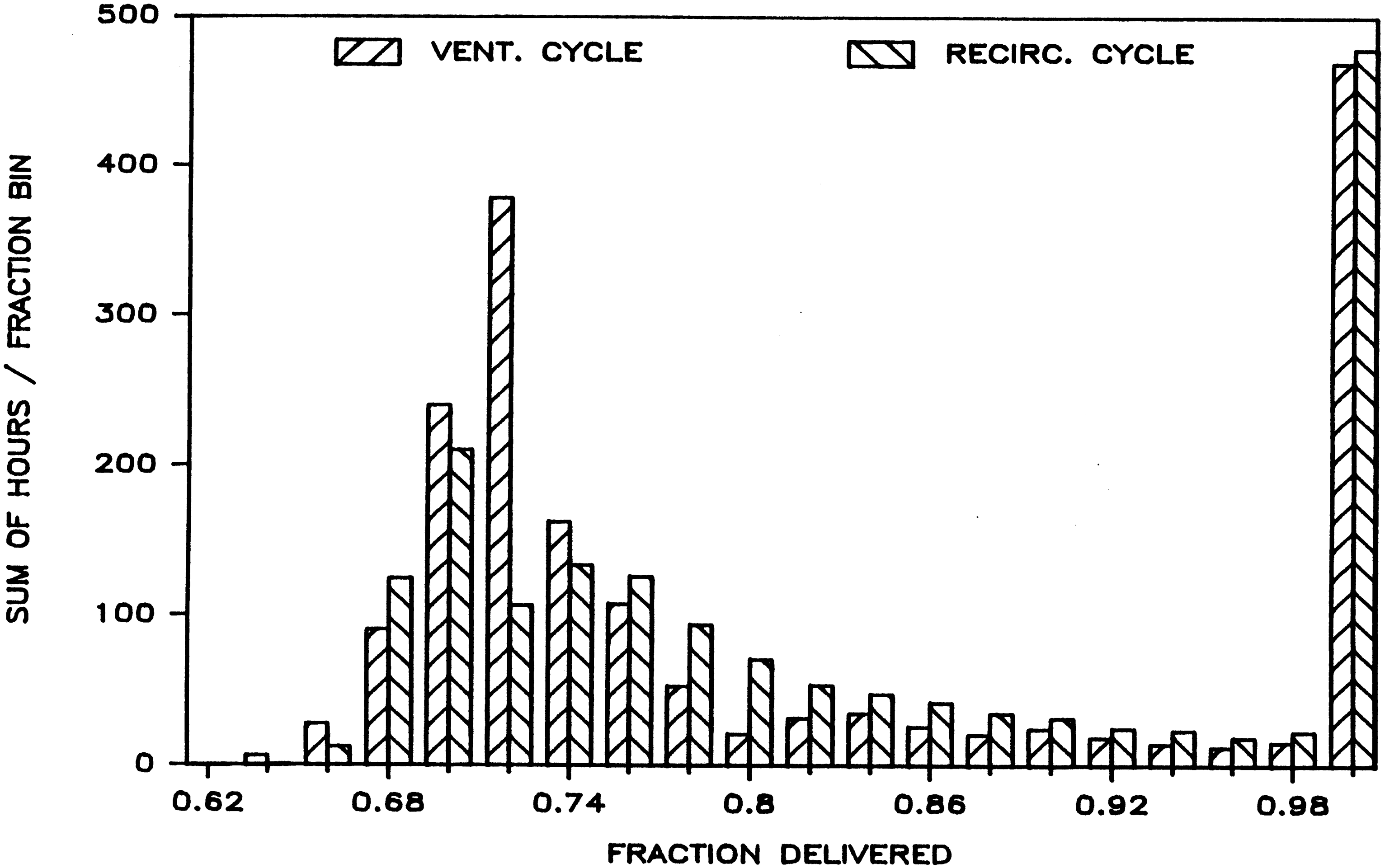

Figure 6.3.1 Histogram of fraction delivered for CT/HX cycle when coupled to typical Wisconsin commercial zone, cooling season, Madison, Wisconsin

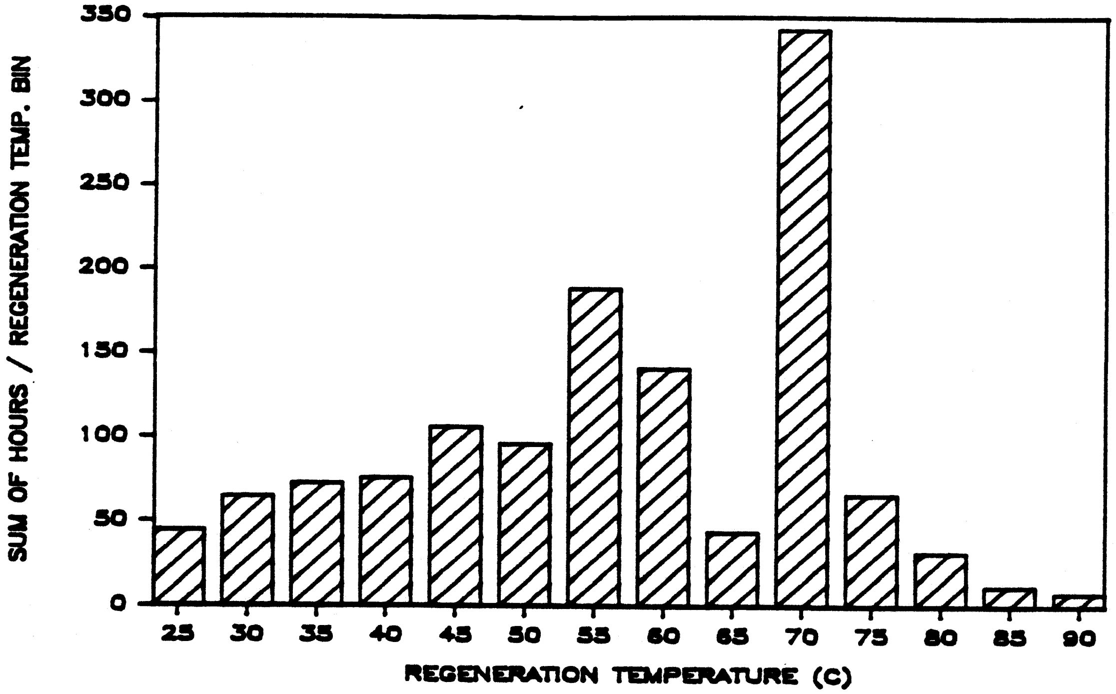

Figure 6.3.2 Histogram of operating hours vs regeneration temperature for ventilation CT/HX cycle, typical Wisc. zone, cooling season, Madison

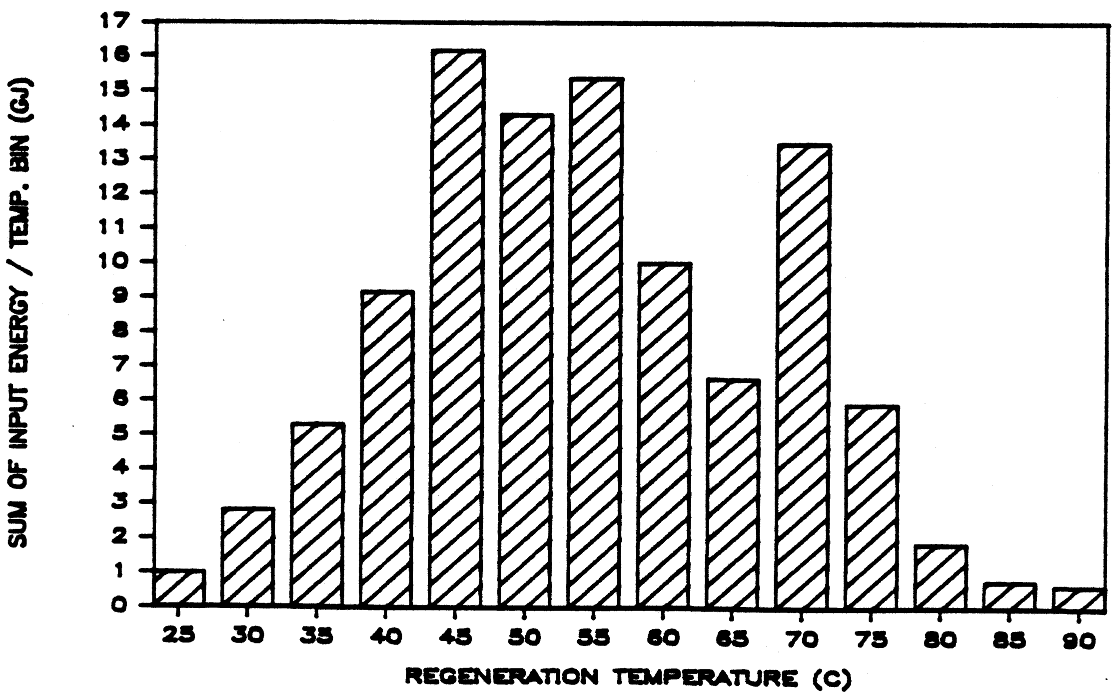

Figure 6.3.3 Histogram of energy input vs regeneration temperature for ventilation CT/HX cycle, typical Wisc. zone, cooling season, Madison

large number of operating hours in the 70°C regeneration temperature bin. These hours correspond to when the control strategy of Section 5.7 is implemented. Here, the air mass flow rate through the dehumidifier is too low and not enough moisture can be removed from the air stream to meet the zone latent cooling load. Return air is then recirculated past the desiccant to increase the latent cooling capacity and the outlet humidity ratio is set to a constant value of 0.004 kg/kg. If the minimum outlet humidity ratio was allowed to be lower then 0.004 kg/kg, then the peak in regeneration temperature would move to higher temperatures. If the minimum were set to higher humidity ratios, then the peak would move more to the left in Fig. 6.3.2.

The energy histogram of Fig. 6.3.3 represents the sum of the thermal energy input to the heater for the entire cooling season at each of the regeneration temperature intervals. Again the peak energy input occurs at the regeneration temperature of 55°C and the energy input decreases at the higher and lower temperature intervals. The seasonal overall energy-averaged thermal COP was 4.06.

Figures 6.3.4 and 6.3.5 show the sum of the hours and the sum of the energy input, respectively, at each of the regeneration temperature intervals for the recirculation cooling tower/heat exchanger cycle. The mean regeneration temperature is 35°C. This is lower then the mean for the ventilation cycle and is due to the relatively low humidity ratio of the air entering the dehumidifier. The season-

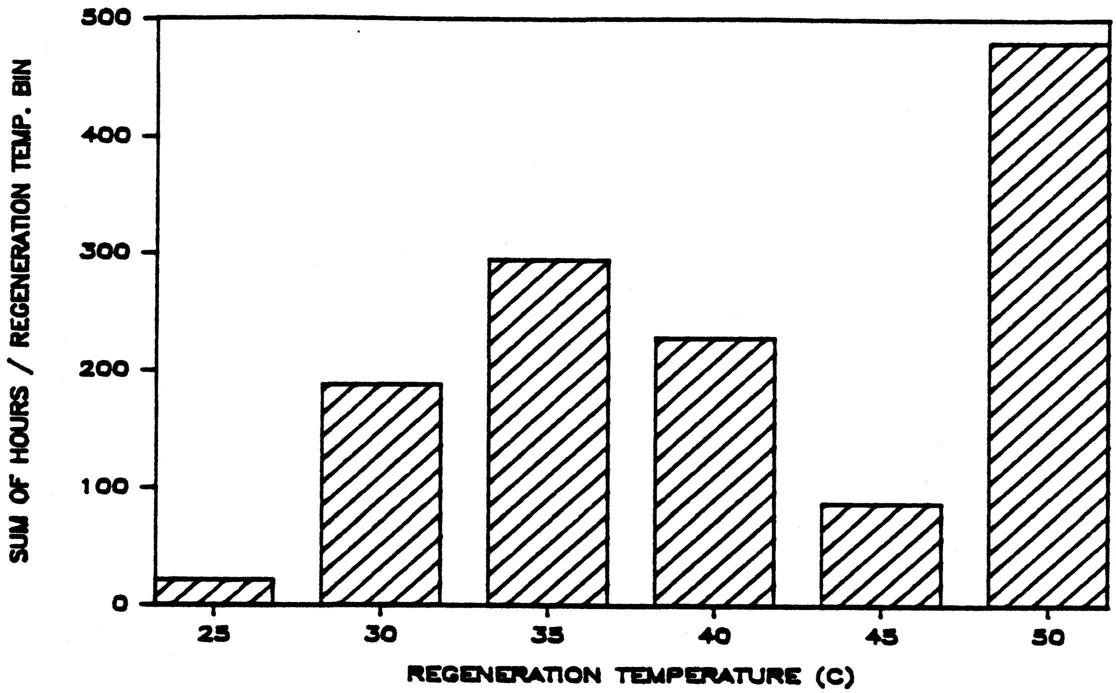

Figure 6.3.4 Histogram of operating hours vs regeneration temperature for recirculation CT/HX cycle, typical Wisc. zone, cooling season, Madison

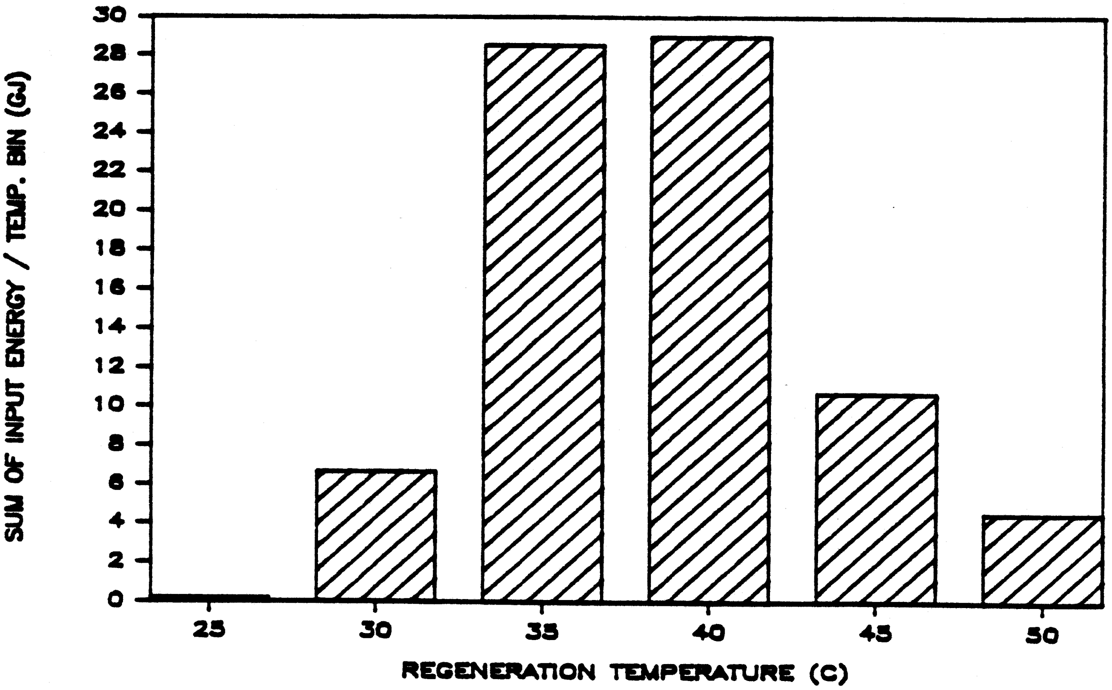

Figure 6.3.5 Histogram of energy input vs regeneration temperature for recirculation CT/HX cycle, typical Wisc. zone, cooling season, Madison

al COP for the recirculation cycle when mated with the sample building zone of Section 6.1 is 5.26.

As a means of comparison with the standard ventilation and recirculation cycle, the same sample zone was conditioned with the classical desiccant air conditioning cycles. Figure 6.3.6 and 6.3.7 show the time and the energy histograms as functions of regeneration temperature for both the ventilation and recirculation cycles. The mean regeneration temperature for both cycles is 50°C. The seasonal energy-averaged thermal COP's for the ventilation and recirculation cycles are 1.39 and 1.36, respectively.

Table 6.3.1 summarizes the seasonal COP's for the systems simulated in this chapter. Listed, also, in this table is the performance for a conventional vapor compression air conditioning unit. The performance of this unit was predicted by a TRNSYS component that models a split-system heat pump manufactured by Carrier Corporation [1985]. Because the energy input to the compressor is in electrical form and not thermal, the listed coefficient of performance is for the energy input multiplied by a weighting factor of 3.0. This weighting factor takes into account the efficiencies in converting nonrenewable fuel into high grade electrical energy. By using this weighting factor, the energy input to the desiccant and vapor compression systems may be fairly compared on a common "resource energy" basis [Jurinak, 1982].

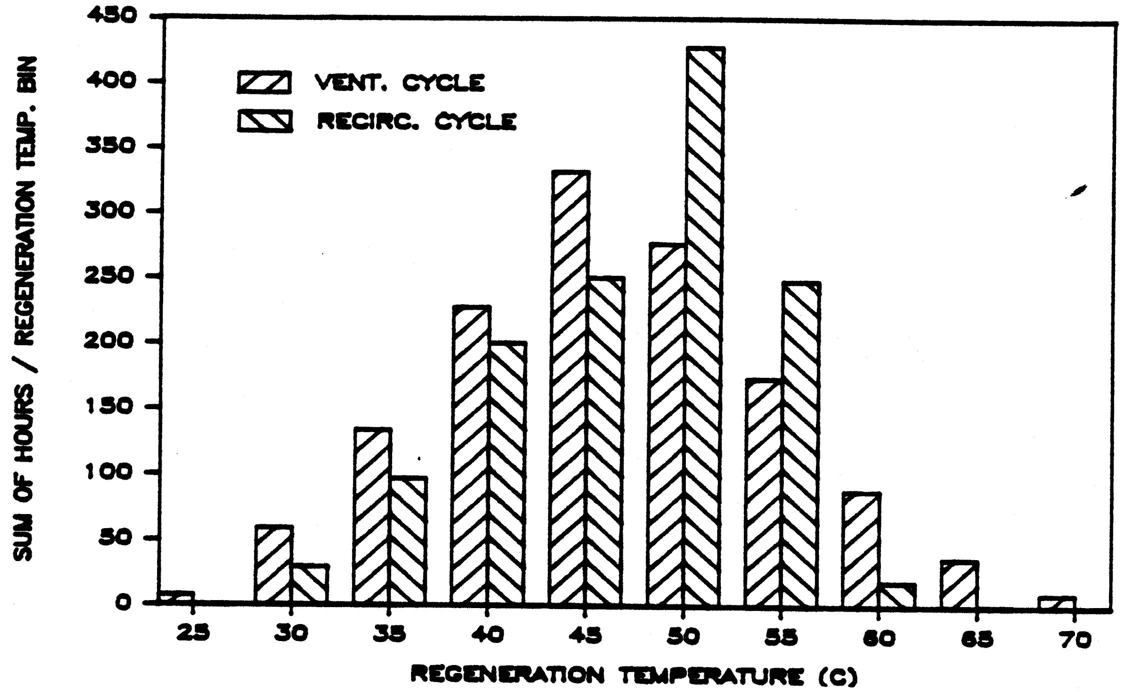

Figure 6.3.6 Histogram of operating hours vs regeneration temperature for classical desiccant cycles, typical Wisc. zone, cooling season, Madison

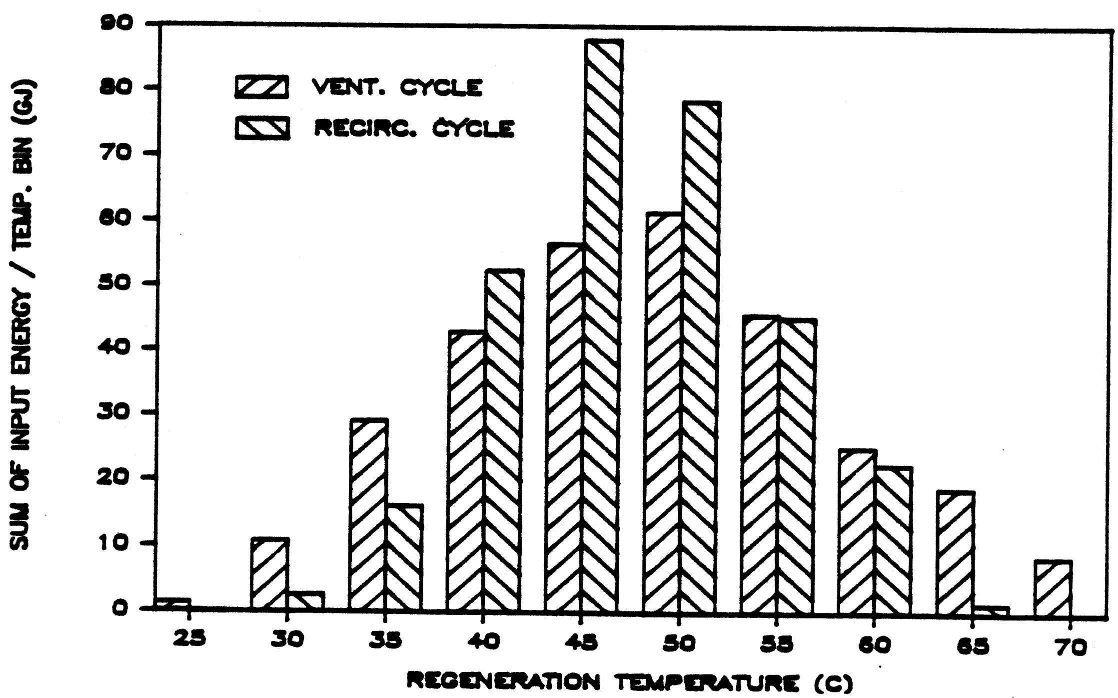

Figure 6.3.7 Histogram of energy input vs regeneration temperature for classical desiccant cycles, typical Wisc. zone, cooling season, Madison

SEASONAL COEFFICIENTS OF PERFORMANCE
MADISON, WISCONSIN

SYSTEM	THERMAL COP
1) CLASSICAL RECIRCULATION	1.36
2) CLASSICAL VENTILATION	1.39
3) COOLING TOWER/H.X.-VENT.	4.06
4) COOLING TOWER/H.X.-RECIRC	5.26
5) VAPOR COMPRESSION UNIT	0.96 *

$$\text{THERMAL COP} = \frac{\text{COOLING LOAD}}{\text{THERMAL ENERGY INPUT}}$$

* INCLUDES RESOURCE ENERGY WEIGHTING FACTOR = 3.0

Table 6.3.1 Summary of seasonal coefficients of performance for classical and CT/HX desiccant cycles, typical Wisc. zone, Madison cooling season

Section 6.4: Conclusions

The advanced cooling tower/heat exchanger cycle studied earlier presents a 190% and 280% increase in thermal COP over the classical ventilation and recirculation cycles, respectively. These large increases in thermal COP may be attributed to two points. First, a large benefit is gained by operating the desiccant cycles with sensible coolers in place of the traditional direct evaporative coolers. The reduction in the degree of required dehumidification brought about by the addition of the sensible coolers yields a substantial boost in the thermal COP. Second, all of the results generated for this chapter are for cycles whose component NTU's are equal to 9.0. This represents very high performance air conditioning devices and marks the upper limit on the cooling tower/heat exchanger unit's utility. If the heat exchangers and cooling tower were reduced in size relative to the conditioned air flow rates, the increase in COP would be less pronounced.

It was also shown in this chapter that the scheduling of the internal loads on the zone resulted in two operating regions for the CT/HX air conditioning unit. During the day-time hours, when a high degree of sensible cooling is required, the unit operates at low fractions delivered. During the evening and early morning hours, less sensible cooling is required and the resultant fractions are near unity. The existence of two distinct operating regions means that a thermostat-type controller could be used to automatically set the regeneration temperature and fraction delivered with the time of day.

Finally, as the size of the components in the CT/HX cycles increases with respect to the conditioned air mass flow rate, the significance of the second rotary heat exchanger decreases. At high heat exchanger NTU, the first heat exchanger performs very well and cools the process air close to the ambient temperature. At these conditions, there is no longer much potential for further heat transfer with the cooling tower exhaust air.

CHAPTER 7: SYSTEM COMPARISONS

To draw conclusions about the potential impact of desiccant air conditioning on Wisconsin Power and Lights utility demand, it is first necessary to determine if any desiccant system, classical or advanced, will ever compete on an energy and cost basis with vapor compression units. This chapter presents an analytical means for comparing the two competing air conditioning systems. The results of this comparison, which show the relative cost of the two systems on a dollar basis, will be given. A list of potential commercial users in the WPL territory is given and favorable match-ups between application and desiccant systems are made. Finally, forecasts are made on the possible electrical energy reduction and the natural gas increase which might be seen in the WPL utility network as a result of any future switch to desiccant air conditioning systems.

Section 7.1: Method of Comparison for Rival Air Conditioning Systems

To compare desiccant cycles with the conventional vapor compression cycles, information regarding the total cost of the cycle to the consumer must first be understood. If the desiccant cycles can never successfully air condition a building space at an economically feasible cost, then these new systems will never displace the conventional vapor compression systems. In this section, the maximum that a desiccant system can cost and still be economically competitive against a vapor compression unit will be determined.

The total cost associated with any piece of air conditioning equipment may be broken down into two parts; the initial investment in the equipment and the operating costs associated with the installed system. Brandemuehl and Beckman have developed an analytical means of calculating the total life cycle cost of solar heating systems [1979]. This economic evaluation technique is further extended by Mitchell to all energy related equipment [1983]. From Mitchell, the life cycle cost associated with a piece of equipment may be written as:

$$\begin{aligned} LCC = {} & \text{investment cost} + \text{fuel cost} + \text{miscellaneous cost} \\ & + \text{property tax} - \text{tax savings} \end{aligned} \tag{7.1.1}$$

The investment cost is that cost associated with the initial down payment on the equipment and future loan payments, as well as installation costs. The sum of the fuel costs, miscellaneous costs and property taxes are annual expenditures whose present worth must be determined. The tax savings are from income tax deductions due to the interest paid on the loan, property tax and any tax credits.

Equation (7.1.1) may be rewritten as:

$$LCC = P_1 * \$F + P_2 * \$E \tag{7.1.2}$$

where \$F is the cost associated with the first year fuel consumption and \$E is the equipment investment. The multipliers P_1 and P_2 are present worth factors that take into account all of the economic factors discussed above. P_1 may be written as:

$$P_1 = (1 - ct) * PWF(n,f,d) \tag{7.1.3}$$

where c is a flag which is set to 1.0 for commercial investments and 0.0 for residential investments, t is the effective income tax rate, and PWF(n,f,d) is a present worth factor which is a function of the number of years in the economic study, the fuel price inflation rate and the market discount rate, respectively. P_2 may be written as:

$$P_2 = D + (1 - D) * \frac{PWF(n_1,0,d)}{PWF(n_L,0,m)} - t(1 - D) * \left[PWF(n_1,m,d) * \left(m - \frac{1}{PWF(n_L,0,m)} + \frac{PWF(n_1,0,d)}{PWF(n_L,0,d)}\right)\right] + \left[p(1 - t) + M(1 - ct)\right] * PWF(n,i,d) - \frac{ct}{n_d} PWF(n_2,0,d) - S - r \tag{7.1.4}$$

where D is the ratio of the down payment to the initial investment, m is the mortgage rate, p is the property tax rate, r is the tax credit, S is the ratio of the salvage value to the initial investment, M is the ratio of miscellaneous costs to the initial investment, n_d is the depreciation life time, n_1 is the minimum of n or the term of the loan, and n_2 is the minimum of n and n_d. Typical values of P_1 and P_2 range from 5 to 20 and 0.5 to 1.5, respectively.

Applying Eq. (7.1.2) to an air conditioning system yields:

$$\text{LCC (A/C unit)} = \$F\text{ (A/C)} * P_1 + \left(\frac{\$E\text{ (A/C)}}{\text{Ton}} * \text{Tons required}\right) * P_2 \tag{7.1.5}$$

Equation (7.1.5) applies to both vapor compression and desiccant systems. Setting the two life cycle costs equal to each other and solving for the allowable first cost of a desiccant air conditioning unit per tonnage of equipment yields:

$$\frac{\$E_{DES}}{\text{Ton}} = \frac{\$E_{v/c}}{\text{Ton}} + \frac{P_1}{P_2} * \left(\frac{\$F_{v/c} - \$F_{DES}}{\text{Installed Tons}}\right) \tag{7.1.6}$$

Here, $\$F_{DES}$ may be written as:

$$\$F_{DES} = \left(\frac{\$}{\text{thermal energy}}\right)\left(\frac{\text{A/C Load}}{\text{COP}_{\text{thermal}}}\right) + \left(\frac{\$}{\text{electricity}}\right)\left(\frac{\text{A/C Load}}{\text{EER}}\right) \tag{7.1.7}$$

where EER is the ratio of the cooling load to the electrical energy input to the fans and pumps in the desiccant systems.

Two points may be drawn from Eq. (7.1.6). First, there is now only one variable, P_1/P_2, that takes into account all of the economic factors previously discussed. By varying the range of P_1/P_2, all of the possible combinations of economic factors may be taken into account. Second, it is seen that under certain instances, the allowable first cost may be less then zero depending on the system seasonal operating costs. Under these circumstances, the desiccant system would never be economically feasible.

The seasonal cost of the energy input to either system is dependent on the costs of energy available from the local power utility. A list of current Wisconsin Power and Light electrical and natural gas rates are listed in Table 7.1.1 for the customer category CG-1. The CG-1 billing category includes all commercial customers with a peak electrical demand less then 75 KW. This one billing group includes 27,600 customers and comprises approximately 95% of all of WPL's commercial users. 85% of these users are billed with the standard electrical rates. The price of electrical energy for the standard electrical service is approximately 3.5 times more than an equivalent amount of energy supplied by natural gas. These rates are used as inputs to the TRNSYS decks that simulate each of the previously discussed air conditioning systems.

All of the desiccant cycles studied in this thesis use both electricity to operate fans and natural gas to dry the desiccant matrix. The vapor compression units use electricity, only, to operate the refrigerant compressor and required fans. The vapor compression system that was simulated for the same conditions was modeled after a Carrier split-system heat pump [Product literature, 1985]. The installed cost of the conventional vapor compression unit was estimated at $750/ton [Means, 1984].

WISCONSIN POWER & LIGHT RATE SCHEDULE

TYPE OF SERVICE	FIXED CHARGE	ENERGY CHARGE
STANDARD ELECTRICAL	1-Ø \$4.25 / mo. 3-Ø \$11.50 / mo.	6.56 ¢ / KW-Hr (\$18.22 / GJ)
TIME-OF-DAY ELECTRICAL	1-Ø \$4.25 / mo. 3-Ø \$11.50 / mo.	8AM-10PM: 12.26 ¢ / KW-Hr (\$34.05 / GJ) 10PM-8AM: 2.89 ¢ / KW-Hr (\$7.94 / GJ)
NATURAL GAS	\$6.00 / mo	56.02 ¢ / THERM (\$5.31 / GJ)

Table 7.1.1 Wisconsin Power and Light rate schedule for customer category CG-1.

Section 7.2: Zone Model Used for System Comparisons

A typical Wisconsin commercial zone was described in detail in Section 5.1. The model used to simulate the air conditioning load on that zone took into account the envelope conductance gains, infiltration gains, solar gains, and internally generated sensible and moisture gains. From that section, it was also found that the primary contributer to the sensible cooling load for commercial zones in Wisconsin climate is the internally generated sensible gains. The zone model of Section 5.1 was therefore simplified for use in the economic evaluation to include only the internal gains and the moisture generation within the zone. The less significant load contributers, such as infiltration and conductance gains are neglected. With this simplified zone model, it is possible to use TRNSYS forcing functions to simulate the zone loads and it is further possible to exactly control the latent load on the zone by changing the proportion of sensible cooling while maintaining a constant total load on the zone.

Maintaining a constant latent load on the zone during a simulation is important because the latent load ratio is the primary load characteristic available for comparing the building types found in Wisconsin Power and Light's territory. Maintaining a constant latent load simplifies matching up generated simulation results with the appropriate building types.

The building loads imposed by the TRNSYS forcing functions total to 139KW. This is equivalent to approximately 40 Tons of air conditioning capacity.

Section 7.3: Simulation Comparison Results

In the comparisons presented in this chapter, an attempt was made to simulate a broad range of desiccant air conditioning systems. These systems range from the more basic classical cycles, through the two-stage IEC cycles and up to the higher performance cooling tower/ heat exchanger cycles. All three of these cycles were simulated in both the ventilation and recirculation modes. Furthermore, each of the advanced cycles were operated at two distinct thermal sizes; one at a NTU equal to 3 and the other at an NTU of 9.0. This variety of system component size provides output for units of both a practical size that could be manufactured today, and units that present upper limits on the cycle's performance.

Each of the cycles just described, was simulated with the cooling load outlined in Section 7.2 while the zone latent load was varied from 0 to 0.6. Tables 7.3.1 and 7.3.2 show a matrix of the allowable first costs for the different systems and the latent composition of the air conditioning loads. These results were generated using Madison, Wisconsin weather data. The zone state was maintained at ARI design conditions for all system simulations.

The number recorded for each system represents the allowable first cost per ton of installed desiccant air conditioning equipment

ALLOWABLE INSTALLED COST OF DESICCANT AIR CONDITIONING EQUIPMENT

EER=5, P1/P2=5

DESICCANT AIR CONDITIONING CYCLE	MODE	LATENT LOAD RATIO 0.0	0.1	0.2	0.3	0.4	0.5	0.6
COOLING TOWER/ H.X.								
NTU=9	RECIRC	809	908	950	984	1018	1054	1091
NTU=3		617	762	865	919	960	998	1034
NTU=9	VENT	792	891	928	946	956	981	1012
NTU=3		513	717	846	893	907	922	952
TWO-STAGE IEC								
NTU=9	RECIRC	235	789	913	966	1016	1062	1104
NTU=3		-550	189	771	910	964	1012	1055
NTU=9	VENT	0	774	876	925	967	1005	1039
NTU=3		-1107	39	748	859	914	957	993
CLASSICAL (ε_{hx}=.95, ε_{ec}=.98)	RECIRC	654	752	806	850	884	913	935
	VENT	625	727	787	843	867	880	888

Table 7.3.1 Allowable installed cost of desiccant air conditioning equipment. EER=5, P1/P2=5

ALLOWABLE INSTALLED COST OF DESICCANT AIR CONDITIONING EQUIPMENT

EER=10, P1/P2=5

DESICCANT AIR CONDITIONING CYCLE	MODE	LATENT LOAD RATIO 0.0	0.1	0.2	0.3	0.4	0.5	0.6
COOLING TOWER/ H.X.								
NTU=9	RECIRC	957	1056	1098	1132	1167	1202	1239
NTU=3		765	910	1013	1067	1108	1146	1182
NTU=9	VENT	940	1041	1076	1094	1104	1129	1160
NTU=3		660	865	993	1041	1054	1070	1101
TWO-STAGE IEC								
NTU=9	RECIRC	383	937	1060	1113	1164	1210	1252
NTU=3		-403	337	919	1058	1112	1159	1202
NTU=9	VENT	149	923	1024	1073	1116	1153	1187
NTU=3		-959	186	896	1007	1062	1105	1141
CLASSICAL								
(ε_{hx}=.95, ε_{ec}=.98)	RECIRC	802	901	955	998	1031	1061	1083
	VENT	774	875	935	990	1015	1028	1036

Table 7.3.2 Allowable installed cost of desiccant air conditioning equipment. EER=10, P1/P2=5

that, when combined with the seasonal operating cost, would just equal the total cost of a vapor compression system. A large allowable first cost signifies that a relatively expensive desiccant system could still be cost effective against a vapor compression system. The lower the actual first cost is relative to the allowable first cost, the greater the savings will be.

The numbers in Tables 7.3.1 and 7.3.2 were generated assuming a desiccant system EER of 5 and 10, respectively. These EER's represent the performance that a desiccant cycle must match if the desiccant system is to compete with vapor compression systems. Both Tables 7.3.1 and 7.3.2 were generated with a P_1/P_2 value of 5.0. This is a representative ratio of the present worth factors that would be encountered in commercial investments.

Several points can be drawn from Tables 7.3.1 and 7.3.2. First, as the zone latent load ratio increases, the allowable first cost of all of the systems increase. The lowest allowable first costs exist at latent loads equal to 0.0. At this loading condition, the competing vapor compression system operates with the highest efficiency and the desiccant system operates at its lowest efficiency. The only negative first costs occur at latent loads equal to 0.0 and for the ventilation two-stage IEC. It would never be economically feasible to install these desiccant systems in situations where the air conditioning load is entirely sensible.

At lower latent loads, the best systems are the cooling tower/ heat exchanger and then the classical desiccant cycles. At higher latent loads, the two advanced desiccant cycles slightly outperform the classical cycles.

At higher latent loads, the significance of using the larger thermal sizes for the components is reduced for both the staged IEC and the cooling tower/heat exchanger cycles. As an example, for the cooling tower/heat exchanger cycle, the difference between the allowable installed cost for cycles with NTU's of 3 and 9 decreases from 31% to 5% as the latent load ratio increases from 0 to 0.6.

The effect of EER on the allowable desiccant system installed cost is seen by comparing Tables 7.3.1 and 7.3.2. At lower latent loads, the purchased thermal energy is the dominant contributer to the seasonal operating costs. In going from an EER of 10 to 5, the effect of the decrease in EER is not very noticeable. At higher latent loads, the purchased electrical energy contributes a larger percentage to the total seasonal operating costs then it did at low LLR's. The resulting allowable first costs increase as much as 20% when the EER is increased from 5 to 10.

Figure 7.3.1 is a graph of the allowable installed first cost for the recirculation two-stage IEC, CT/HX and the classical desiccant air conditioning cycles as a function of latent load ratio for a cycle EER of 10 and P_1/P_2 equal to 5. The wide disparity between cycles is evident at lower latent load ratios, especially for the two-stage IEC cycle. At the higher latent loads, the allowable installed costs vary by about 9%. The dashed horizontal line on this plot represents the allowable installed cost of the rival vapor com-

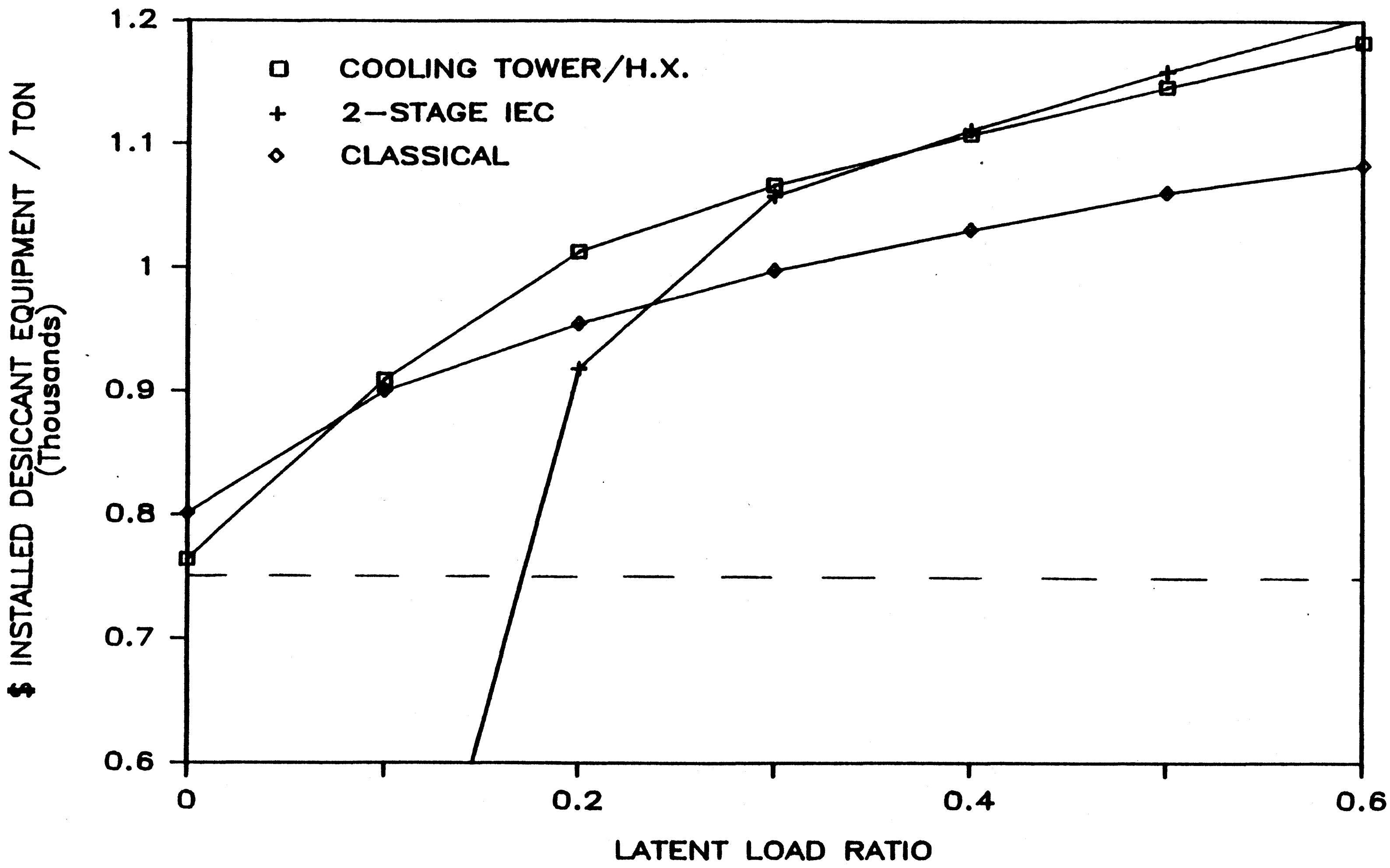

Figure 7.3.1 Allowable installed cost for recirculation CT/HX, two-stage IEC and classical desiccant air conditioning cycles, NTU's=3.0, EER=10, P1/P2=5

pression air conditioning unit which is priced at $750 per ton. In all ranges of latent loading conditions, desiccant cycles are able to compete with the vapor compression system provided the installed desiccant system may be purchased for a price equal to or less than that indicated. In general, desiccant systems could cost greater than a vapor compression machine and still be cost effective.

Table 7.3.3 presents a breakdown of the types of commercial users in Wisconsin Power and Light's territory. Listed in this table are the nine different building types which are found in the CG-1 electrical billing category that was outlined in Table 7.1.1. The users are further broken down into groupings of similar zone latent load ratios. The latent load category was estimated based on the functions occurring inside the building.

The total 1985 electrical energy consumption is recorded in the third column of Table 7.3.3 for each of the building types in each latent load group. The predominant group of buildings is in the LLR of 0.15 category and together they account for approximately 65% of the total electrical energy usage of all the groups combined. The approximate percentage of the total 1985 seasonal electrical usage that is attributed to air conditioning requirements is also tabulated in column four of Table 7.3.3. This percentage was determined from an electrical energy end-use disaggregation study conducted by WPL and was compiled from their Commercial and Apartment Conservation Service (CACS) data base. With the percentage air conditioning approximation and the total 1985 energy usage, the energy usage

1985 COOLING SEASON ELECTRICAL ENERGY USAGE

LATENT LOAD RATIO	BUILDING TYPE	1985 ELECTRICAL ENERGY USAGE (KW-Hr)	% A/C	1985 A/C ELECTRICAL ENERGY USAGE (KW-Hr)
0 - 0.1	WAREHOUSES	32,336,700	2.6	840,750
0.15	OFFICES	192,215,600	8.4	16,146,000
	RETAIL	140,864,300	6.6	9,297,000
	SCHOOLS	21,596,500	4.3	928,650
	HOTELS	26,525,000	11.5	3,050,400
	HEALTH	20,540,100	9.2	1,889,700
	MISCELANEOUS	78,865,800	2.2	1,735,000
0.35	RESTAURANTS	128,260,800	12.2	15,647,800
0.6	GROCERIES	42,435,400	2.6	1,103,300

Table 7.3.3 Breakdown of 1985 cooling season electrical energy usage by building type

directly attributed to air conditioning requirements was calculated and is listed in column 5 of Table 7.3.3. Overall, the energy required for air conditioning is 7.1% of the total 1985 energy expenditures.

Table 7.3.4 illustrates the potential reduction in electrical energy consumed for air conditioning purposes. Again, this list is broken down into groups with common latent load ratios. The sum of electrical energy usage from the 1985 cooling season attributed to air conditioning is repeated from Table 7.3.3 and is tabulated in column 2. The column entitled "Seasonal Desiccant A/C Electric Usage" lists the electrical energy required of the desiccant air conditioning cycles if the desiccant cycles were to completely displace all vapor compression air conditioning units. These numbers were calculated assuming a vapor compression COP of 4 and a desiccant cycle EER of 10. This amounts to a 60% reduction in electrical energy use. The total reduction in electrical energy consumed by WPL's customers would sum to approximately 30,383,100 KW-Hours if all customers were to switch to desiccant air conditioning systems.

The thermal energy input that would be required of the classical recirculation cycle and the more advanced cooling tower/heat exchanger desiccant cycle are listed in the last two columns of Table 7.3.4 for each latent load category. The former represents a cycle that, at present, is technologically feasible and is similar to desiccant systems that may soon be marketed. The latter represents the best possible desiccant air conditioning system that might be

SUMMARY OF POTENTIAL REDUCTION IN ENERGY DEMAND DUE TO DESICCANT CYCLES

BASED ON: VAPOR COMP. COP=4, DESICCANT EER=10

LATENT LOAD RATIO	1985 SEASONAL A/C ELECT. USAGE (KW-Hr)	SEASONAL DESICCANT A/C ELECT. USAGE (KW-Hr)	THERMAL ENERGY INPUT: CLASSICAL RECIRC. CYCLE (THERMS*)	THERMAL ENERGY INPUT: C.T./H.X. RECIRC. CYCLE (THERMS)
0 - 0.1	840,750	336,300	16,050	4,350
0.15	33,046,750	13,218,700	729,100	257,190
0.35	15,647,800	6,259,120	429,150	188,050
0.60	1,103,300	441,320	35,600	19,400
	50,638,600	20,255,440	1,209,900	468,990

* 1 THERM = 10^5 BTU

Table 7.3.4 Summary of potential reduction in energy demand due to desiccant cycles. Calculations based on vapor compression COP=4, desiccant system EER=10 produced and marketed in the future. The numbers listed in columns 4 and 5 were generated by dividing the air conditioning load for each latent load ratio category by the thermal COP observed at that latent load ratio. The classical desiccant cycles would require an increase in natural gas sales in an amount equal to 1,209,900 therms whereas the advanced cycles would require 468,990 therms of energy.

The net effect of desiccant systems on revenues to WPL can be estimated using an electrical price of 6.5 ¢/KW-Hour and a natural gas price of 56 ¢/Therm. The loss in electrical revenue due to a total implementation of desiccant air conditioning systems would amount to about $2,000,000. This loss would be partially offset by increased natural gas revenues. With the classical desiccant system, the increase in natural gas sales would be about $700,000 and the increase would be about $260,000 for the advanced desiccant cycles.

CHAPTER 8: CONCLUSIONS AND RECOMMENDATIONS

This thesis has presented an analysis of open cycle desiccant air conditioning systems. This analysis offered both a review of the more classical desiccant air conditioning cycles as well as a look at two new advanced desiccant cycles. The objective behind analyzing these different systems was to generate performance data to compare the different desiccant cycles against vapor compression air conditioners. With this data, it was then further possible to calculate the possible shifts in utility demand felt by WPL as well as to study the feasibility of these new systems in the Wisconsin climate. The following conclusions may be made with regard to the findings of this study:

1) High performance desiccant systems may be constructed by replacing the traditional evaporative coolers with sensible air cooling devices. The two most promising sensible air coolers were the two-stage indirect evaporative cooler (IEC) and the combination cooling tower/heat exchanger (CT/HX). Both of these devices exhaust a portion of the cooled process air to the ambient as a means of producing a heat sink for the warmer process air. Both coolers can cool inlet air to temperatures below the inlet wet bulb temperature. The CT/HX cooler has the potential of cooling inlet air to near the inlet dew point temperature with one stage of cooling.

2) Design point simulations were conducted for all of the discussed desiccant cycles; the classical cycles, the two-stage IEC cycles, and the more advanced cooling tower/heat exchanger cycles. At ARI design point simulations, the cooling tower/heat exchanger cycle performed the best with a thermal COP = 2.08 when operated in the ventilation operating mode. The two-stage IEC cycle performed next best and for the same operating mode had a design point COP = 0.96. The COP for the classical ventilation cycle at the same conditions is 0.77.
3) Season simulations were run for the cooling tower/heat exchanger cycle and the classical cycle. When the advanced cycle was sized with components of NTU = 9.0, the seasonal thermal COP was 4.06 and was 190% higher then the COP for the classical cycle.
4) The regeneration temperatures observed in the conducted simulations ranged between 40°C and 90°C. These temperatures are within the range of temperatures attainable in solar collectors.
5) An economic evaluation was performed on all studied cycles. An allowable first cost for the installed desiccant systems was calculated and provided a comparison between the cycles. The advanced cooling tower/heat exchanger cycle performed the best for latent loads up to 0.5. The staged IEC cycle performed poorly at lower latent loads but slightly outperformed the CT/HX cycle at the higher latent loads. The classical cycles performance and allowed first cost was slightly less than the advanced cycles but was still in a feasible first cost range of $600 to $1000 per ton

of cooling capacity. The allowable first cost for all systems studied increased as the latent load on the zone increased.

6) Because of the large price disparity between electrical energy and natural gas, desiccant cycles can compete on a cost basis with vapor compression cycles. Desiccant cycles can, in general, cost more than a vapor compression system and still be cost effective.

7) WPL commercial users were categorized both by building type and by latent load ratio. The total commercial seasonal air conditioning energy usage was determined to be 50.6 GW-Hours. If desiccant air conditioning systems were to totally replace vapor compression systems, a sixty percent reduction in electrical consumption could be expected. This reduction totals to 30.4 GW-Hours and about $2,000,000. The corresponding expected increase in natural gas sales would vary with the type of desiccant system installed. The advanced CT/HX cycle would require 468,000 Therms of thermal energy while the classical recirculation cycle would consume 1,209,000 Therms. The increased revenue would be about $700,000 and $260,000 for the classical and advanced cycles, respectively.

8) Desiccant air conditioning, although under study for more than twenty years, is still in the development stage. Testing of equipment in field settings has just begun and desiccant systems have still not broken into the energy market. The best systems proposed in this thesis have not been built or tested. These

high performance systems serve merely to point to the potential that desiccant systems may someday attain.

The following recommendations point out further research that could be conducted to more conclusively determine the impact of desiccant air conditioning on the Wisconsin consumer and WPL's future utility demand.

1) It is recommend that a desiccant system be purchased when they become available for test purposes. While system computer simulations are helpful in drawing initial conclusions regarding the potential impact of these systems, they are no substitute for the actual testing and monitoring of real equipment. The tested system should be installed in an occupied building that is easily accessible to researchers for constant monitoring. The system should be fully instrumented to record information such as unit cooling capacity and thermal and electrical energy consumption.
2) The sales of future desiccant systems should be closely monitored. Increasing sales and consumer inquires should serve as good indicators of impending change.
3) Finally, the desiccant cycles studied in this thesis should be simulated when combined with solar collectors. This study has assumed that the source of the thermal energy supplied to the system originated from a gas fired heater. This may not always be the case.

APPENDIX A

The following is a derivation of the equations used to model the cooling tower used throughout this thesis. This derivation is as specified in the paper, "A General Theory of Wet Surface Heat Exchangers" by Maclaine-Cross and Banks [1981].

The general psychrometer equation for an adiabatic saturation process is:

$$h_a + (\omega_a' - \omega_a) * h_f = h_a' \qquad (A.1)$$

Replacing the moist air specific enthalpy with Eq. (A.2) yields Eq. (A.3).

$$h_a = c_{P,da} * (T_a - T_{ref}) + \omega_a * h_g \qquad (A.2)$$

$$T_a - T_a' = (\omega_a' - \omega_a) \frac{h_{fg}}{c_{P,da}} \qquad (A.3)$$

An energy balance on the differential element in the moist air stream of the wet surface heat exchanger shown in Fig. A.1 yields:

$$\dot{m}_a h_a |_y + h_D \Delta y W (\omega_w - \omega_a) h_g + h_c \Delta y W (T_w - T_a) - \dot{m}_a h_a |_{y+\Delta y} = 0 \qquad (A.4)$$

Dividing Eq. (A.4) by Δy and taking the limit as Δy goes to zero produces Eq. (A.5).

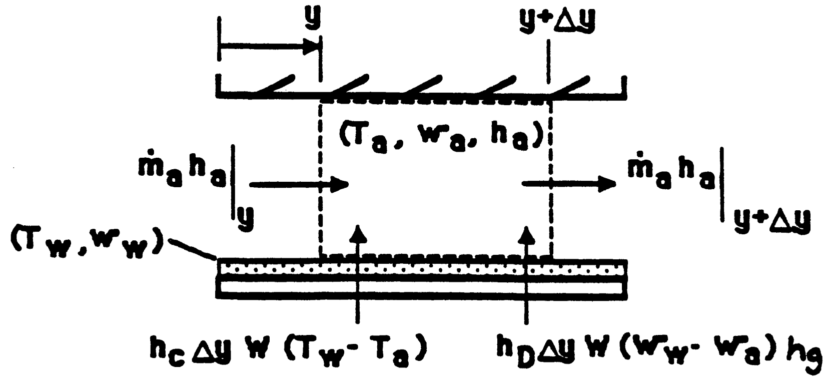

Figure A.1 Differential element in air stream of wet surface heat exchanger

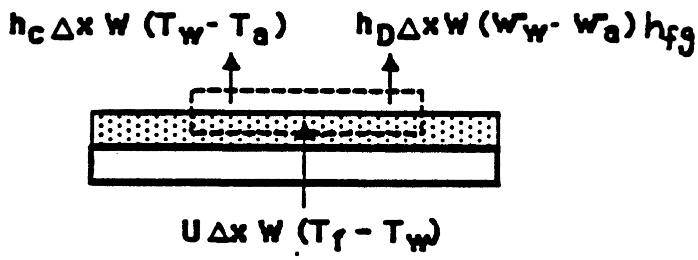

Figure A.3 Differential element at water/air interface in wet surface heat exchanger

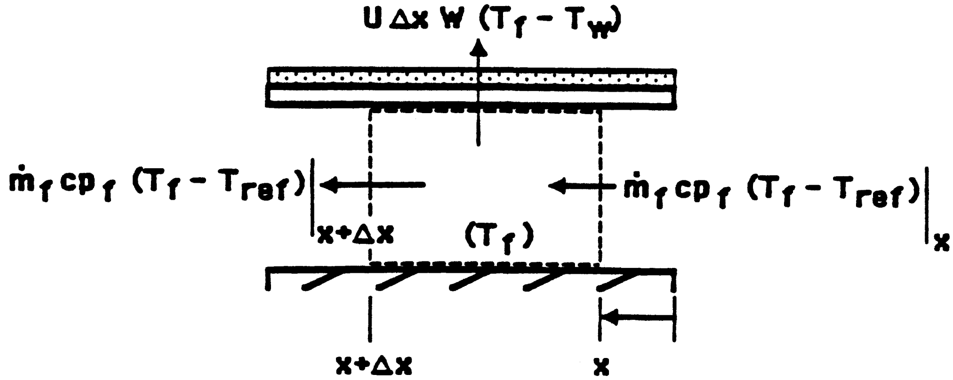

Figure A.2 Differential element in fluid side of wet surface heat exchanger

$$\dot{m}_a \frac{dh_a}{dy} = h_D W(\omega_w - \omega_a)h_g + h_c W(T_w - T_a) \tag{A.5}$$

An energy balance on a differential element in the fluid side of the wet surface heat exchanger in Fig. A.2 yields:

$$\dot{m}_f C_{P,f} T_f|_x - \dot{m}_f C_{P,f} T_f|_{x+\Delta x} - U\Delta x W(T_f - T_w) = 0 \tag{A.6}$$

Dividing by Δx and taking the limit as Δx goes to zero produces:

$$\dot{m}_f c_{P,f} \frac{dT_f}{dx} = UW(T_w - T_f) \tag{A.7}$$

Likewise, an energy balance on a differential element at the air/water interface shown in Fig. A.3 yields:

$$U(T_f - T_w) = h_c(T_w - T_a) + h_D(\omega_w - \omega_a)h_{fg} \tag{A.8}$$

A mass balance on the water vapor in the air side of the exchanger shown in Fig. A.1 yields:

$$\frac{d\omega_a}{dy} = \frac{h_D W}{\dot{m}_a}(\omega_w - \omega_a) \tag{A.9}$$

Substituting Eq. (A.9) into the derivative of Eq. (A.2) with respect to y gives:

$$\frac{dh_a}{dy} = c_{P,da}\frac{dT_a}{dy} + \frac{h_g h_D W}{\dot{m}_a}(\omega_w - \omega_a) \tag{A.10}$$

Substituting Eq. (A.10) into Eq. (A.5) for dh_a/dy yields:

$$\dot{m}_a c_{P,da}\frac{dT_a}{dy} = h_c W(T_w - T_a) \tag{A.11}$$

An assumption is now made that the saturation curve is linear in the range of conditions experienced in the wet surface heat exchanger. In equation form, this may be expressed:

$$\omega_w = d + e^*T_w \tag{A.12}$$

where e is the slope of the assumed linear saturation line and d is a constant. Equation (A.12) may then be substituted into the psychometer equation, (A.3), to obtain Eq. (A.13).

$$T_a - T_a' = \frac{(d + e^*T_a - \omega_a)^*h_{fg}}{(c_{P,da} + e^*h_{fg})} \tag{A.13}$$

Equation (A.11) is now multiplied through by the quantity $eh_{fg}/(c_{P,da} + eh_{fg})$ to obtain:

$$\frac{\dot{m}_a c_{P,da} e\, h_{fg}}{(c_{p,da} + eh_{fg})}\frac{dT_a}{dy} = \frac{h_c W e h_{fg}}{c_{P,da} + eh_{fg}}(T_w - T_a) \tag{A.14}$$

Multiplying Eq. (A.9) through by the group $c_{P,da}h_{fg}/(c_{P,da} + eh_{fg})$

yields:

$$\frac{\dot{m}_a c_{P,da} h_{fg}}{(c_{P,da} + eh_{fg})} \frac{d\omega_a}{dy} = \frac{h_D W c_{P,da} h_{fg}}{(c_{P,da} + eh_{fg})} (\omega_w - \omega_a) \qquad (A.15)$$

Subtracting Eq. (A.15) from (A.14) and bringing constants inside the derivative sign yields:

$$\dot{m}_a c_{P,da} \frac{d}{dy} \left[\frac{(eT_a - \omega_a)h_{fg}}{(c_{P,da} + eh_{fg})}\right] = Wh_{fg} \frac{[h_c e(T_w - T_a) - c_{P,da} h_D (\omega_w - \omega_a)]}{(c_{P,da} + eh_{fg})} \qquad (A.16)$$

Assuming that the Lewis number is unity and substituting the equation for the assumed linear saturation curve into Eq. (A.16) yields:

$$\dot{m} c_{P,da} \frac{d}{dy} \left[\frac{(d + eT_a - \omega_a)h_{fg}}{c_{P,da} + eh_{fg}}\right] = -Wh_c \left[\frac{(d + eT_a - \omega_a)h_{fg}}{c_{P,da} + eh_{fg}}\right] \qquad (A.17)$$

Replacing the two bracketed groups of terms with Eq. (A.13), multiplying through by Y and rearranging yields:

$$\frac{d}{dy} (T_a - T_a') = - \frac{h_c A_a}{\dot{m} c_{P,da} Y} (T_a - T_a') \qquad (A.18)$$

The solution to this linear first order differential equation is:

$$T_a - T_a' = k_1 * \exp \left(\frac{h_c A_a}{\dot{m} c_{P,da}} * \frac{y}{Y}\right) \qquad (A.19)$$

The boundary condition for this O.D.E. is that at y = 0, the air dry and wet bulb temperatures at the inlet to the exchanger are both known quantities. Therefore, the solution to the O.D.E. at the exchanger exit, where y/Y = 1.0, is:

$$(T_a - T_a')|_{outlet} = (T_a - T_a')|_{inlet} * \exp\left(- \frac{h_c A_a}{\dot{m} c_{P,da}}\right) \quad (A.20)$$

Equation (A.20) may now be used to calculate the wet bulb depression of the air as it passes through the wet surface exchanger once the parameters in the exponent parenthesis are specified.

To obtain equations for the exiting wet bulb temperature, Eq. (A.13) is first multiplied through by $(1.0 + eh_{fg}/C_{P,da})$ to yield:

$$(T_a - T_a')*(1.0 + eh_{fg}/c_{P,da}) = (d + eT_a - \omega_a)\, h_{fg}/c_{P,da} \quad (A.21)$$

Cancelling common terms in the above equation results in:

$$T_a + (\omega_a - d)\, h_{fg}/c_{P,da} = T_a' \,(1.0 + eh_{fg}/c_{P,da}) \quad (A.22)$$

Equation (A.8) may also be simplified by assuming the Lewis number is unity and using the linear approximation for the saturation line.

$$U(T_f - T_w) = h_c(T_w - T_a) + \frac{h_c h_{fg}}{c_{P,da}} (d + eT_w - \omega_a) \quad (A.23)$$

Substituting Eq. (A.22) into the right hand side of the above equation yields:

$$U(T_f - T_w) = (T_w - T_a') * h_c\ (1.0 + eh_{fg}/c_{P,da}) \tag{A.24}$$

A wet bulb heat transfer coefficient is now defined as:

$$h_{wb} \triangleq h_c * (1.0 + eh_{fg}/c_{P,da}) \tag{A.25}$$

and is used to simplify Eq. (A.24) to:

$$U(T_f - T_w) = h_{wb} * (T_w - T_a') \tag{A.26}$$

Substituting Eq. (A.11) into Eq. (A.18) for dT_a/dy yields:

$$\frac{dT_a'}{dy} = \frac{h_c L}{\dot{m}c_{P,da}} * (T_w - T_a') \tag{A.27}$$

A wet bulb specific heat is now defined as:

$$c_{wb} \triangleq c_{P,da} * (1.0 + eh_{fg}/c_{P,da}) \tag{A.28}$$

to simplify Eq. (A.27) to:

$$\dot{m}_a c_{wb} \frac{dT_a'}{dy} = h_{wb} W(T_w - T_a') \tag{A.29}$$

The three resulting equations, (A.7), (A.26) and (A.29), are of the same form as the governing equations seen in sensible heat exchanger theory. The effectiveness-NTU equations for counter-flow heat exchangers may therefore now be used to solve for the exiting air wet bulb temperature once the previously defined wet bulb specific heat and heat transfer coefficient are calculated. Finally, Eq. (A.20) may be used to calculate the exiting air wet bulb depression and together with the exiting wet bulb temperature fixes the air state exiting the wet surface heat exchanger.

APPENDIX C

The following is the seasonal performance data for the Carrier heat pump and the desiccant cycles used to generate Tables 7.3.1 through 7.3.4.

TABLE C.1

SEASONAL PERFORMANCE DATA FOR CARRIER SPLIT SYSTEM HEAT PUMP, MADISON, WISCONSIN

LATENT LOAD RATIO	$Q_{EVAPORATOR}$ (GJ)	VAPOR COMPRESSION WORK (GJ)
0	704.4	178.4
0.1	879.6	221.8
0.2	988.5	249.1
0.3	1093.0	275.5
0.4	1200.0	302.3
0.5	1309.0	329.5
0.6	1419.0	357.3

TABLE C.2

SEASONAL THERMAL COEFFICIENTS OF PERFORMANCE

MADISON, WISCONSIN

DESICCANT AIR CONDITIONING CYCLE	MODE	LATENT LOAD RATIO 0.0	0.1	0.2	0.3	0.4	0.5	0.6
COOLING TOWER/ H.X.								
NTU=9	RECIRC	7.334	7.243	5.339	3.975	3.147	2.610	2.235
NTU=3		1.679	2.053	2.553	2.445	2.181	1.926	1.712
NTU=9	VENT	5.670	5.629	4.148	2.908	2.134	1.789	1.570
NTU=3		1.183	1.676	2.279	2.121	1.709	1.429	1.282
TWO-STAGE IEC								
NTU=9	RECIRC	0.662	2.365	3.606	3.378	3.079	2.736	2.398
NTU=3		0.295	0.538	1.620	2.335	2.232	2.064	1.870
NTU=9	VENT	0.483	2.183	2.734	2.537	2.275	2.004	1.750
NTU=3		0.212	0.450	1.489	1.817	1.765	1.623	1.465
CLASSICAL								
(ϵ_{hx}=.95, ϵ_{ec}=.98)	RECIRC	1.977	1.960	1.882	1.744	1.562	1.385	1.220
	VENT	1.739	1.755	1.730	1.692	1.469	1.251	1.071

REFERENCES

ASHRAE, ASHRAE handbook 1983 Equipment Volume, American Society of Heating, Refrigerating and Air-Conditioning Engineers, Atlanta, GA (1983).

Brandemuehl, M.J. and Beckman, W.A., "Economic Evaluation and Optimization of Solar Heating Systems," Solar Energy, 23, 1 (1979).

Curt, C.W., "Control Concepts for Evaporative Cooling Systems," for inclusion in ASHRAE Transactions 1986, Vol. 92, Pt. 1.

DILHR, Wisconsin Administrative Code, Rules of the Department of Industry, Labor and Human Relations, Vol. 7, Building and Heating Ventilation and Air Conditioning Code (1986).

Dunkle, R.V., "A Method of Solar Air Conditioning," Mech. and Chem. Engr. Trans., Inst. Engs. Australia, MC1, 73 (1965).

Jurinak, J.J., "Open Cycle Solid Desiccant Cooling-Component Models and System Simulations," Ph.D. thesis, University of Wisconsin-Madison (1982).

Kang, T.S., "Adiabatic Desiccant Open Cooling Cycles," MS thesis, School of Mechanical and Industrial Engineering, University of New South Wales (1985).

Kays, W.M. and London, A.L., Compact Heat Exchangers, McGraw-Hill, N.Y. (1984).

Klein, S.A., et al., "TRNSYS - A Transient Simulation Program," University of Wisconsin-Madison Engineering Experiment Station Report 38-12, Version 12.1, December (1983).

Maclaine-cross, I.L., "High Performance Adiabatic Desiccant Open Cooling Cycles," Solar Energy, 107, 102 (1985).

Maclaine-cross, I.L. and Banks, P.J., "A General Theory of Wet Surface Heat Exchangers and Its Application to Regenerative Evaporative Cooling," ASME Journal of Heat Transfer, 103, 579 (1981).

Maclaine-cross, I.L. and Banks, P.J., "Coupled Heat and Mass Transfer in Regenerators - Prediction Using an Analogy with Heat Transfer," International Journal of Heat and Mass Transfer, 15, 1225 (1972).

Means, R.S., "Means Mechanical Cost Data," Robert Snow Means Co., Kingston, MA (1984).

Mitchell, J.W., Energy Engineering, John Wiley and Sons, New York (1983).

Nelson, J.S., Beckman, W.A., Mitchell, J.W. and Close, D.J., "Simulations of the Performance of Open Cycle Desiccant Systems Using Solar Energy," Solar Energy, 21, 273 (1978).

Product Literature, "Applied Split System Heat Pumps," Application Data, Form 38AQ-5XA, Carrier Corporation, Syracuse, NY, USA.

SOLMET Typical Meteorological year, Tape Deck 9734, National Oceanic and Atmospheric Administration, Environmental Data Service, National Climate Center, Asheville, NC.

Van den Bulck, E., Mitchell, J.W. and Klein, S.A., "Design Theory for Rotary Heat and Mass Exchangers - I. Wave Analysis of Rotary Heat and Mass Exchangers with Infinite Transfer Coefficients," International Journal of Heat and Mass Transfer, Vol. 28, No. 8, 1575 (1985).

Van den Bulck, E., Mitchell, J.W. and Klein, S.A., "Design Theory for Rotary Heat and Mass Exchangers, II. Effectiveness-Number-of-Transfer-Units Method for Rotary Heat and Mass Exchangers," International Journal of Heat and Mass Transfer, Vol. 28, No. 8, 1587 (1985).

Van den Bulck, E., Mitchell, J.W. and Klein, S.A., "The Use of Dehumidifiers in Desiccant Cooling and Dehumidification Systems," ASME paper 84-HT-32, Journal of Heat Transfer (in press).

APPROVED:

Date

John Mitchell, Professor
Mechanical Engineering